NASA-CR-132648

COMPUTER PROGRAM TO ASSESS IMPACT OF FATIGUE AND FRACTURE CRITERIA ON WEIGHT AND COST OF TRANSPORT AIRCRAFT

C. J. Tanner
G. S. Kruse
B. H. Oman

June 1975

Prepared Under
Contract NAS 1-12506
for
National Aeronautics and Space Administration
LANGLEY RESEARCH CENTER
Hampton, Virginia

Prepared by
GENERAL DYNAMICS CONVAIR DIVISION
P.O. Box 80847
San Diego, California 92138

FOREWORD

This report describes the methodology and data used in developing fatigue and fracture analysis routines which were integrated into an existing computer program which performs weight and cost analysis of transport aircraft. This work was sponsored by the NASA Langley Research Center. The contributions of Mr. C. C. Poe, Jr., NASA/LRC contract monitor, are gratefully acknowledged. He provided the stress intensity factor coefficients for stiffened panels used in the crack growth and residual strength analysis routines.

The work was accomplished by the Structural Analysis and Mass Properties groups of the Convair Division of General Dynamics, San Diego, California, under the supervision of J. E. Ashton, Director of Structures and Design. The Program Manager was C. J. Tanner. The structural synthesis module, APAS, which includes the added fatigue and fracture routines was developed by G. S. Kruse. Phil Thorndyke aided in developing fatigue data and analysis procedures. Work on the weight and cost computer program is continuing under the leadership of B. H. Oman. Significant contributions were made by T. F. Reed and A. R. Stone in computer programming to produce the resultant Vehicle Design Evaluation Program, VDEP-II.

TABLE OF CONTENTS

LIST OF FIGURES

LIST OF FIGURES (Contd.)

LIST OF FIGURES (Contd.)

LIST OF TABLES

LIST OF SYMBOLS

A	cross sectional area
A_t	enclosed area
a	half crack length
B	structural element dimensions (See figure 2-3)
b	stiffener spacing
C	Erdogan equation coefficient, fatigue equation coefficient
C_f	Shanley frame equation coefficient
C_1, C_2	fatigue notch factor equation coefficients
CP	optimization procedure critical constraint parameter
c	mean geometric wing chord
D	fuselage diameter
E	modulus of elasticity, error of integration
E*	error of integration limit
F_{tu}	ultimate tensile strength
g	acceleration due to gravity
H	growth rate integration operator
I	moment of inertia
I_{xx}	moment of inertia about an axis thru the centroid parallel to the X axis
I_{zz}	moment of inertia about an axis thru the centroid parallel to the Z axis
J	number of loading conditions, torsional stiffness constant
K	opening mode stress intensity factor
K_c	opening mode fracture toughness
K_f	fatigue notch factor (ratio of unnotched to notched fatigue strength)

K_{fs}	lower limit of K_f (at one cycle)
K_{fe}	upper limit of K_f (at endurance limit)
K_g	gust alleviation factor
L	frame spacing, number of static strength failure modes
L(a)	stiffener load concentration factor
M	number of flights in a spectrum, maximum resultant fuselage bending moment, $\sqrt{M_x^2 + M_z^2}$
MC	side constraint parameter
MS	margin of safety
M_x	net bending moment about a horizontal axis thru centroid
M_z	net bending moment about a vertical axis thru centroid
m	slope of lift curve, sub-element of a panel, Erdogan equation exponent, fatigue equation exponent
N	number of allowable stress cycles (fatigue analysis)
N_s	number of load cycles in a spectrum
n	number of applied stress cycles (fatigue analysis), fatigue equation exponent
P	optimization procedure criticality parameter, axial load
p	Erdogan equation exponent
R	stress ratio
S	wing area
S_{max}, σ_{max}	maximum stress in a cycle
S_{min}, σ_{min}	minimum stress in a cycle
S_s	net section static strength, (F_{tu} x SF)
S_e	maximum cyclic stress at endurance limit
SF	net section factor
T, t_i	structural element thicknesses (See figure 2-3)
$\bar{t}$	effective thickness of a panel element (i.e., panel area divided by panel width)

U_{de}	derived gust velocity
V_e	equivalent airspeed
W	aircraft weight
X, Z	section coordinate axes
x, z	distance along coordinate axes
α	ply angle for composite materials
ρ	air density
ρ_o	air density at sea level
μ_g	aircraft mass ratio (See page 2-7)
ϵ	optimization closure tolerance
σ	stress
$\bar{\sigma}$	equivalent stress for flaw growth calculations (see equation 2.7-8)
$\lambda(a)$	correction factor which accounts for geometric effects

SUMMARY

This report presents the results of a research and development study performed under NASA Contract NAS1-12506. The objective of the study was to develop a "Computer Program to Assess the Impact of Fatigue and Fracture Criteria on Weight and Cost of Transport Aircraft." Its intended use is as a preliminary design analysis tool to enable the user to rapidly perform trade-off studies involving fatigue, fracture, static strength, weight, and cost.

The approach consisted of developing analysis subprograms for fatigue life, crack growth life, and residual strength; and linking these to a structural synthesis module which in turn was integrated into a "Computer Program to Perform Cost and Weight Analysis of Transport Aircraft" developed under Contract NAS1-11343. The fatigue routine utilizes a flight profile to calculate damage and is named PRODAM. The second routine uses the same flight profile to calculate crack growth and is called PROGRO. The third routine RESIDS, determines residual strength of flawed structures.

The structural synthesis module, APAS, was originally developed under a Convair IRAD study in 1972. Beam type structures (i.e., wing boxes and fuselages) are synthesized in a multi-station approach to obtain optimum design for static strength for several structural configurations. As a user option PRODAM, PROGRO, and RESIDS may then be called to check the design for fatigue and fracture criteria. A redesign loop is employed to augment the section until the input criteria are met.

Under this study the part definition module of the cost and weight analysis program (NAS1-11343) was expanded to be compatible with the upgraded structural synthesis capability.

The resultant Vehicle Design and Evaluation Program is named VDEP-II. It is an accurate and useful tool for estimating purposes at the preliminary design stage of airframe development. A sample case along with an explanation of program applications and input preparation is presented in the User's Manual. Table 1 is a summary of the program functional capability and Figure 1 is a program block diagram.

Table 1. Summary of the Program Functional Capability

Vehicle Synthesis (Sizing)	Manufacturing Cost
Aircraft Balance	Material Cost
Mission Center of Gravity Envelope	Engineering Cost
Area Ruled Fuselage Geometry	Tooling Cost
General Curve Plotting	Total Vehicle Program Cost
Structural Synthesis	Return-on-Investment
Parts Definition and Weight	Airline Route Analysis

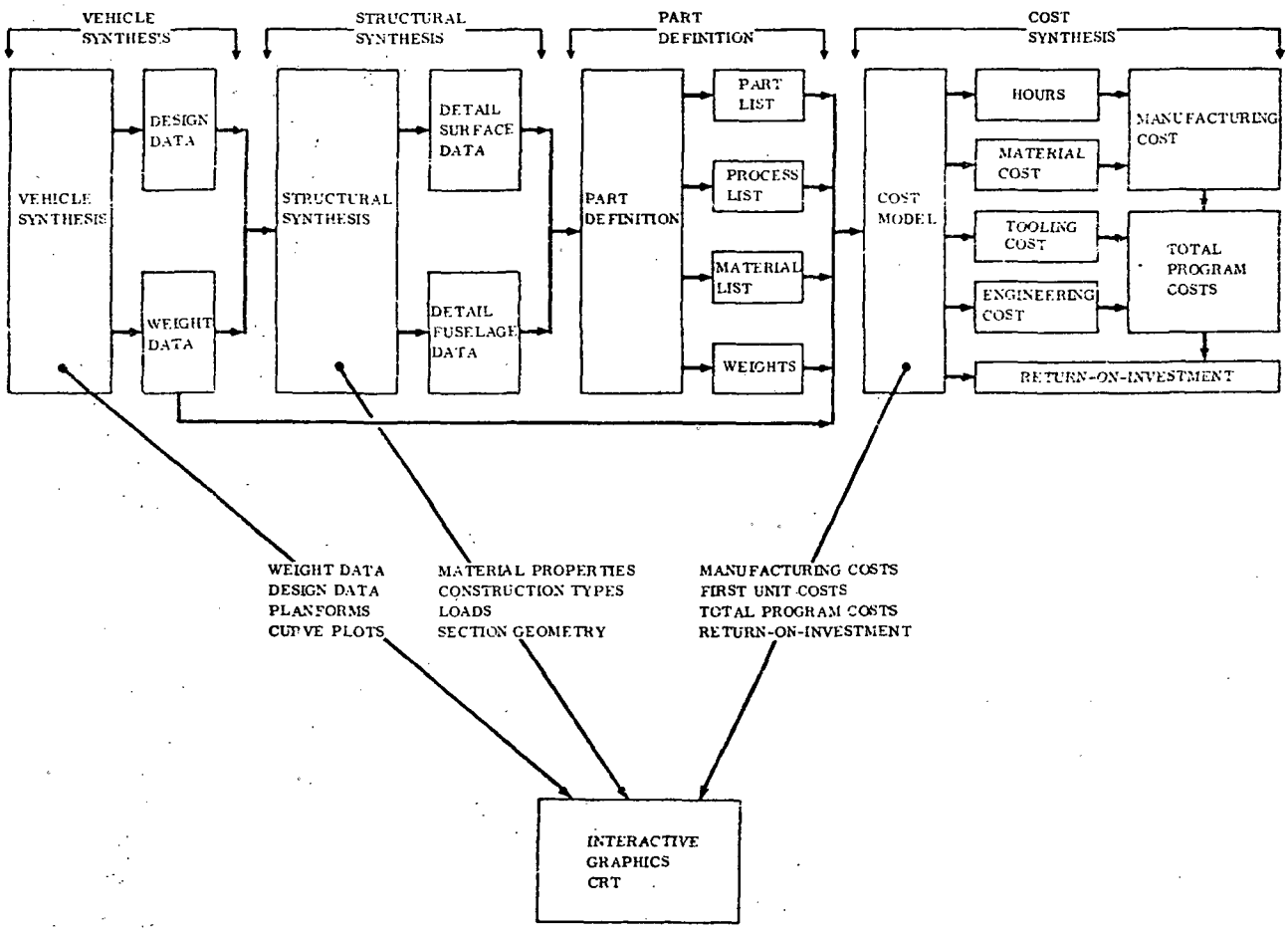

Figure 1. Vehicle Design and Evaluation Program (VDEP-II) Block Diagram

SECTION 1

INTRODUCTION

With the steadily rising cost of aircraft production and operation, and with the large number of materials and structural design concepts applicable to flight vehicles, it becomes increasingly important to be able to assess the impact of aircraft design alternatives in terms of weight and cost. Advances in technology have produced components of increased specific strength, and hence, decreased weight, but at the expense of requiring increasingly exotic materials and fabrication complexities. The result has been an inversion in the typical cost/weight relationship. One way of combating rising operating cost is to design new aircraft for longer service lives. This combination of opposing constraints requiring high structural efficiency on one hand and long service life on the other has focused the attention of airframe designers on fatigue and fracture considerations.

Fatigue analysis has been applied in varying degrees of rationality in the design of most transport aircraft developed in the last three decades. Over-simplified approaches (such as setting an arbitrary limit on allowable tensile stress) have frequently been used in preliminary design. On the other extreme, methods have been devised, and used to solve special problems, which account for non-linear damage accumulation under complex load spectra. In this program an intermediate approach has been developed which permits a realistic evaluation of fatigue criteria and at the same time provides the necessary computational efficiency. This approach employs a simplified flight profile, component S-N data, and linear damage summation.

A major obstacle to applying fatigue analysis in preliminary design is the sparsity of S-N data for the many structural configurations which need to be evaluated. Fatigue life is affected by a wide range of parameters that include cyclic stress, mean stress, product form and orientation, temperature, environment, structural geometry, notch effects, metallurgical effects, and surface finish. An almost infinite variety of materials and fabrication methods would have to be tested to build an adequate S-N data bank. Since this is out of the question, the fatigue life of most aerospace vehicles is verified by tests and analysis performed late in the development of the structure. This after-the-fact analysis cannot produce optimum structures. Tradeoff studies performed in the preliminary design phase are compromised by lack of rational fatigue considerations. Two methods for generating component S-N curves from unnotched coupon data have been applied in this program. Results are presented in Appendix A and B. A third approach utilizing an S-N equation directly within the computer program is proposed for future development. See "Recommendations", page 5-1.

Fracture mechanics is still a developing technology even though problems with slow crack growth as well as catastrophic cracking have afflicted various types of structure for many years. World War II military aircraft structures were designed using methods that accounted for the stiffness and static strength of the undamaged structure

only. Low-strength, highly ductile alloys such as 2024-T3 were used. Fabrication consisted primarily of forming and riveting sheet metal. Conventional sheet-stringer construction gave sufficiently stiff covers for the subsonic flight loads, along with reasonable structural efficiencies. The combination of low-strength ductile material, riveted sheet-stringer construction, and thin sheet metal sections made these structures inherently highly damage tolerant.

Post-war military aircraft were designed for supersonic flight, heavier payloads, and increased structural efficiency to save weight. Thick, monolithic, integrally stiffened, machined components replaced sheet-stringer construction to provide smooth, nonbuckling covers. High-strength materials such as the 7000 series aluminum alloys and heat-treated steels replaced the low-strength ductile materials previously used and resulted in increased design stress levels. The combination of construction type, higher design stresses, more severe usage and more fracture-prone material produced an ever-increasing number of catastrophic service and test failures. In most instances, the failures originated at points of high stress concentration, or at metallurgical defects. Most often, the fatigue cracks, before failure, were hidden or were not large enough to be detected by close visual inspection. As a result, most high-performance military aircraft used during the 1950's and 1960's have gone through costly structural test, structural modification, and life monitoring programs to remain flightworthy. Primary reliance has been placed on a safe-life approach to maintain serviceable aircraft. Extensive element, component, and complete airframe test programs are used to prove the safe-life of the structure.

Commercial aircraft designed before and during World War II used material and structural concepts similar to those military aircraft. Again, the combination of low-strength ductile material and thin sheet metal sections made the designs highly damage tolerant. Later, two ill-fated airplane programs caused commercial aircraft designers to adopt a fail-safe design approach. These were the Martin 404, with heavy monolithic spar cap brittle fractures; and the De Haviland Comet pressurized cabin failures. Since these two instances, commercial aircraft have been designed with a strength capability of 80% of limit flight loads and 100% of normal cabin pressure with single structural members failed in compliance with FAR Part 25. These obvious partial failures are usually chosen to be sufficiently large to be apparent during normal preflight inspections.

The design task of providing damage tolerance was made easier by the reduced stress levels and increased toughness provided by the almost exclusive use of a low-strength, ductile aluminum alloy (2024-T3) in these tension critical applications. The proof of the fail-safe load capability of the flawed structures was accomplished largely by fail-safe tests.

In 1958, the Department of Defense, motivated by several fracture problems in rocket propellant tanks, initiated a study of fracture phenomena within the American Society for Testing and Materials (ASTM). The ASTM, through its E-24 Committee, provided considerable impetus to the advancement of fracture mechanics analysis. The committee's work has resulted in standardized test methods and test specimens for the

proper measurement of material toughness (K_{Ic}). Reference 1 presents these results and has been used extensively as the text on fracture mechanics by the aerospace community. Reference 2 is a comprehensive summary of fracture data for commonly used aerospace materials.

Irwin (Ref. 3) developed equations that related the crack phenomenon to terms that are common to the designer or stress analyst (or, in his words, "suitable for stress analysis"). Later, Paul Kuhn developed practical guidelines that more or less guaranteed fail-safe structures without rigorous use of linear elastic fracture mechanics (Ref. 4). While Irwin's work provided insight into the cause of previous brittle fracture service problems, his analysis methods were applicable only to the simplest structural components. Similarly, Kuhn's guidelines were not always compatible with the emphasis on improved structural efficiency and minimum weight.

Stress intensity factor solutions for numerous load/geometry combinations are now available. Reference 5 summarizes many of these. Special computer programs have been developed to solve additional complex geometries. Methods and programs are also available to predict crack growth under sustained and cyclic loading. The problem of crack propagation thru stiffened panels is of particular interest to aircraft designers. Methods and data required to solve this type problem are presented in Reference 6 and are the basis of the crack growth and residual strength analysis routines developed in this program.

There is a danger that this proliferation of design criteria, and analysis methods relating to fatigue and fracture criteria may reach a point of diminishing return, and even negative return. Therefore it is appropriate to evaluate and balance the possible improvements in service life and operating costs versus weight penalties and manufacturing costs. That was the primary objective of this program--to develop a computer program to assess the impact of fatigue and fracture criteria on the weight and cost of transport aircraft.

The starting point of this effort was a computer program developed under NASA Contract NAS1-11343, "A Computer Program to Perform Cost and Weight Analysis of Transport Aircraft", (Reference 7). This program, intended for use at the preliminary design level, incorporates both batch mode and interactive graphics run capability. The basis of the weight and cost estimation method developed is a unique way of predicting the physical design of each detail part of a vehicle structure at a time when only configuration concept drawings are available. Encompassing the areas of manufacturing and material cost, engineering cost, tooling cost, total vehicle program cost, and return-on-investment, this program represents a significant extension and refinement of the methods originally formulated in Reference 8.

Weight data are generated in four areas of the program. Overall vehicle system weights are derived on a statistical basis as part of the vehicle sizing process. Theoretical weights, actual weights, and the weight of the raw material to be purchased are derived as part of the structural synthesis and part definition processes based on the computed part geometry.

The manufacturing cost analysis, based at the individual detail part level, is made by considering the actual manufacturing operations required to produce that part. A list of shop operations is called out with each detail part, and a series of equations associated with each operation is used to compute the shop hours necessary to make the part.

By applying the appropriate labor rates to the calculated hours, the direct and indirect manufacturing labor costs are found. Material costs are computed based on the amount of material required to manufacture each part.

Engineering costs are computed based on the number of manhours necessary to perform the various tasks associated with the development and production of aircraft. The computation has as its basis equations originally developed by Levenson and Barro of the Rand Corporation (Reference 9). Initial engineering hours are broken down and distributed among the various engineering disciplines based on studies made of historical data.

Tooling costs are computed as a function of the number of basic tool manufacturing hours, initial and sustaining aircraft production rates, and tooling labor rates. Basic tool manufacturing hours are derived as a function of the number of dissimilar parts to be produced, the average number of tools required per dissimilar part, and the average number of hours required to produce each tool.

Total vehicle program costs are computed based on a cost model that was assembled primarily from the work of Kenyon (Reference 10). Cost elements that are computed elsewhere in the program are brought across and substituted into the model. A learning curve approach is utilized to derive costs of a given unit or lot as a function of the first unit cost.

A comprehensive measure of the total economic viability for a commercial transport operation is reflected in the return-on-investment analysis. Direct operating costs are computed using the 1967 Air Transport Association formula updated to 1972 cost levels. Indirect operating costs and return-on-investment are computed by applying aircraft acquisition and direct operating costs to a defined traffic structure. Output includes direct operating costs, indirect operating costs, revenue, load factors, profit, return-on-investment, and fleet size.

An important feature of the program is its capability to make trade studies from several levels of consideration. For example, weight and cost data can be related directly to key system parameters at the vehicle mission level such as payload, speed, range, and landing field length requirements. At the vehicle configuration level, data can be related directly to surface areas, span, sweep, taper, etc., and fuselage length, slenderness, etc. At the major component level comparisons can be made between different materials, modes of construction, detail part make-up, etc. Tradeoffs can be made to determine the overall vehicle weight and cost sensitivities at each of these levels, and in this manner the proposed aircraft design may be further and further refined down to high degree of detail. Thus, engineering functions can gain insight into the cost effectiveness of alternate aircraft systems, perform design trade studies, as well as perform studies to determine the impact of fatigue and fracture criteria.

SECTION 2

STRUCTURAL SYNTHESIS

The structural synthesis procedure used by VDEP-II is known as APAS. This procedure was originally developed earlier under a company sponsored IRAD program and is reported in Reference 11.

The pertinent information of that report is restated in this section for convenience. Also reported in this section is a complete description of the technical approach used to include fatigue and fracture criteria in the structural synthesis procedure.

2.1 COMPONENT GEOMETRY

The geometry of each component, (fuselage, wing, horizontal and vertical stabilizer) is represented by the coordinates of a set of nodes at each of the various stations along the component. This nodal geometry describes the shape of the component which is used for the computation of section properties.

2.1.1 FUSELAGE NODAL GEOMETRY. The fuselage is represented by 18 nodes at each of 10 stations. The nodes are located at 20 degree intervals around the fuselage. Nodal geometry for a typical transport fuselage is presented in Figure 2-1. Nodes are numbered starting at the top centerline and proceeding clockwise looking aft.

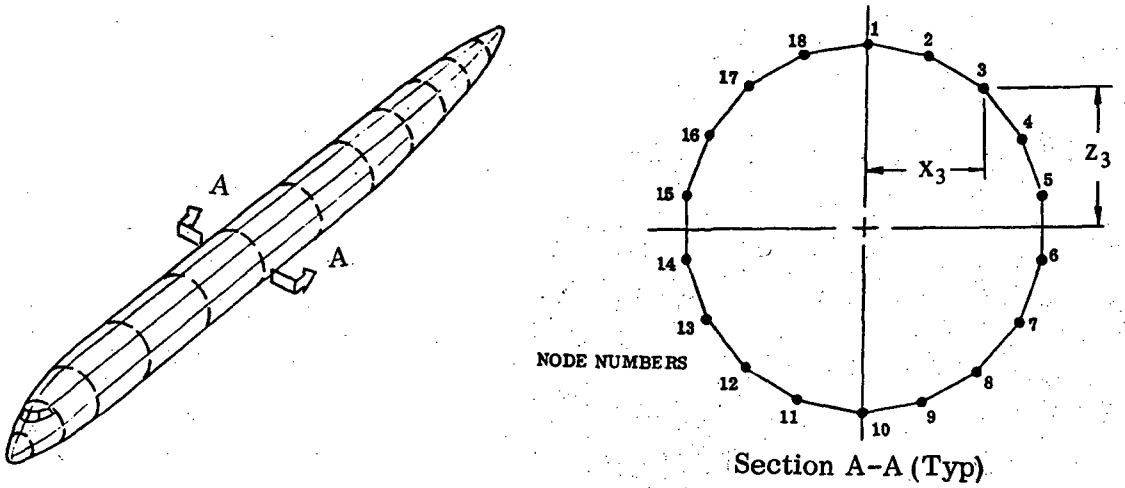

Figure 2-1 Fuselage Nodal Geometry

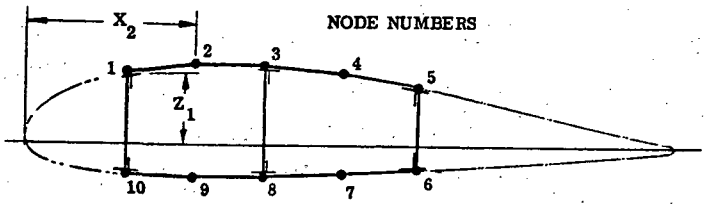

Section B-B (Typ.)

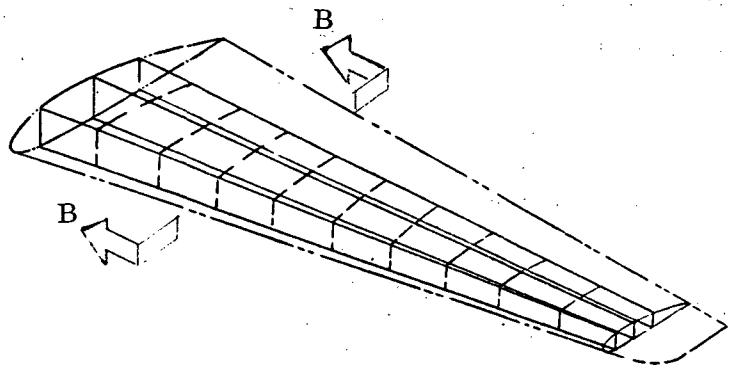

Figure 2-2 Aerodynamic Surface Nodal Geometry

2.1.2 AERODYNAMIC SURFACE NODAL GEOMETRY. The wing, horizontal and vertical stabilizer are represented by 10 nodes at each of 10 stations. The nodal geometry describes the box structure for a surface with up to 5 spars. The nodes are numbered beginning at the upper sparcap of the front spar and proceeding clockwise to the lower front sparcap. A typical surface nodal geometry is presented in Figure 2-2.

2.2 STRUCTURAL ELEMENTS, RIBS AND FRAMES

2.2.1 STRUCTURAL ELEMENTS. Structural elements include skin panel, spar webs and spar caps. Each element is described by a type number and by from one to eight dimension variables. The dimension variables are of two types, thickness variables and non-thickness variables such as stiffener spacing, stiffener height, corrugation angle, etc. In general, non-thickness variables may have either equality or inequality constraints imposed, whereas thickness variables may have equality or lower bound inequality constraints imposed.

2.2.1.1 Skin Panel Elements. The structural synthesis program includes twelve types of panel elements as presented in Figure 2-3. The stiffeners on panel types one through nine are assumed to be oriented parallel to the elastic axis of the structure. The 0 degree ply of panel type 12 is also assumed to be parallel to the elastic axis.

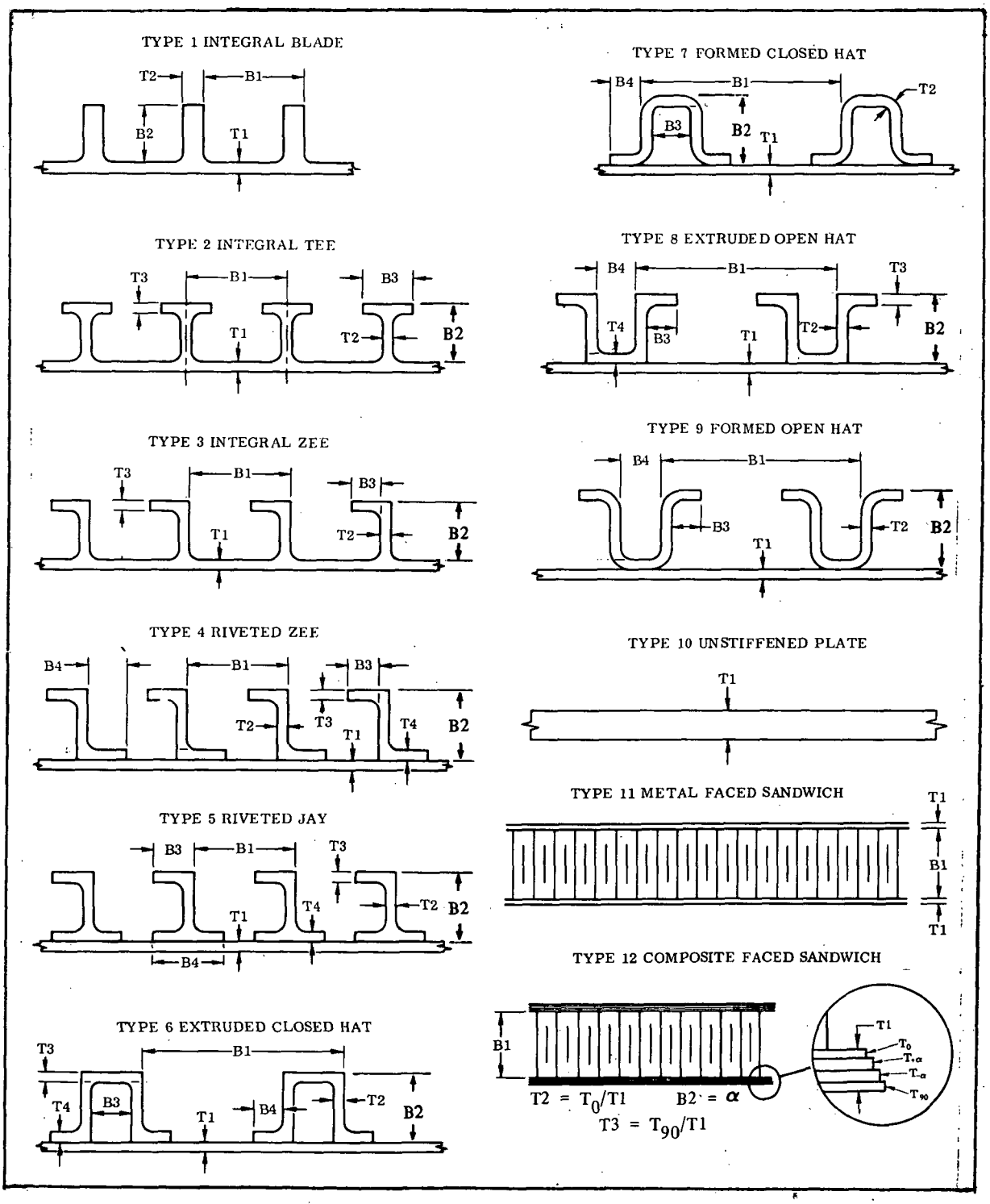

Figure 2-3. Skin Panel Elements

2.2.1.2 "Spar Web" Elements. The structural synthesis program contains seven types of "spar web" elements. Four of these are truss type elements, two are stiffened webs and the remaining one is a corrugated web. These elements are presented in Figure 2-4. "Spar Web" elements are assumed to resist only shear and crushing loads, the axial stiffness of these elements is assumed to be zero for the purpose of computing section properties.

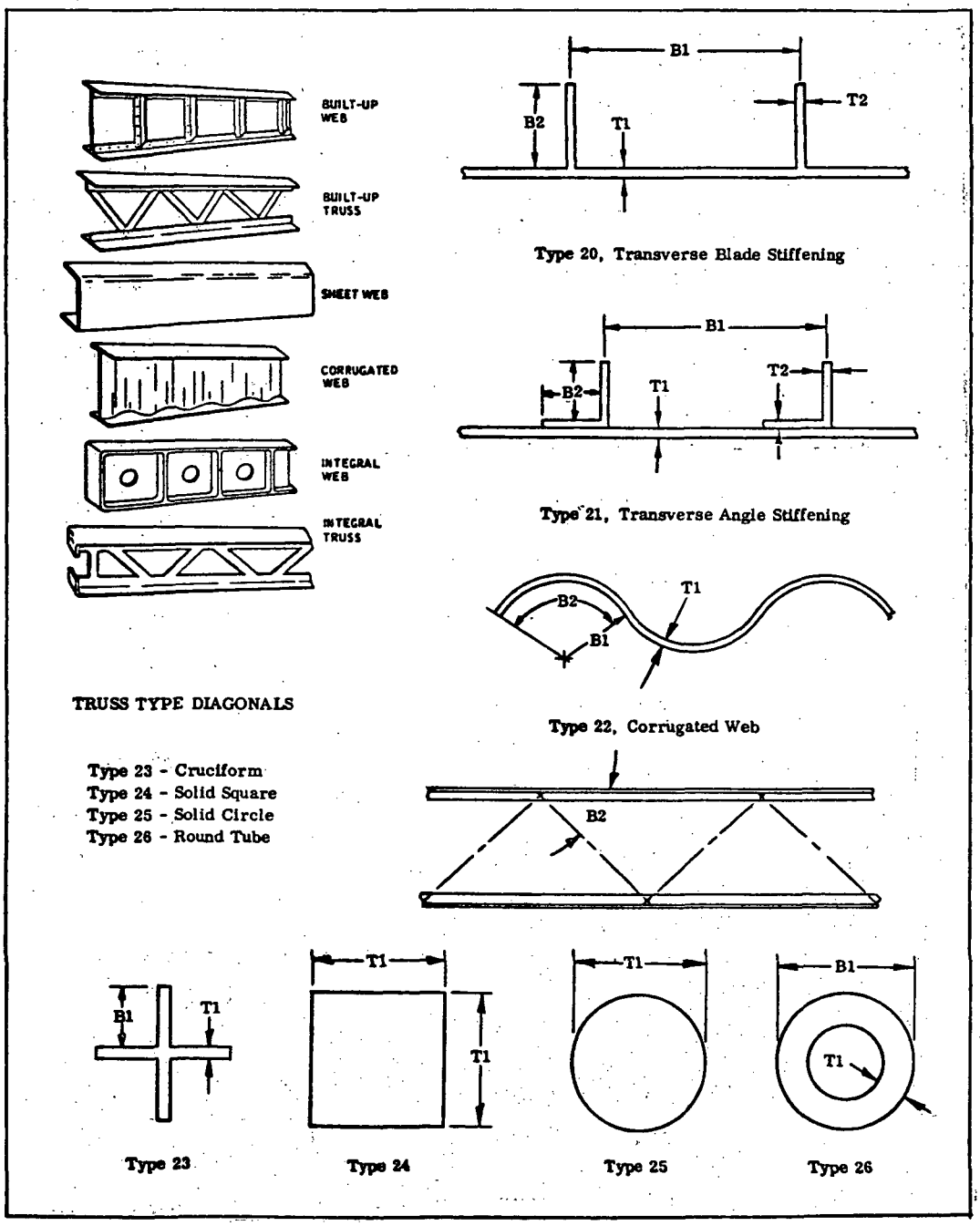

Figure 2-4 Spar Web Elements

2.2.1.3 Spar Cap Elements. Four types of spar caps are currently available. They include integral tee and angle and riveted tee and angle as shown in Figure 2-5.

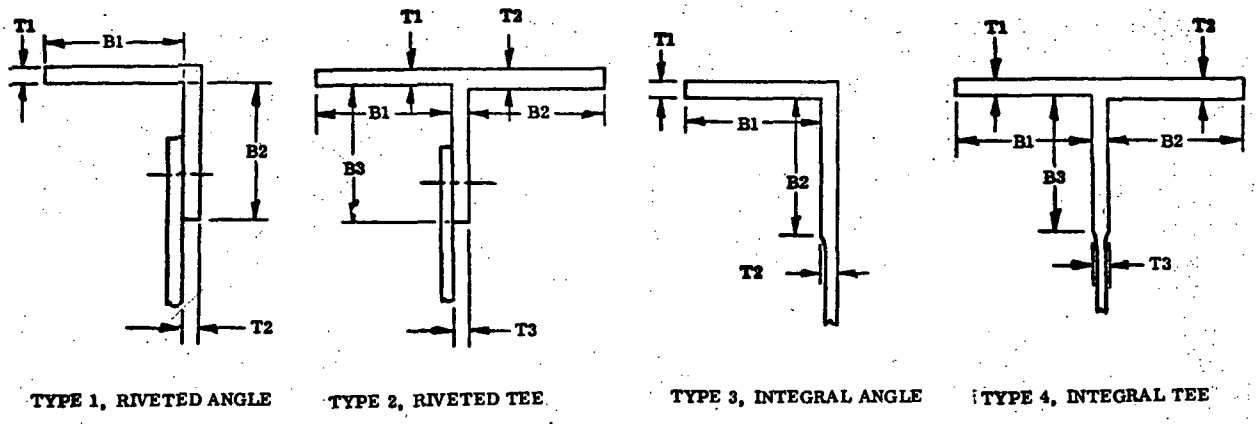

Figure 2-5 Spar Cap Elements

2.2.2 RIBS. The types of ribs available within the program are presented in Figure 2-6. The ribs are comprised of caps and webs or truss elements. Rib caps are sized to react a moment at the rear spar due to the loading on the surface aft of the rear spar. Rib webs are sized to carry shear and to support crushing loads.

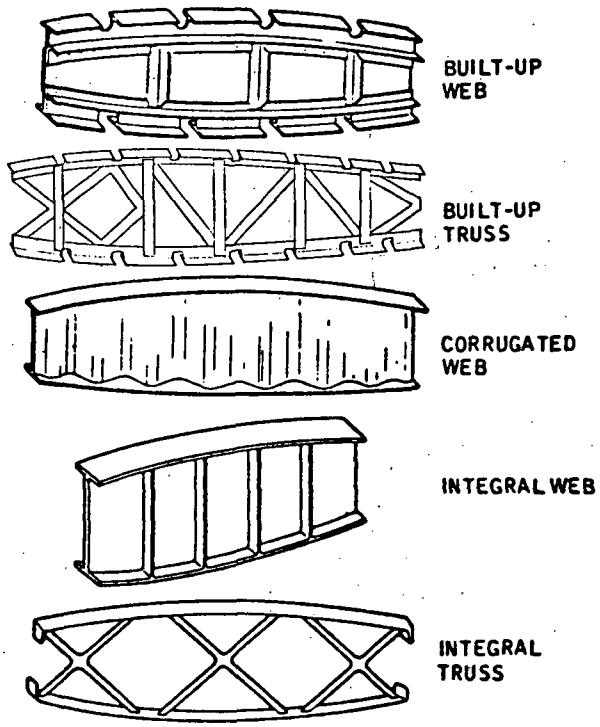

Figure 2-6 Ribs

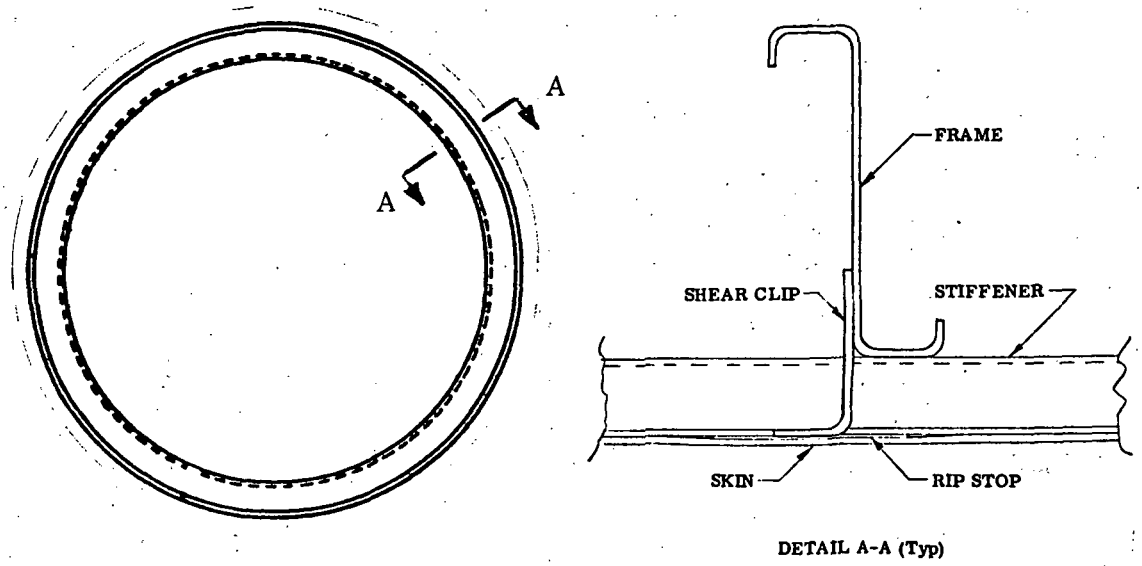

Figure 2-7 Typical Ring Frame

2.2.3 FRAMES. A typical ring frame is shown in Figure 2-7. The frames are sized so that the outer flange clears all of the skin stiffeners. The inner flange is maintained at 14 cm (5.5 inches) from the outer skin contour. The frame is sized using Shanley's criteria to set a minimum frame bending stiffness. The frame is set to minimum gage for non-critical areas.

$$EI = \frac{C_f M D^2}{L}$$ Shanley's criteria (Ref. 18)

where:

EI = frame bending stiffness

M = maximum resultant fuselage bending moment, $\sqrt{M_x^2 + M_z^2}$

D = fuselage diameter

L = frame spacing

C_f = fit coefficient (.00025)

2.3 FLIGHT PROFILE AND LOAD SPECTRUM

The fatigue load spectrum defines the number of times that incremental loads of given magnitudes are encountered during the design life of the aircraft. Experimental data is available which defines the probable magnitudes and frequency of occurrence of these incremental loads as a function of aircraft type, configuration parameters, and flight parameters.

The configuration and flight parameters are defined using a typical flight profile, which is divided into segments. Parameters are averaged for each segment, and these average values are used in finding the incremental loads. See Figures 2-8 and 2-9.

The typical flight profile used for fatigue and flaw growth analysis is based on medium range operation of a contemporary transport aircraft.

The parameter values for each segment are listed in Table 2-1 . The segments are divided into subsegments, with each subsegment representing a particular magnitude of incremental load. Using the segment parameters and the subsegment load, frequency of occurrence of the incremental load is found for each subsegment using the methods and information in Reference 13.

For gust loads, curves showing gust velocity vs frequency of occurrence are found in Reference 13, Figure C13-32 through C13-37. From Reference 13, Page C13-24,

$$\Delta g = m S V_e U_{de} K_g \rho_{o/2W}$$

For speeds below critical Mach number:

$$K_g = \frac{.88\mu_g}{5.3+\mu_g} \qquad \mu_g = \frac{2W}{m g c S \rho}$$

where

- Δg = incremental load factor
- m = slope of lift curve
- S = wing area
- V_e = equivalent airspeed
- U_{de} = derived gust velocity
- K_g = gust alleviation factor
- ρ_o = air density at sea level
- W = aircraft weight
- μ_g = aircraft mass ratio
- g = acceleration of gravity
- c = mean geometric wing chord
- ρ = air density

Figure 2-8. Typical Flight Profile

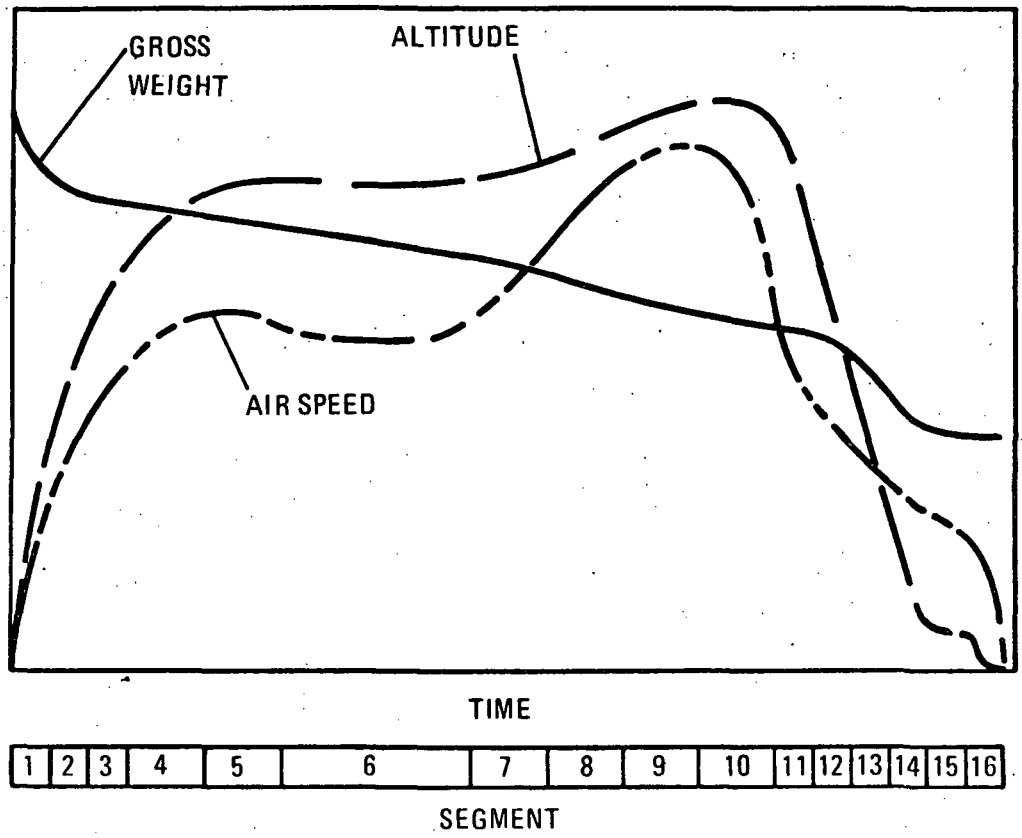

Figure 2-9. Typical Segment Load Frequency Curve

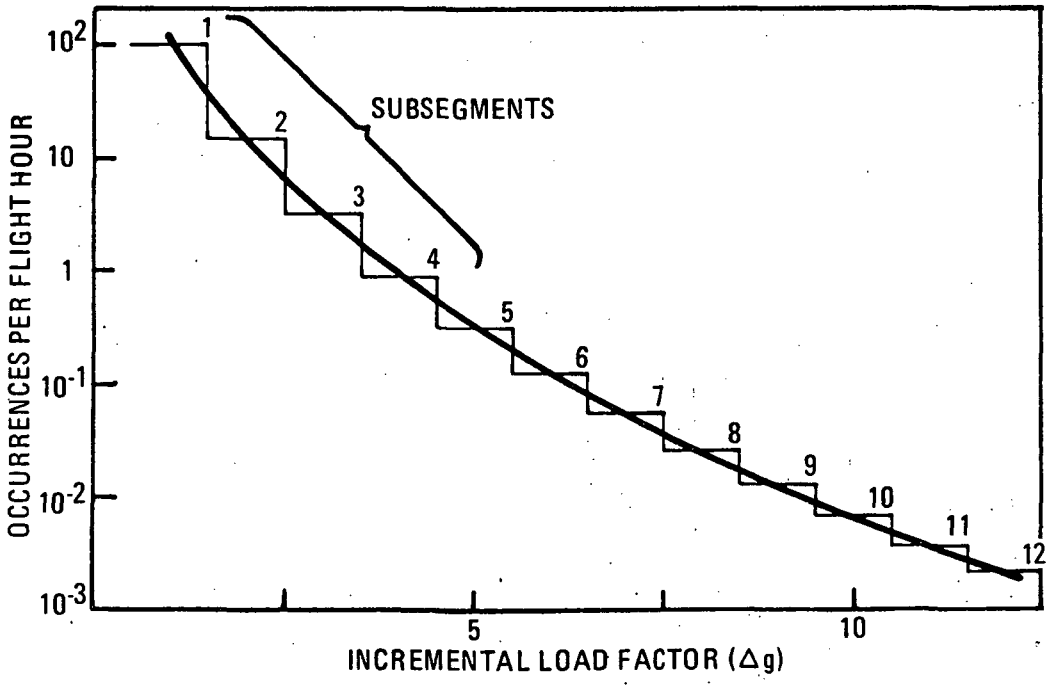

solving for U_{de}

$$U_{de} = \frac{\Delta g}{m S V_e K_g \rho_{o/2W}}$$

U_{de} is then calculated for each subsegment, and the curves of Figure C13-37 are used to find the frequency of occurrence.

For maneuver loads, Figure C13-41 of Reference 13 shows incremental load factor vs frequency of occurrence. For taxi loads, Figure C13-46 of Reference 13 shows incremental load factor vs frequency of occurrence. Incremental load factor vs frequency of occurrence for landing loads was averaged from data for two commercial transport aircraft.

The resulting fatigue load spectrum is shown in Table 2-2. The number of cycles is based on 10,000 flights. The variation between cycles and flights is linear, so that linear ratioing of cycles and design life is valid.

Table 2-1. TYPICAL TRANSPORT FLIGHT PROFILE

	Segment Description	Gross Weight (kips)	Altitude ($ft \times 10^3$)	* KEAS	Mach No.	Distance Statute Miles
1	Taxi; takeoff run, ldg. roll	358.3	S.L.			
2	Climb (Flaps down 25°)	352.2	0 - 5	223	.355	8.15
3	↑	↑	5 - 10	250	.435	12.51
4	↓	↓	10 - 20	340	.684	47.53
5	Climb	352.2	20 - 35	319	.836	150.70
6	Cruise	341.4	35	273	.85	395.58
7	Descent	335.4	35 - 20	319	.836	53.29
8	↑	↑	20 - 10	340	.684	33.33
9	↓ (Flaps down 15°)	↓	10 - 5	250	.435	23.45
10	Descent (Flaps down 50°)	335.4	5 - 0	223	.355	14.11
11	Climb (Flaps down 25°)	352.2	0 - 5	223	.355	8.15
12	↑	↑	5 - 10	250	.435	12.51
13	↓	↓	10 - 20	340	.684	47.53
14	Climb	352.2	20 - 35	319	.836	150.70
15	Cruise	341.4	35	273	.85	395.58
16	Descent	335.4	35 - 20	319	.836	53.29
17	↑	↑	20 - 10	340	.684	33.33
18	↓ (Flaps down 15°)	↓	10 - 5	250	.435	23.45
19	Descent (Flaps down 50°)	335.4	5 - 0	223	.355	14.11
20	Landing	334.7	S.L.	128		

*Knots equivalent airspeed

Table 2-2. TYPICAL TRANSPORT FATIGUE SPECTRUM - CYCLES PER 10,000 FLIGHTS

SUBSEGMENT		1	2	3	4	5	6	7	8	9	10	11	12	13	14	15	16
SEGMENT NO.	LOAD TYPE •	Δ g .10	Δg .15	Δ g .20	Δg .25	Δ g .30	Δ g .35	Δ g .40	Δ g .45	Δ g .50	Δg .60	Δ g .70	Δ g .80	Δ g .90	Δg 1.00	Δ g 1.10	Δ g 1.20
1	2-2	2349957		249957		15070		882		43							
2	2-1	246970		10867		823		120		26	8	3	1	.4			
3	2-1	41700		5212		834		199		54	17	7	3	1	.6		
4	2-1					6990		2502		951	336	190	90	45	24	14	8
5	2-1	100467		13700		3014		685		196	60	24	11	6			
6	2-1	113023		8417		1236		283		75	25						
7	2-1	48446		5921		1211		296		85	28	11	5	2			
8	2-1					6060		2083		833	333	159	79	42	22	12	7
9	2-1			13794		2468		558		156	52	20	8	4	2	.9	
10	1-1	486552		22397		1987		282		61	18	7	3	1			
11	1-1	4320	1328	448	151	51	18	7	3	2							
12	1-1	6630	2039	688	231	78	28	11	5	2							
13	1-1	25191	7747	2614	879	295	106	42	19	9							
14	1-1	79871	24564	8288	2788	934	347	132	59	30							
15	1-1	209657	64480	21757	7318	2453	882	347	154	77							
16	1-1	28244	8686	2931	986	330	119	47	21	10							
17	1-1	17665	5433	1833	617	207	74	29	13	6							
18	1-1	12428	3822	1290	434	145	52	21	9	5							
19	1-1	7478	2300	776	261	87	31	12	6	3							
20	3-2				508.	7030.	1500.			845.		104.		13.			

• 1-1 MANEUVER
3-2 LANDING IMPACT
2-2 TAXI
2-1 GUST

2.4 EXTERNAL LOADS

Net limit loads due to the air loads, inertia loads and landing gear loads of various flight and ground conditions are input to the program.

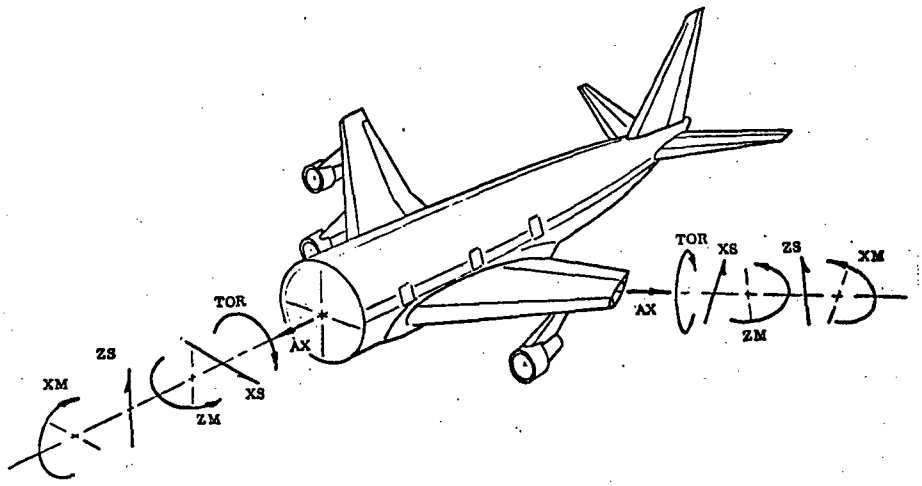

Figure 2-10. External Loads Sign Convention

The loading conditions are separated into two groups. The first group consists of from one to six conditions. These conditions are specified by the user and are used to size the structure so as to preclude static strength failures and to meet residual strength requirements. The second group consists of the six conditions listed in Table 2-3. These conditions are used to define the fatigue stress spectrum described in Section 2.7.

Table 2-3. Fatigue Spectrum Loading Conditions

Condition Number	Description
1	1G Taxi
2	1G Level Flight
3	2G Vertical Gust
4	2G Maneuver
5	1G Landing Impact
6	Maximum Pressure (Fuselage)

Each loading condition defines the six components of load (AX, XS, ZS, TOR, XM, ZM) at up to twenty stations along the structure. The sign convention used is presented in Figure 2-10. A typical fuselage loading condition is illustrated in Figure 2-11. Steps in the loading curves are represented by repeating stations with the two

different load component values. The reference axis used for input loads is the centerline for fuselages and a line midway between the front and rear spars for aerodynamic surfaces.

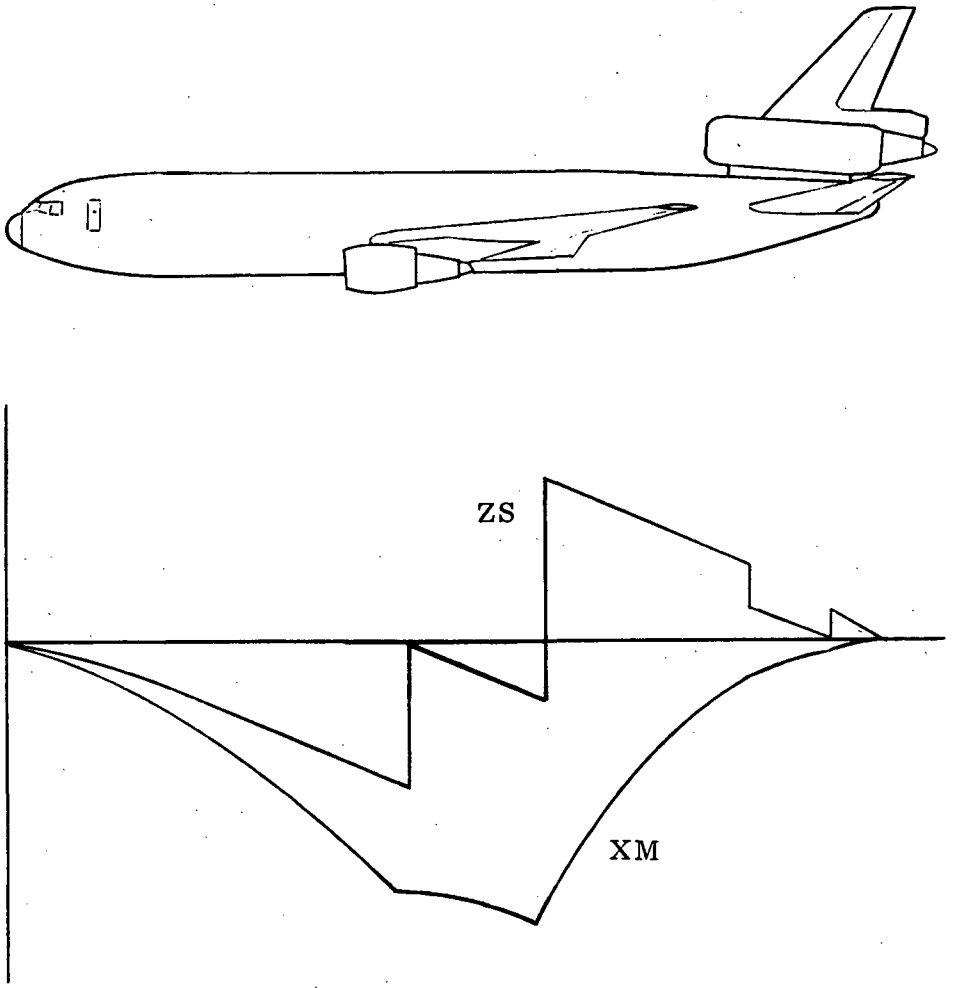

Figure 2-11. Typical Fuselage Load Condition

2.5 STRUCTURAL DESIGN PROCEDURE

The structural design procedure starts with the input design, then through a series of design analysis and redesign iterations produces a final design. The iteration process continues until the lightest weight design which satisfies design criteria and constraints is found.

The design analysis involves the comparison of applied stresses and allowable stresses. The internal load solution described in Section 2.7 is used to calculate the applied stresses. The box beam internal load solution was selected instead of a finite element solution in order to keep computer execution time at an acceptable level. This selection restricts this procedure to relatively clean beam-like structures. However, decoupling of internal loads from one station to the next is basic to the box beam theory. Hence, the overall design problem is reduced to a series of cross-section design problems at any number of desired locations along the structure.

The procedure used to design the cross section is a two part procedure. The first part, the section sizing procedure, adds or subtracts material from the structural elements of the cross section in order to produce a zero margin or minimum gage design. The second part employs a non-linear programing technique to minimize the "criticality" of each element while maintaining a constant weight design. This element optimization procedure, is then iterated with the section sizing procedure until the design converges. Convergence occurs when two successive iterations produce a change in weight that is within a specified tolerance.

2.5.1 SECTION SIZING PROCEDURE. During this part of the design process only the thickness variables are changed. Figure 2-12 illustrates a typical cross-section design problem.

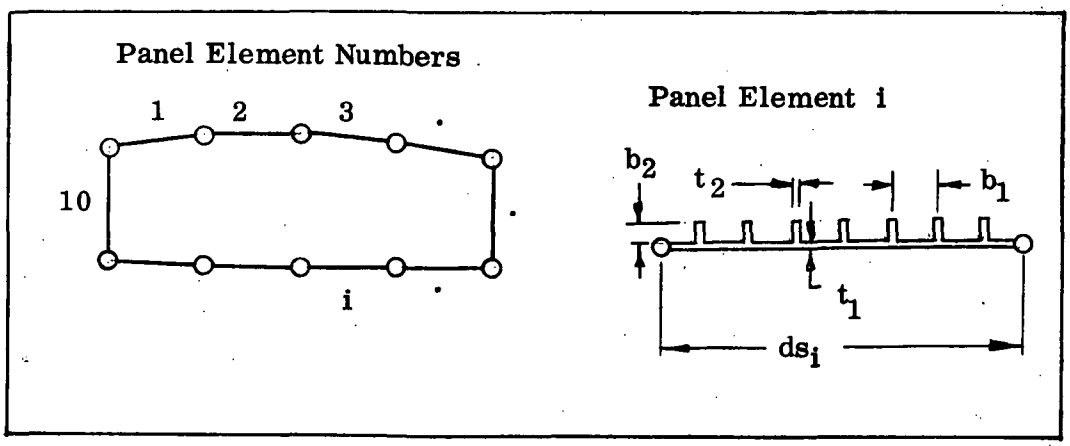

Figure 2-12. Typical Cross Section

The equivalent thickness of the panel, $\bar{t}$, is defined as the panel section area divided by its width. For the panel illustrated, $\bar{t}$ is given by

$$\bar{t}_i = t_{i,1} + b_{i,2} \cdot t_{i,2} / b_{i,1} \quad = (\text{Area of panel } i)/ds_i$$

The following steps are used to find critical $\bar{t}$'s. A critical $\bar{t}$ is defined as the $\bar{t}$ for which the panel's critical margin of safety is zero or for which the most critical margin of safety is positive and the panel is minimum gage.

1. Determine the section properties of the cross-section.

2. Determine the internal loads of each element of the cross section for each load condition.

3. Calculate the applied stresses.

4. Perform a stress analysis of each element for each load condition and produce the structural margins of safety.

5. Starting with the 1st element of the cross-section and proceeding to the last find the critical constraint parameter, i.e., lowest margin of safety or minimum gage margin.

6. Change the $\bar{t}$ of each element to drive it towards its critical $\bar{t}$.

7. Return to step one and iterate the process until all panels have critical $\bar{t}$'s.

The technique employed in step 6 to predict new $\bar{t}$'s is described below. The new $\bar{t}$ of a structural element is predicted by passing a second degree parabola through the points (0, -1), ($\bar{t}^{k-1}$, CP^{k-1}) and (t^k, CP^k) then solving for the proper root of the resulting equation. The critical constraint parameter, CP, is the margin of safety or the side constraint margin defined in Section 2.5.2. The superscript is used to denote the iteration number; i.e., $\bar{t}^k$ is the current $\bar{t}$, CP^k is the critical constraint parameter for $\bar{t} = \bar{t}^k$, and ($\bar{t}^{k-1}$, CP^{k-1}) are corresponding values for the previous iteration. The process, illustrated in Figure 2-13, is started by passing a straight line through the points (0, -1) and ($\bar{t}^1$, CP^1).

2.5.2 ELEMENT OPTIMIZATION PROCEDURE. The object of the element optimization procedure is to adjust detail dimensions of an element so as to make the most efficient use of the material while maintaining a given weight. As an example refer again to Figure 2-12. The panel element shown contains four design variables, t_1, t_2, b_1 and b_2.

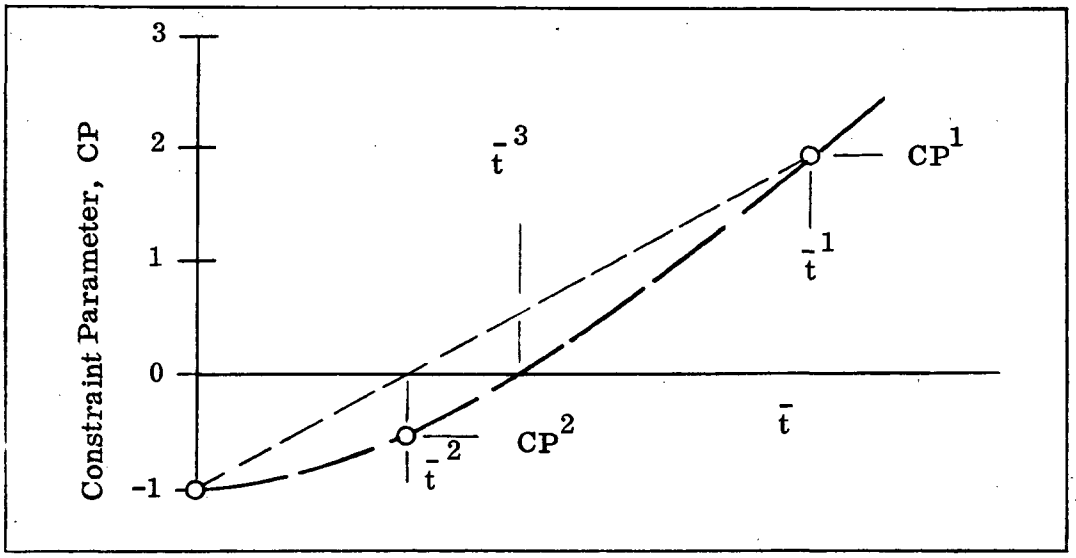

Figure 2-13. Section Sizing Procedure

The object is to find the optimum set, i.e., that set which represents the "least critical" panel possible. Since this procedure requires that $\bar{t}$ remain constant, there are only three independent design variables. Given any three variables the fourth is found by solving the following equation for the appropriate variable.

$$\bar{t} = t_1 + t_2 b_2 / b_1$$

The "least critical" design is defined as that design for which the following criticality parameter is a minimum

$$P = \sum_{\ell=1}^{L} \sum_{j=1}^{J} F(MS_{\ell,j}) + \sum_{m=1}^{M} F(MC_m)$$

where

ℓ denotes the failure mode
j denotes the loading condition
m denotes the sub element of each panel element

MS = margin of safety

MC = side constraint margin e.g., $(t_m - t_{min\ m})/t_{min\ m}$

$$F(x) = \frac{1}{x} \qquad x > \epsilon$$

$$F(x) = \frac{1}{\epsilon}\left[\frac{x}{\epsilon}\left(\frac{x}{\epsilon} - 3.\right) + 3.\right] \qquad x \leq \epsilon$$

where

$$\epsilon = 10^{-5}$$

A typical plot of the criticality function, F, is illustrated in Figure 2-14.

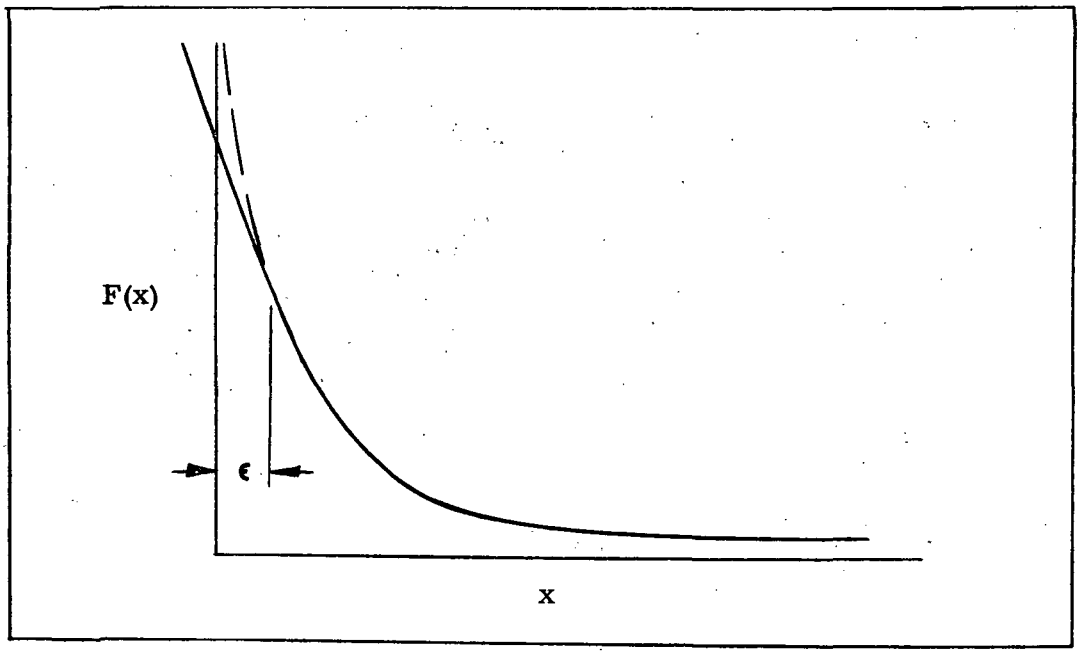

Figure 2-14. Criticality Function

There are a number of techniques available to minimize P, the method used by APAS is the Fletcher-Powell-Davidon unconstrained minimization technique (Ref. 14). P is the objective function and $[t_2, b_1, b_2]$ is the design variable vector for the example problem. Optimization is performed on each element of the cross section in order to minimize weight.

2.6 STRUCTURAL ELEMENT SYMMETRY GROUPS

A symmetry group is a group of structural elements which have identical designs. When a number of structural elements are placed into the same symmetry group only

one design is produced. The design of the element respects all of the margins of safety for all of the elements in the group. This technique provides a means by which fuselage centerplane symmetry can be respected without duplicating reversible loading conditions. It is often desirable to make adjacent panel elements identical for ease in manufacturing. This can be accomplished with symmetry grouping also. Since the use of symmetry groups reduces the number of independent design variables of the structure it can be of significant use in reducing execution time and should be employed wherever possible.

2.7 STRUCTURAL ANALYSIS

This section presents the techniques used to calculate the applied stresses, including the fatigue stress spectrum and the methods used to calculate margins of safety for static strength, fatigue, flaw growth, and residual strength criteria.

2.7.1 INTERNAL LOADS ANALYSIS. The internal loads analysis is based on classical box beam theory (Ref. 13). The assumptions made are; plane sections remain plane under the action of bending moments and axial loads, cross sections are free to warp when torque is applied, and the structure obeys a linear elastic stress-strain law.

2.7.1.1 Axial Stress. The axial stresses are made up of stresses due to axial loads and stresses due to bending moments. The equation used to calculate the axial stresses is,

$$\sigma = \frac{M_x I_{xz} - M_z I_{xx}}{I_{xx} I_{zz} - I_{xz}^2}(x-\bar{x}) + \frac{M_z I_{xz} - M_x I_{zz}}{I_{xx} I_{zz} - I_{xz}^2}(z-\bar{z}) + \frac{P}{A}$$

where,

M_x = Net bending moment about a horizontal axis passing through the centroid

M_z = Net bending moment about a vertical axis passing through the centroid

P = Axial load

x, z = Coordinates of the element, see Figure 2-15

$\bar{x}, \bar{z}$ = Coordinates of the centroid, see Figure 2-15

$I_{xz}, I_{xx}, I_{zz}, A$ = Section properties, see Section 2.7.2.

2.7.1.2 Shear Stresses. The shear stresses resist the external shear forces and the torque applied to the section. Under the basic assumptions the shear flow is calculated using a VQ/I distribution for the shear forces. The resultant applied torsion is due to the applied torque, TOR, and the couples resulting from shifting the shear forces XS and ZS to the shear center. This net torsion is resisted internally by a shear flow which is distributed according to a T/2A distribution. In the case of multiple cell structures, such as multi-spar wings, the cells are assumed to have equal twisting angles. For a further description of the method see Paragraph 17.9 thru 17.11 of Reference 19.

2.7.2 SECTION PROPERTIES. Section properties of the cross section of the wing or fuselage are calculated at each station where structural sizing is performed. These properties are used to calculate the internal loads distribution and to provide stiffness information. In order to simplify the calculation of section properties the following assumptions are made; (1) the material which resists bending moments is assumed to be smeared uniformly between nodal points, (2) only the skin and shear webs are effective for resisting shear loads and torsion. The following equations are used to calculate section properties, (see Figure 2-15).

$$A = \int da$$

$$\bar{x} = \frac{1}{A} \int x\,da$$

$$\bar{z} = \frac{1}{A} \int z\,da$$

$$I_{xx} = \int z^2 da - A \cdot \bar{z}^2$$

$$I_{zz} = \int x^2 da - A \cdot \bar{x}^2$$

$$I_{xz} = \int xz\,da - A \cdot \bar{x} \cdot \bar{z}$$

$$J = 4A_T^2 / \oint ds/t$$

where,

x, z are the coordinates of the incremental area da

A is the total area of the cross-sectional material

$\bar{x}, \bar{z}$ are the coordinates of the centroid of A

I_{xx} is the moment of inertia of A taken about an x axis passing through the centroid

I_{zz} is the moment of inertia of A taken about a z axis passing through the centroid

I_{xz} is the product of inertia of A with respect to the centroid

J is the tortional stiffness constant

A_T area enclosed by the cross section

ds incremental distance along the box contour

t thickness of the shear resisting material associated with ds

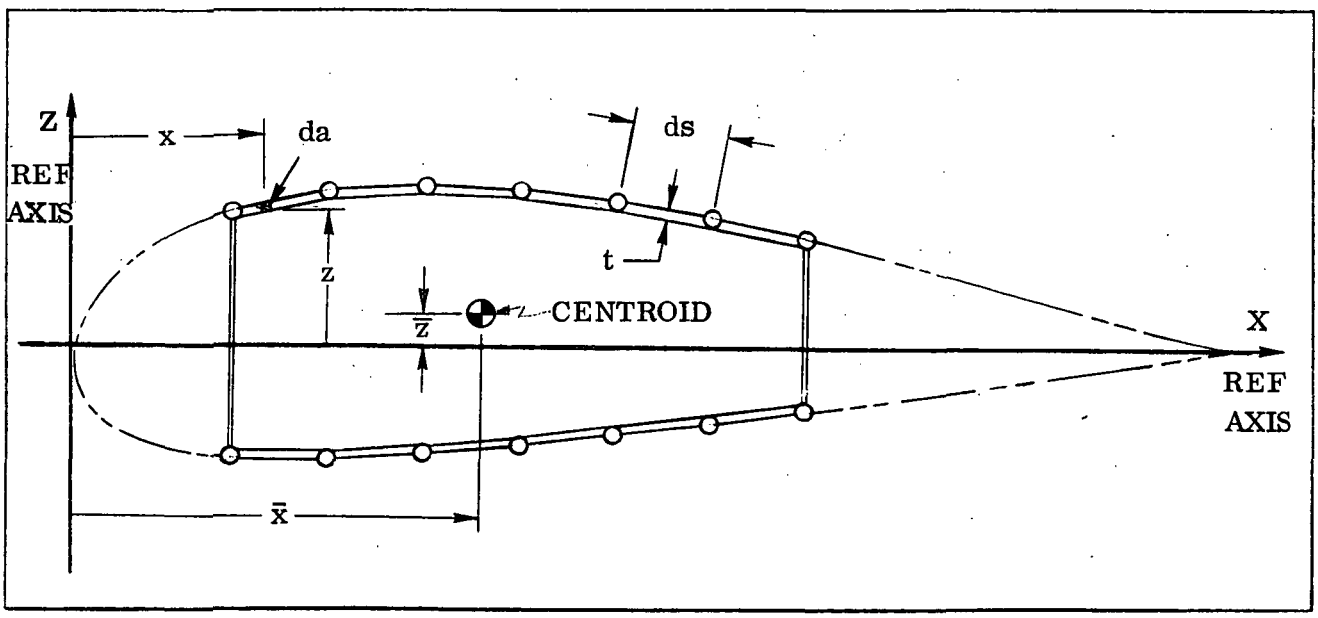

Figure 2-15. Typical Wing Section

2.7.3 STATIC STRENGTH ANALYSIS. The static strength analysis consists of calculating margins of safety for a number of failure modes. The failure modes are listed in Table 2-4. The analysis procedures are taken from Reference 13 . Simplifying assumptions are made regarding the buckling coefficients used for calculating local buckling stresses. Buckling coefficients for long narrow plates with simply supported edges or one long edge free and the others simply supported are used. The general instability of panel elements is checked using wide column analysis and assumes simple supports at ribs or frames. For multi-spar construction using thick plates or sandwich elements an orthotropic panel general instability analysis is made. The panel is checked for general buckling due to inplane loading, the lowest buckling load obtained from any combination of up to five half waves in each direction is used. The depth of analysis is generally consistent with typical predesign stress analysis.

Table 2-4. Panel Element Failure Modes

FAILURE MODE	PANEL CONSTRUCTION TYPE (See Fig. 2-3)											
	1	2	3	4	5	6	7	8	9	10	11	12
Local Buckling	•	•	•	•	•	•	•	•	•			
Crippling	•	•	•	•	•	•	•	•	•			
Inter-Rivet Buckling				•	•	•	•	•	•			
Panel General Instability										•	•	•
Wide Column Buckling	•	•	•	•	•	•	•	•	•			
General Yielding	•	•	•	•	•	•	•	•	•	•	•	
Maximum Shear Stress	•	•	•	•	•	•	•	•	•	•	•	
Von Mises Equivalent Stress	•	•	•	•	•	•	•	•	•	•	•	
Maximum Fiber Strain in a Laminate												•
Diagonal Tension	•	•	•	•	•	•	•	•	•			
Shear Buckling	•	•	•	•	•	•	•	•	•	•	•	•

Margins of safety for the critical failure modes for each element and load condition are output. The margins of safety are calculated using standard interaction formula and are estimates of the additional load carrying capability of the element for each loading condition. See Section 3 of Reference 20.

2.7.4 FATIGUE STRESS SPECTRUM. The fatigue stress spectrum is based on the flight profile and load spectrum discussed in Section 2.3. It is made up of a group of minimum and maximum stresses and the number of applications expected during the design life. This spectrum is used for the fatigue analysis and the flaw growth analysis of the element discussed in this section.

Minimum and maximum stresses are calculated for each subsegment of the fatigue spectrum (see Table 2-2). These stresses are calculated from the segment constant stress σ_c and the segment alternating stress σ_a.

$$\sigma_{min} = \sigma_c - \Delta g \cdot \sigma_a$$

$$\sigma_{max} = \sigma_c + \Delta g \cdot \sigma_a$$

The value of σ_c and σ_a are in general different for each segment and are calculated by forming linear combinations of the stress due to the fatigue spectrum conditions (see Table 2-3).

$$\sigma_{cj} = \sum_{i=1}^{6} c_{ij} \sigma_i$$

$$\sigma_{aj} = \sum_{i=1}^{6} a_{ij} \sigma_i$$

where i denotes the fatigue spectrum condition number and j denotes the segment number. The constants c_{ij} and a_{ij} are based on the flight profile (See Table 2-1) and are stored within the program.

The ground-air-ground (G-A-G) cycle shown in Figure 2-16 is not defined in Section 2.3. It dominates fatigue damage and flaw growth in many areas of the structure of transport aircraft. This stress excursion is due in part to the difference between the groundborn load distribution and the airborn distribution, and in part to cabin pressurization. A G-A-G spectrum is calculated automatically within the program at each analysis point. The G-A-G cycle is defined as the maximum stress excursion between the peak inflight stress (i.e. the maximum gust occurring in that flight) and the peak/valley groundborn stress (i.e. the maximum taxi Δg). Several high peaks of cyclic loads,

such as those due to gust encounters in stormy weather, tend to occur on the same flight. It would therefore be conservative to use all peak loads expected in the total aircraft life in building the G-A-G spectrum. To avoid this over conservatism a frequency factor is introduced which has the effect of skipping over some of the peak loads. A frequency factor equal to two is considered appropriate for transport aircraft. Thus, every other peak is included in the G-A-G spectrum. Frequency factor is a user input.

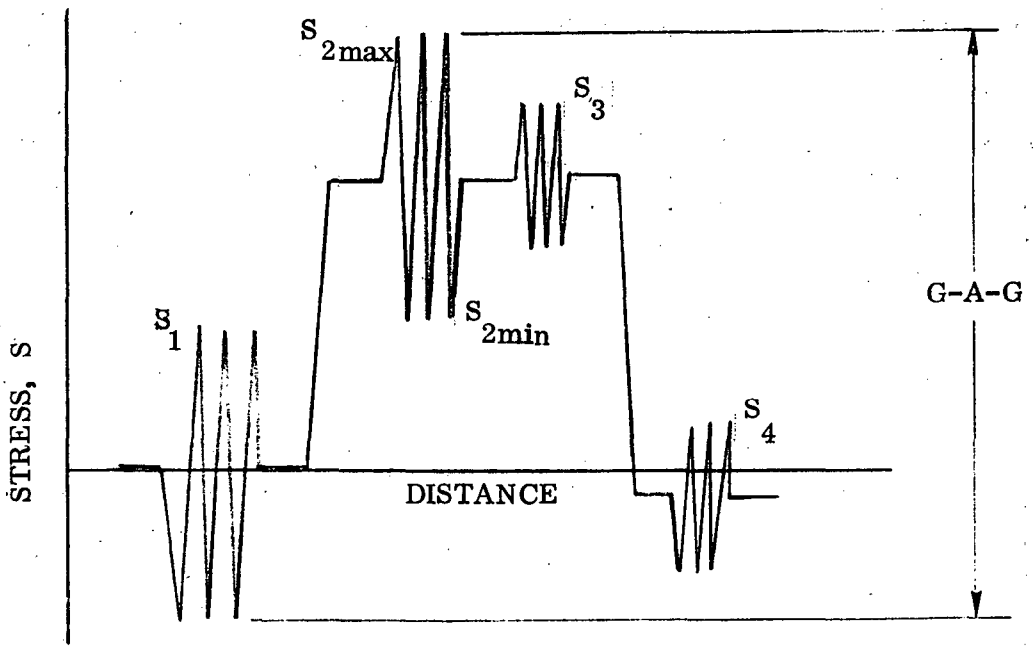

Figure 2-16. Simplified Flight Profile

A unique stress spectrum is generated for each structural element based on the local stress history and is used for the fatigue analysis and flaw growth analysis also reported in this section. No provision is currently available for changing the load profile, however additional load spectra can be incorporated into the existing program with very little programming effort.

2.7.5 FATIGUE ANALYSIS. Fatigue damage is defined as the ratio of the number of applied stress cycles, n, of a given stress magnitude to the number of allowable stress cycles, N, of the same stress magnitude. Miner's Rule (Ref. 16) is the basis of fatigue damage analysis performed within the program. Under this concept

fatigue damage is assumed to be linearly cumulative, and fatigue failure is assumed to occur when the damage summation equals unity.

$$\text{Fatigue Damage} = \frac{n_1}{N_1} + \frac{n_2}{N_2} + \frac{n_3}{N_3} + \cdots \frac{n_m}{N_m}$$

$$\text{Fatigue Failure} = \sum_{i=1}^{m} \frac{n_i}{N_i} = 1$$

To facilitate the analysis, S-N curves are plotted from test data for several values of stress ratio, R. Allowable cycles for each subsegment are read from the curves as shown in Figure 2-17.

where, $R = \frac{S_{min}}{S_{max}}$ (Also see Figure 2-16)

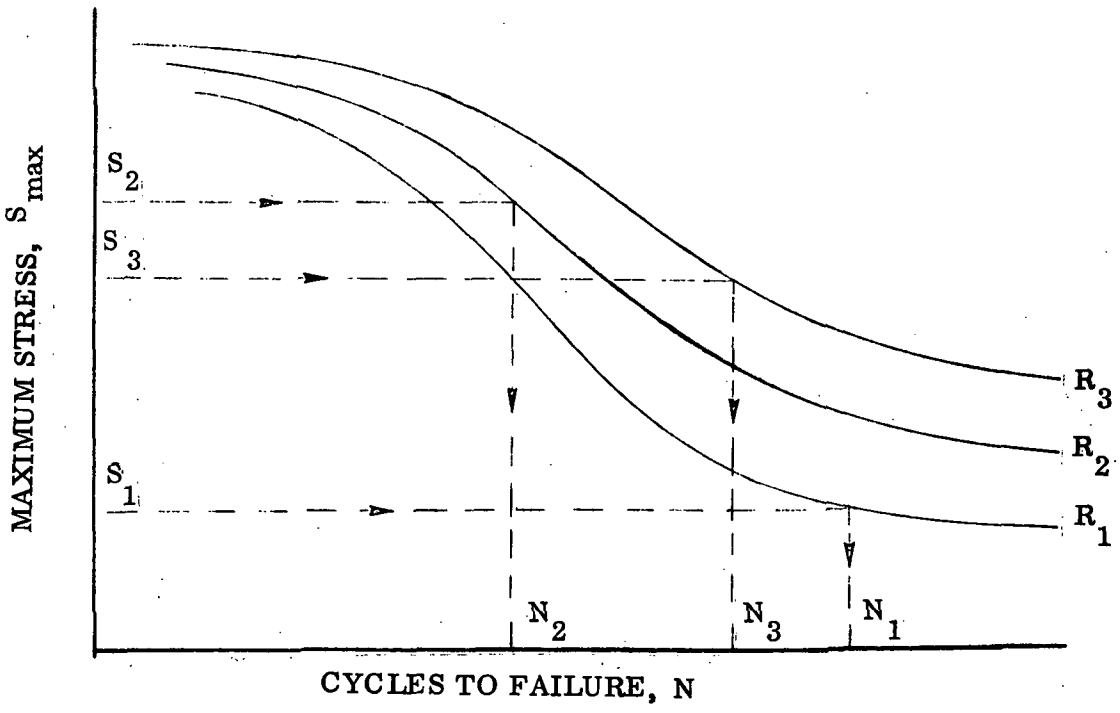

Figure 2-17. Fatigue Damage Determination

A review of previous General Dynamics programs and other sources did not produce nearly enough component S-N data to fill the required data bank indicated by Table 2-5. Much of the data reviewed was generated for specific configurations and load spectra. Manufacturers usually test splices and other fatigue critical details but seldom develop S-N curves for typical structure and spectra. Even less data is published because component test results are frequently considered proprietary or sensitive to a particular project.

Table 2-5. Availability of Fatigue Data

Material	Fabrication Method	Wing Box	Fuselage	General Structure	Coupon S-N
Aluminum	Riveted	◒	◒	●	
	Integral	◒	○	◒	●
	Bonded	○	○	○	
	Welded	○	○	○	
Titanium	Riveted	○	○	○	
	Integral	◒	○	◒	●
	Bonded	○	○	○	
	Welded	○	○	○	
Graphite/ Epoxy	Riveted	○	○	○	
	Integral	○	○	○	◒
	Bonded	○	○	○	
Boron/ Epoxy	Riveted	○	○	◒	
	Integral	○	○	○	◒
	Bonded	○	○	◒	

○ = No data
● = Complete data

In some cases the component data was incomplete. To facilitate extrapolation, curves of stress vs. stress ratio at constant cycle values were plotted from the original data. Expanded S-N curves were then drawn based on the extrapolated data. For the many cases where component data was not available, reduction factors were applied to un-notched coupon data for the appropriate material. A complete set of data was generated by this method. However, S-N curves plotted from this data did not show the trends and consistency expected. Anomalies in the component data due to inconsistent test parameters were still present in the expanded S-N curves. A complete and consistent set of S-N curves for all required component types could not be obtained with this approach.

Subsequently, a second method, Reference 15, for plotting S-N curves from limited data was employed. This procedure utilizes two Hewlett-Packard 9100B computer programs to curve fit and plot data. More reliance is placed on un-notched coupon data, and component fatigue strength factors are plotted versus life to ensure that smooth and consistent S-N curves are generated. All of the S-N curves shown in Appendix A were generated by this method. The Reference 15 procedure is presented in Appendix B for convenience.

Data from constant life cuts of these curves is stored in the program. An interpolation routine is used in the program to retrieve allowable cycles from the stored data.

This rather simple approach is widely used in fatigue life predictions of transport aircraft. The more severe load spectra of fighter type aircraft produce more significant residual stresses at points of stress concentration and may warrant a more sophisticated analytical treatment.

2.7.6 FLAW GROWTH ANALYSIS. This section presents the flaw growth analysis used in the VDEP II Program. The flaw growth analysis predicts how a crack grows under the influence of a fatigue load spectrum. The growth analysis is based on an integration technique developed under this contract. The technique currently used is conservative, making no provision for growth retardation effects due to spectrum loading.

Crack growth predictions are usually based on the integration of empirical growth rate laws. The integration techniques range from simple cycle by cycle summations to more sophisticated techniques involving high powered numerical methods. Cyclic growth rate equations are usually expressed as functions of the stress intensity factor range, ΔK, the cyclic stress ratio, R, and certain empirical constants determined from tests data.

$$\frac{da}{dN} = F\ (\Delta K\ ,\ R,\ \text{empirical constants})$$

where $\frac{da}{dN}$ is the cyclic growth rate.

The stress intensity factor range, ΔK, is a measure of the change in the intensity of the stress field near the tip of the crack, (see Figure 2-18).

$$\Delta K = \lambda\,(a)\,\Delta\sigma\sqrt{\pi\, a} = K_{max} - K_{min}$$

where,

$\Delta\sigma$ range of the remotely applied cyclic stress

a half crack length

$\lambda(a)$ correction factor which accounts for geometric effects

The amount of growth, Δa, which occurs during one cycle of applied stress can be predicted using a growth rate equation, i.e.,

$$\Delta a = f(\Delta K, R, \text{empirical constants})$$

After a load cycle is applied the new crack length is longer by Δa at each tip. The ΔK calculated for the next load cycle is then based on the new crack size. Crack growth can in this way be predicted for cyclic loading. This process is cumbersome if the number of load cycles is very large.

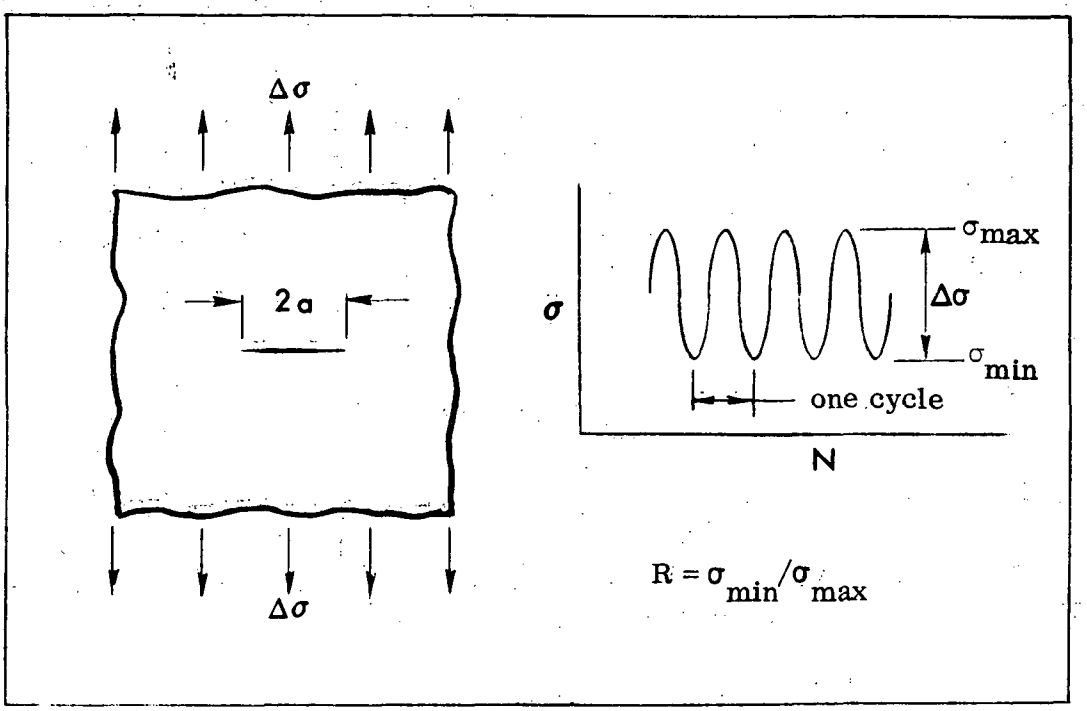

Figure 2-18. Fatigue Crack Loading

Crack growth analysis of transport aircraft often involves millions of cycles of applied loads during service life. Computer routines written to predict flaw growth based on the method just described were found to be too slow to use for this program. A technique based on averaging the cyclic growth rates during a flight and then performing the integration on a flight by flight basis was developed. A curve of average flight crack growth rate da/dF versus crack length is obtained for the specific crack geometry and load spectrum. Such a curve is obtained by summing the growth rates due to each of the load cycles in the spectrum and then dividing by the number of flights represented by the spectrum. By performing this process at various crack sizes a curve can be constructed as shown in Figure 2-19.

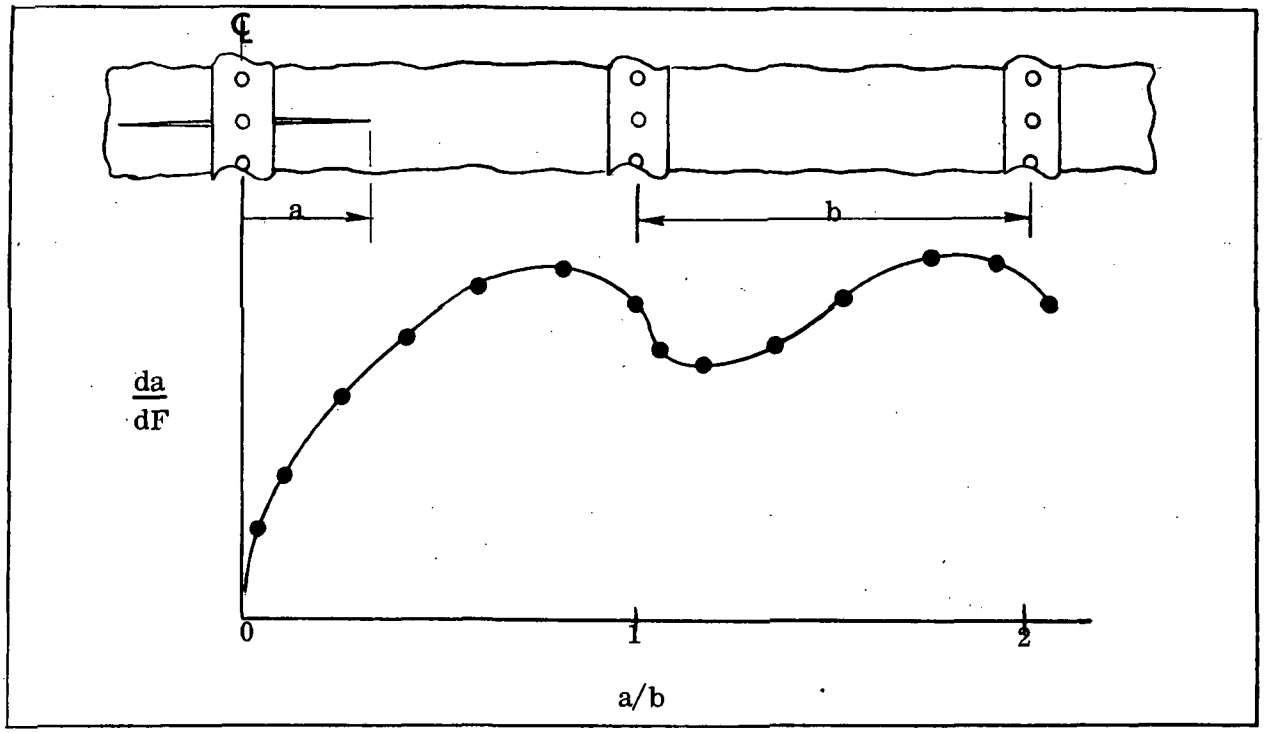

Figure 2-19. Flight by Flight Growth Rate

The inverse of this curve, i.e. dF/da, is integrated numerically over the desired crack interval. A technique based on the Erdogan growth rate equation was developed in order to simplify and automate the procedure needed to generate the da/dF curves.

Erdogan growth rate equation:

$$\frac{da}{dN} = CK_{max}^{m} \Delta K^{p} \qquad (2.7\text{-}1)$$

where C, m, and p are empirical constants determined from constant amplitude crack growth tests.

Since $K_{max} = \frac{\Delta K}{1-R}$

$$\frac{da}{dN} = \frac{C(\Delta K)^{m+p}}{(1-R)^{m}} \tag{2.7-2}$$

The average flight growth rate at any crack size a is then,

$$\frac{da}{dF} = \frac{1}{M} \sum_{i=1}^{N_s} C \frac{(\Delta K_i)^{m+p}}{(1-R_i)^{m}} \tag{2.7-3}$$

where,

$$\Delta K_i = \lambda(a)\, \Delta\sigma_i \sqrt{\pi a} \tag{2.7-4}$$

$$R_i = \sigma_{min_i} / \sigma_{max_i} \tag{2.7-5}$$

$$\Delta\sigma_i = \sigma_{max_i} - \sigma_{min_i} \tag{2.7-6}$$

N_s = Total number of cycles contained in the spectrum.

M = Number of flights represented by the spectrum.

Rewriting Equation 2.7-3, assuming the change in a to be small in N_s cycles.

$$\frac{da}{dF} = C\left(\lambda(a)\sqrt{\pi a}\right)^{m+p} \cdot \frac{1}{M} \sum_{i=1}^{N} \frac{(\Delta\sigma_i)^{m+p}}{(1-R_i)^{m}} \tag{2.7-7}$$

Now define $\bar{\sigma}$ as

$$\bar{\sigma} \equiv \left[\frac{1}{N_s} \sum_{i=1}^{N_s} \frac{(\Delta\sigma_i)^{m+p}}{(1-R_i)^{m}}\right]^{\frac{1}{m+p}} \tag{2.7-8}$$

The application of N/M cycles of $\bar{\sigma}$ with an R value of 0, will produce the growth which is equivalent to the growth caused by the actual load cycles of an average flight.

$$\frac{da}{dF} = \frac{N_s}{M} C \left[\lambda(a) \bar{\sigma} \sqrt{\pi a} \right]^{m+p} \tag{2.7-9}$$

The number of flights required to grow a crack from a_i to a_{i+1} can be found by solving the differential equation. Equation 2.7-9 is separable and can be written in integral form as shown by Equation 2.7-10.

$$\Delta F = \frac{M}{N_s C \bar{\sigma}^{m+p}} \int_{a_i}^{a_{i+1}} \frac{da}{[\lambda(a)\sqrt{\pi a}]^{m+p}} \tag{2.7-10}$$

The closed form solution to Equation 2.7-10 can become exceedingly complex and perhaps impossible depending on the form of $\lambda(a)$. The simplest form of $\lambda(a)$ which is useful leads to the following choice.

$$\lambda(a) = \lambda_o + \lambda_i a \tag{2.7-11}$$

Even with this simple form, the closed form of the solution is not practical. Numerical integration techniques must be applied to find the solution. Since $\lambda(a)$ has been chosen to be linear in a, the following form of Equation 2.7-9 can be written.

$$\Delta F = \frac{M}{N_s C [\bar{\sigma} \lambda(a^*)]^{m+p}} \int_{a_i}^{a_{i+1}} \frac{da}{(\sqrt{\pi a})^{m+p}} \tag{2.7-12}$$

where

$$a_i \leq a^* \leq a_{i+1}$$

Performing the integration in Equation 2.7-12 leads to the following solution.

$$\Delta F = \frac{2M}{N_s \cdot C [\bar{\sigma} \lambda(a^*)]^{m+p} \cdot (m+p-2)} \left[a_i^{(2-m-p)/2} - a_{i+1}^{(2-m-p)/2} \right] \tag{2.7-13}$$

where

$$m + p \neq 2$$

The error of integration introduced is dependent on the selection of a*. If a* is chosen to be equal to a_i then the error is

$$E = \left| \left[\frac{\lambda(a^*)}{\lambda(a_i)} \right]^{m+p} - 1 \right| \tag{2.7-14}$$

Since ($a_i \leq a^* \leq a_{i+1}$) the maximum possible error is introduced when $a^* = a_{i+1}$.

$$E_{max} = \left| \left[\frac{\lambda(a_{i+1})}{\lambda(a_i)} \right]^{m+p} - 1 \right| \tag{2.7-15}$$

The greatest potential error can be limited to some prescribed error $E^* > 0$ by proper selection of a_{i+1}.

$$\left| \left[\frac{\lambda_o + \lambda_1 \cdot a_{i+1}}{\lambda_o + \lambda_1 \cdot a_i} \right]^{m+p} - 1 \right| < E^* \tag{2.7-16}$$

An operator H is introduced so that the absolute value bars can be removed.

$$\frac{\lambda_o + \lambda_1 \cdot a_{i+1}}{\lambda_o + \lambda_1 \cdot a_i} < (1 + HE^*)^{1/(m+p)} \tag{2.7-17}$$

Where,

$H = 1$ for $\lambda_1 > 0$

$= -1$ for $\lambda_1 < 0$

Solving Equation 2.7-17 for a_{i+1} results in the following

$$a_{i+1} = (HE^* + 1)^{1/(m+p)} \cdot \left[\frac{\lambda_o}{\lambda_1} + a_i \right] - \frac{\lambda_o}{\lambda_1} \tag{2.7-18}$$

where $\lambda_1 \neq 0$

For the case where $\lambda_1 = 0$ the value of a_{i+1} may be set to the largest value of a for which the linear approximation to λ is valid, in which case the integration is exact.

The following equation is used to supply the (λ_o/λ_1) term for values of λ supplied at two crack sizes.

$$\frac{\lambda_o}{\lambda_1} = \frac{\lambda_j \cdot a_{j+1} - \lambda_{j+1} \cdot a_j}{\lambda_{j+1} - \lambda_j} \qquad (2.7\text{-}19)$$

where (a_j, a_{j+1}) is the interval over which the λ function is to be linearized and λ_j and λ_{j+1} are the values of λ at a_j and a_{j+1} respectively.

The foregoing procedure is applicable to any flaw geometry for which the stress intensity correction factors, λ, are known. The program currently contains factors for a wide range of stiffened panels with through cracks. Curves for L(a) and λ(a) for the case of a crack extending equally on both sides of a riveted stiffener (illustrated in Figure 2-20) are stored within the program in the form of data tables. For furthere information concerning the derivation of these curves the reader is referred to Reference 6.

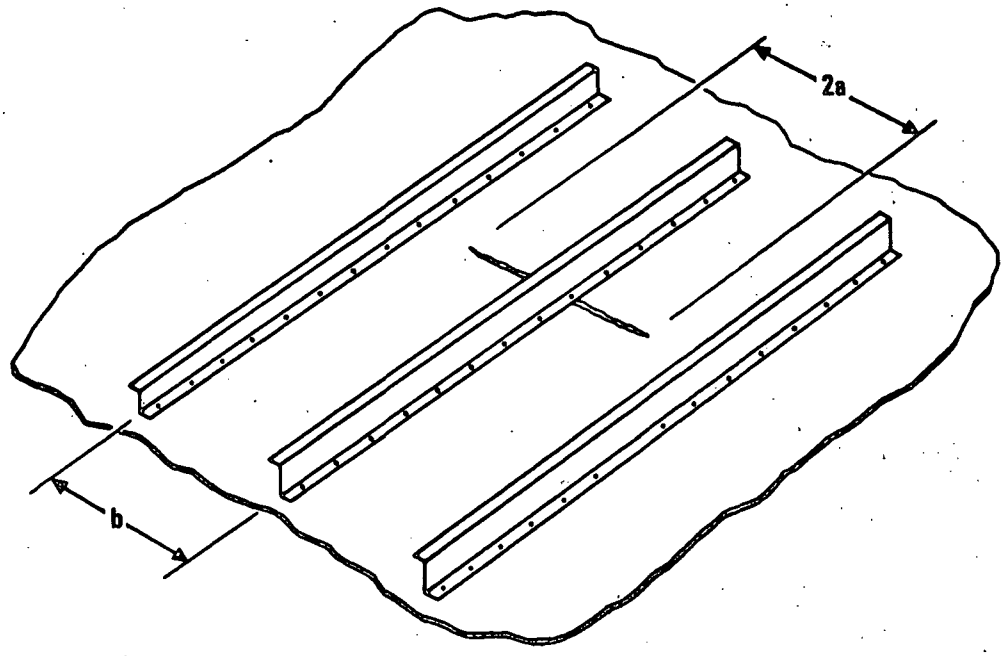

Figure 2-20. Stiffened Panel Crack Geometry

The program currently contains 75 sets of data for L(a) and λ(a) covering a wide range of stiffener spacing and percent stiffening, including cases for broken stiffeners. Figure 2-21 presents a typical set of curves. Linear interpolation is used to determine L(a) and λ(a) curves for cases which lie between data sets. These curves are used for all riveted-stiffener plate combinations, (e.g., panel types 4 through 9 of Figure 2-3).

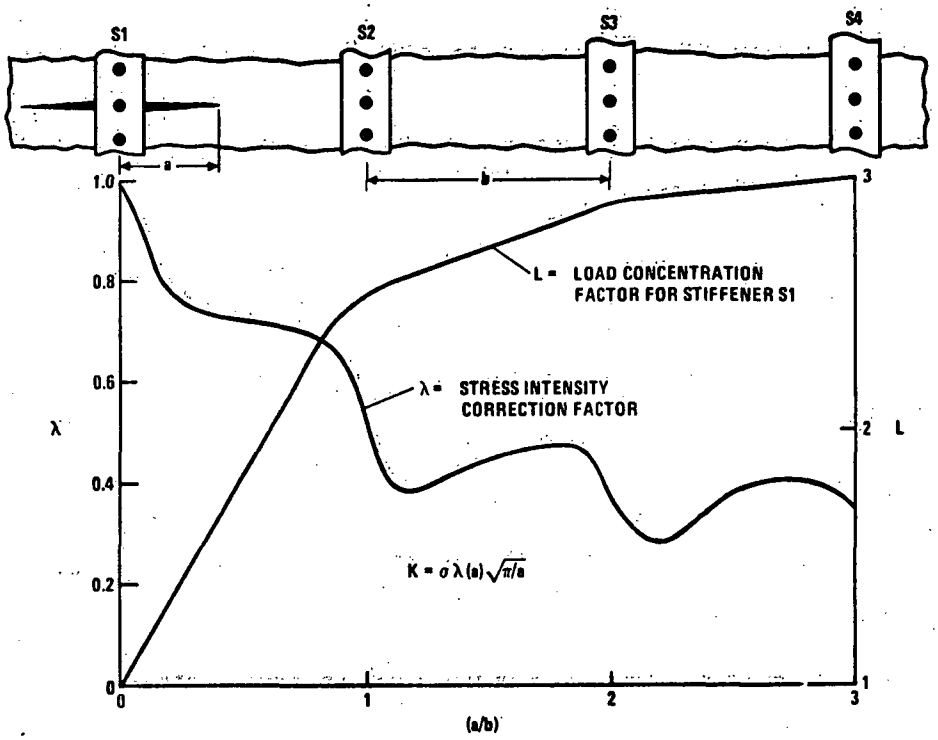

Figure 2-21. Stiffened Panel Stress Intensity Correction Factors

For the case of integral construction (e.g., panel types 1, 2, and 3), the panel is treated as a flat plate without stiffeners with a thickness equal to $\bar{t}$ (i.e., $\lambda(a) = 1.0$).

2.7.7 RESIDUAL STRENGTH ANALYSIS. The residual strength analysis determines the failing strength of a damaged panel. Damage consists of skin cracks and broken stiffeners. The residual strength of a damaged panel is defined as the maximum stress level which can be applied to the panel without the crack growing unstably to failure. Unstable crack growth occurs when the applied stress intensity factor, K, exceeds the fracture toughness of the skin material, K_C.

Unstable crack growth is allowed to occur at stress levels below the residual strength of a panel as long as the crack growth eventually arrests at a larger crack size. Whenever stress level of the most highly loaded stiffener exceeds the ultimate tensile strength of the stiffener, it fails, and the applied stress intensity factors of the skin are recalculated to reflect the broken stiffener.

Figure 2-22 illustrates a typical example of the residual strength analysis procedure. The curves shown are generated by calculating the gross panel stress which causes stiffener failure and the gross panel stress which cause unstable crack growth. Equations 2.7-20 and 2.7-21 are used for these calculations.

$$\sigma_{cr_{(\text{unstable crack growth})}} = \frac{K_C}{\lambda(a)\sqrt{\pi a}} \qquad (2.7\text{-}20)$$

$$\sigma_{cr\ (\text{stiffener failure})} = \frac{F_{tu}}{L(a)} \qquad (2.7\text{-}21)$$

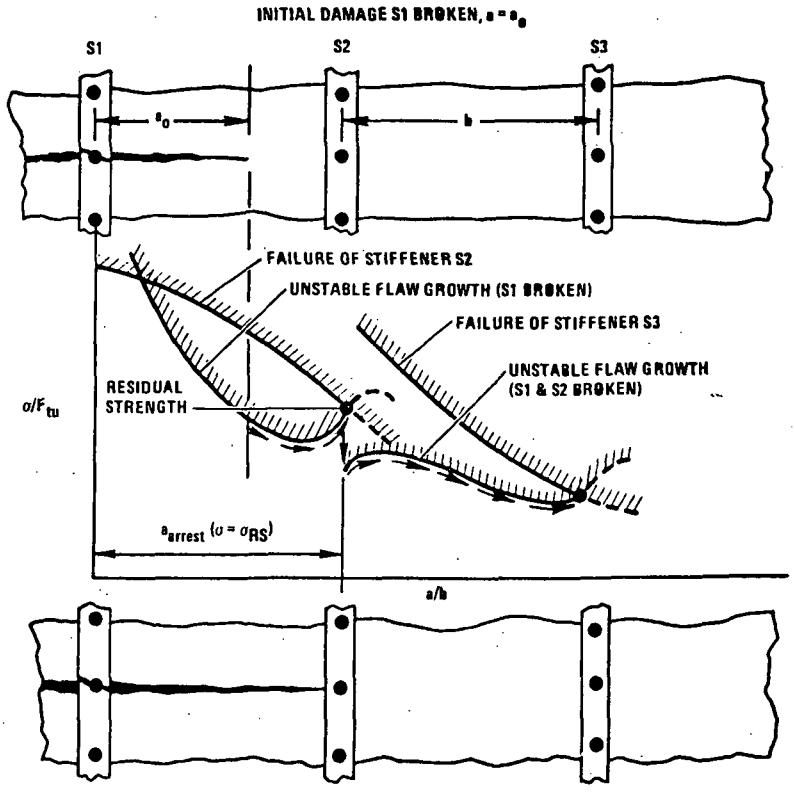

Figure 2-22. Typical Example of Residual Strength Analysis

SECTION 3

PART DEFINITION MODIFICATIONS

During the course of the NASA contract NAS1-11343, methods were developed to predict a generalized detail parts listing based on the output from the structural synthesis analysis. The resultant parts listing provides a complete breakdown of an airframe structure into its most elementary components. This listing of detail parts then represents the basis of a weight and manufacturing cost analysis procedure. As part of this procedure each detail part is looked at individually and analyzed in terms of its weight, cost to manufacture, and cost of material.

A sequence of assembling the detail parts is also modeled. The weight and costs corresponding to each step of the assembly process are included in the computations. Thus, the weight and costs of the complete airframe structure can be obtained by summing the values for the individual parts, and adding in the elements associated with the assembly.

As part of the computer program development tasks a more comprehensive structural synthesis routine, APAS, was substituted for the existing lifting surface synthesis, BOXSIZ. This conversion required changes to the program interfaces with respect to both the preceeding vehicle synthesis routines and the succeeding parts definition routines. As part of this conversion task an effort was made to increase the degree of geometrical consistancy for the components being analyzed in the parts definition routines.

The structural synthesis, both the BOXSIZ and the APAS versions, contain a number of alternative user-selected modes of construction for each of the major components (cover panels, spars, and ribs). Previously, only a single mode of construction existed for each of the components in the parts definition portion of the analysis. As a result of current efforts several additional structural arrangements were made available at the parts definition level. A summary of the various modes of construction currently available is presented in Figure 3-1. The broken lines indicate those areas of analysis performed as part of this study.

Figure 3-1. Summary of Structural Synthesis and Parts Definition Configurations

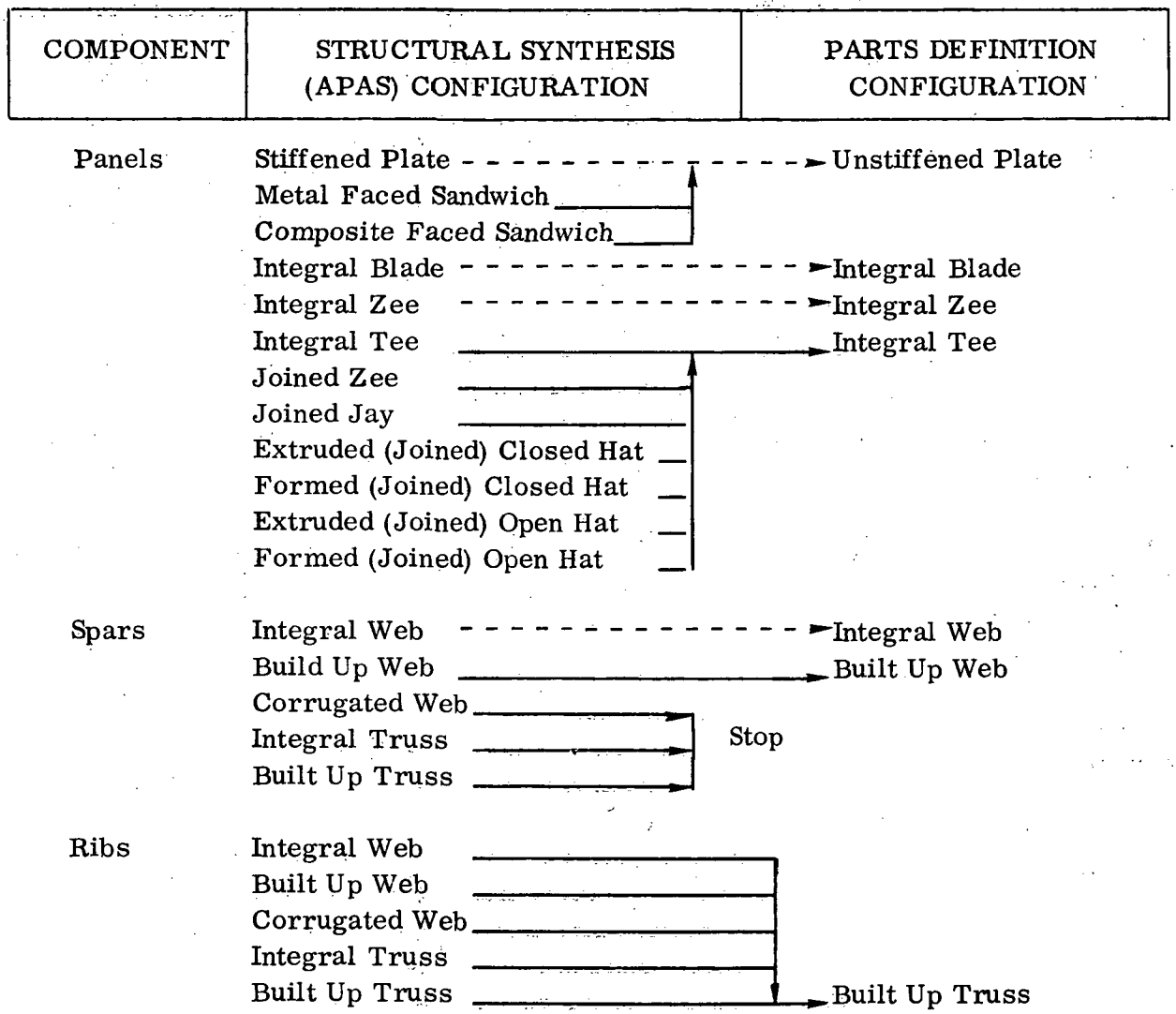

3.1 SKIN PANEL PARTS DEFINITION

As part of the conversion from the BOXSIZ synthesis driver to APAS several new panel configurations were added to the parts definition routines. A summary of the panel concepts currently available in the parts definition is presented in Figure 3-2. Each of the lifting surface cover panels is assumed to be a complete (integral) assembly by itself. There are no other detail parts associated with the panels at this stage. Subassembly operations accounted for in the panel analysis are the spanwise and chordwise panel splices. Assembly of the complete box structure, as illustrated in Figure 3-3, is accounted for in later portions of the parts definition process.

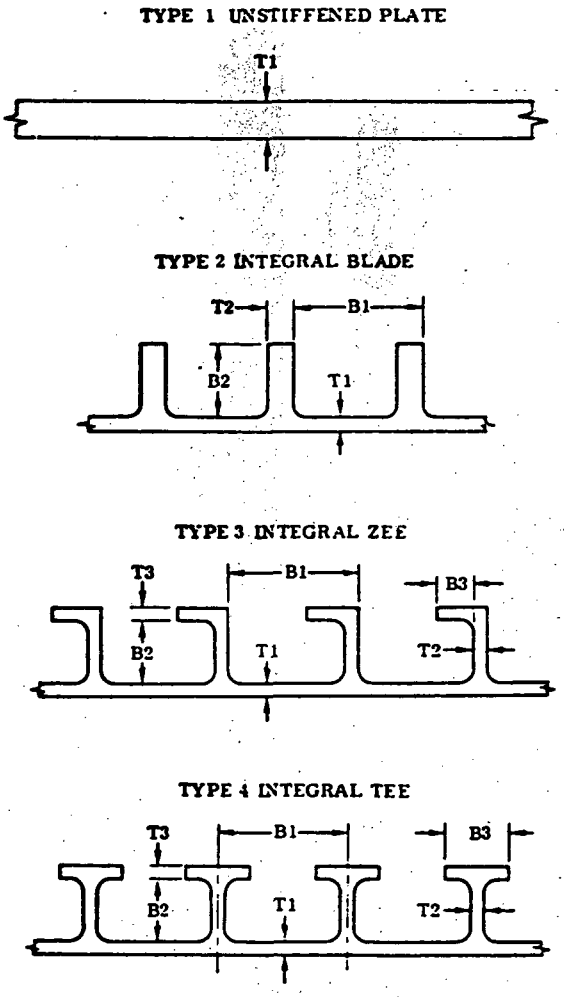

FIGURE 3-2. LIFTING SURFACE COVER PANEL OPTIONS FOR THE PARTS DEFINITION

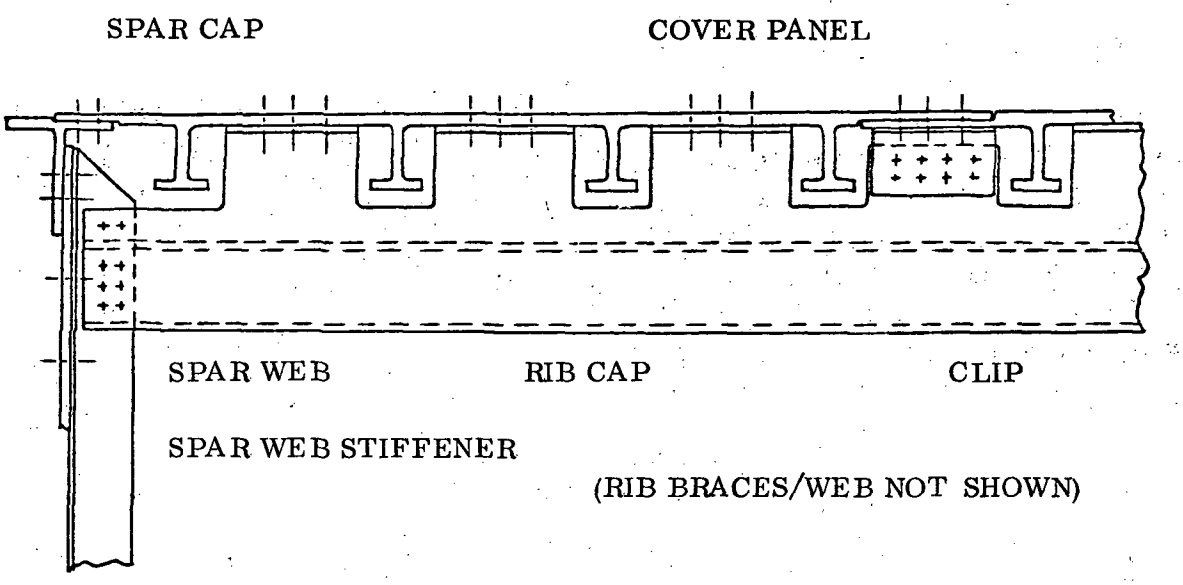

FIGURE 3-3. TYPICAL MODE OF ATTACHMENT FOR A LIFTING SURFACE COVER PANEL.

Input to the panel parts definition routine includes variables from both the lifting surface geometry and the structural synthesis routine. Input from the structural synthesis process is comprised of panel cross section dimensions of each control station. Additional input from the geometry routine includes the number and location of the control stations, and the number of control station nodes. User supplied input accounts for specifying a panel type with an option for also defining a maximum allowable panel length.

As part of the parts definition process the semi-span is divided into a number of constant length panels. In the absence of a user specified panel length, a maximum length of 10.06 m is assumed. Panel widths are assumed to be defined by the node locations, which in turn are defined in the lifting surface geometry routine. A constant number of panels are assumed across the surface in both a spanwise and a chordwise direction.

Panel cross section dimensional data is computed at the actual panel endpoints by a linear interpolation of the geometry at adjacent control stations. The reference geometry of a typical panel in terms of the program Fortran variables is illustrated in Figure 3-4. Corresponding detailed dimensions for the various panel types are presented in Figure 3-2. The panels are assumed to be spliced, using an overlap joint, in both the spanwise and chordwise directions, to form a complete cover ready for attachment to a spar and rib box structure.

Panel weights are computed at three different levels of consideration. A theoretical weight, OPWT, is computed directly from the output of the structural synthesis routines. The theoretical weight is the weight of the basic, idealized structural element. It represents an optimum value that is based on geometry of a component sized simply for load carrying capability. Real world manufacturing and assembly constraints are not considered. Typical features not accounted for are: flanges to serve as attachment points, clearance allowances, material widths for edge distance requirements, joint load path continuity, etc.

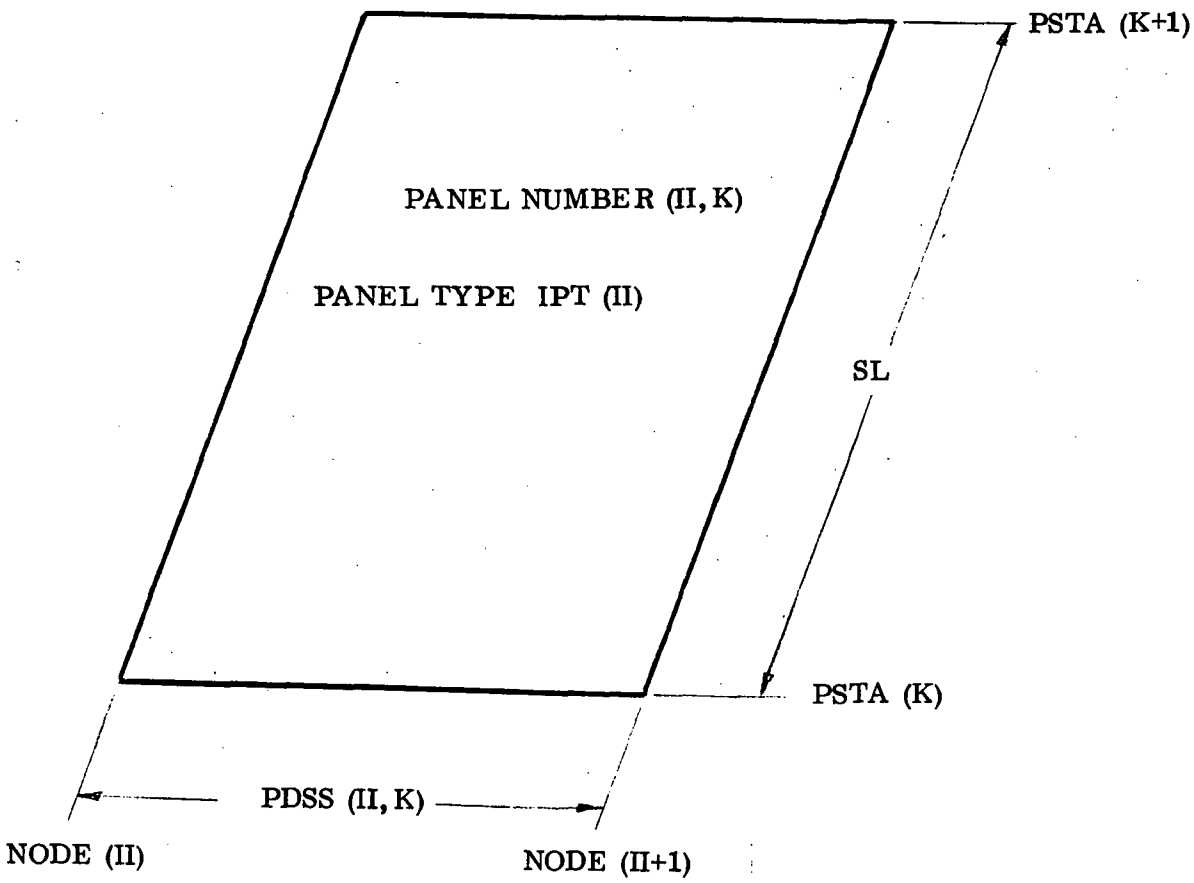

FIGURE 3-4. TYPICAL LIFTING SURFACE PANEL ARRANGEMENT WITH CORRESPONDING FORTRAN VARIABLES.

The actual weight, ACWT, reflects the actual weight of the finished part. It is computed based on the actual geometry of the finished part, and accounts for all design, manufacturing, and assembly considerations that would normally go into producing a real part. The material purchase weight, MAWT, is the weight of raw material stock that must be purchased in order to be able to manufacture a part of actual weight, ACWT. Calculation of the material purchase weight uses the same terms as the actual weight but includes allowances for material removed during manufacturing. Losses occurring between the time the material is purchased and its being utilized to produce a useful part (including losses due to design changes, part duplication, spoilage, waste, overbuy, etc.) are accounted for in the cost analysis portion of the program. Actual manufacturing operations which result in the loss of material include the initial material cut off from the raw stock, initial cutting to size, trimming, milling, turning, drilling, etc. Figure 3-5 illustrates the difference due to fabrication in actual and material purchase weights for the cover panel arrangements which are available.

The general form of the equation used to compute cover panel weight is:

$$\text{weight} = \frac{\text{panel length}}{6} * (\text{area}_1 + \text{area}_2 + 4 * \text{area}_{12}) * \text{density}$$

where area_1 and area_2 are the cross sectional areas at the panel ends, and area_{12} is the cross sectional area at the panel midpoint. The panel midpoint dimensional data needed to compute area_{12} is obtained by a linear interpolation of dimensional data at the panel ends.

The optimum weight for each panel is computed utilizing the dimensions output from the structural synthesis routines directly. The actual weight computation utilizes the dimensions output by the structural synthesis with extra allowances made for manufacturing and assembly clearance requirements, edge distance requirements, flange widths for attachment, fillets, standard and minimum gages, etc. For the current cases involving integrally machined cover panels a minimum gage of .081 cm is assumed for the outer skin portions of the panel which are to be riveted during assembly. Minimum gage for the remaining portions of the panel are specified by the user and are accounted for in the structural synthesis. For the unstiffened plate configuration the thickness of the skin is increased to the nearest standard material stock gage. Because the panels are integrally machined, there are no stiffener attachment flange width requirements or fastener edge distance requirements during assembly to consider. Fillets with a .635 cm radius are added to the stiffener corners.

Material purchase weights are computed based on an assumed raw material stock form of either flat plate or extruded flat plate. Constant dimensions are assumed for the raw material stock. The actual cover panel is assumed to be machined from the raw material stock with skin thickness and stiffener dimensions corresponding to the varied load conditions occurring on different parts of the surface. A constant (linear) rate of taper of panel dimensions is assumed between panel endpoints. Weight of the purchased raw material is computed by using the dimensions of the center,

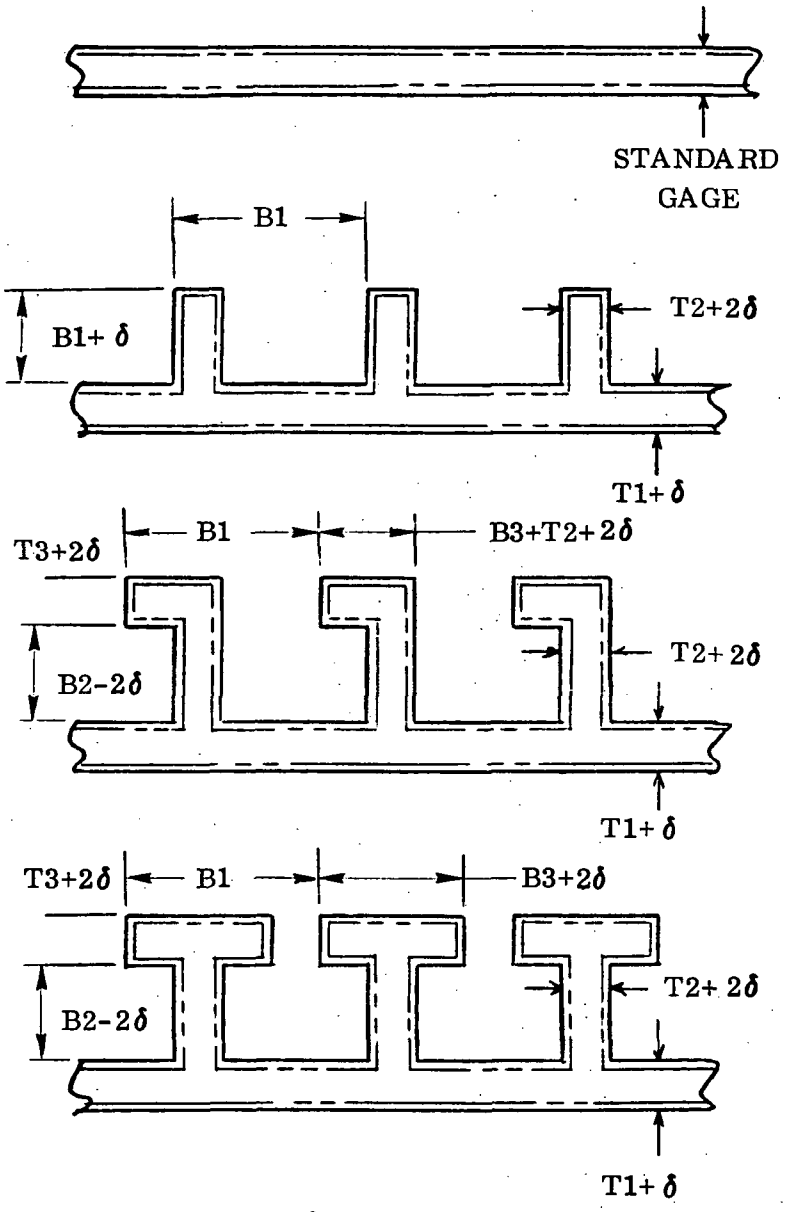

δ = .25 cm

FIGURE 3-5. PURCHASED MATERIAL FORMS FOR LIFTING SURFACE COVER PANEL.

root panel, and adding an allowance to account for machining losses. A single size of raw material stock is assumed for each surface and all panels for that surface are assumed to be machined from this. The assumed raw material forms are illustrated in Figure 3-5.

The next step in the analysis procedure is a manufacturing cost computation. For each detail part defined by the parts definition process, a corresponding sequence of manufacturing operations is automatically specified. This list represents those processes which are required to produce the part in the shop. Each process is represented by an equation from which a calculation is made to determine the number of labor hours required for that process during production of the part. These hours plus corresponding labor rates, overhead rates, and efficiencies form the basis of determining manufacturing cost.

No additions were made to this portion of the program during the current effort. However, the existing analysis encompasses the fabrication of integral tee cover panel configurations, and is reasonably accurate for interim use with the remaining three panel configurations. It is recommended that future refinements to the program include not only the addition of new structural configuration alternatives, but also an updated and expanded process listing for the concepts currently available.

3.2 SPAR PART DEFINITION

As part of the conversion from BOXSIZ to the APAS synthesis driver, several new spar configurations were added to the parts definition routines. These configurations include integrally machined and builtup spar arrangements, each with either an angle or a tee cap. A summary of spar configurations currently available in the parts definition routine is presented in Figure 3-6.

Input to the spar parts definition routines include variables from both the lifting surface geometry and the structural synthesis routine. Input from the structural synthesis process is comprised of spar cap and web cross section dimensions at each control station. Additional input from the geometry routine includes basic surface geometry, the number and location of the control stations, the number of ribs associated with the surface. User supplied input encompasses the rib and spar types, and the total number of spars. A minimum of two spars, a front and rear, is assumed in the absence of an input. A maximum of five spars are allowed.

The program analyses each spar of a surface individually. The true length of the spar is computed by assuming a structural box extending from airplane centerline to the surface tip, minus 30.48 cm allowed for attachment of a tip cap. No separate carry through structure inside the fuselage shell is accounted for. The spars are assumbed to run along constant percent chord lines, and are divided into a number of segments if necessary to attain the full spar length. Maximum segment length may be input by the user. In the absence of an input integrally machined spars are assumed to have a maximum segment length of 4.115 m and builtup spar segments a maximum length of 8.230 m.

Each spar segment is then analyzed separately. Basic elements comprising the spar segment include the caps, web, web stiffeners, and rib stiffeners. Additional spar parts include splice plates for splicing segments, fittings for attachment of leading and trailing edge components, and assembly fasteners.

The structural synthesis process provides basic dimensions for caps, web, and web stiffeners at each control station. Dimensions for the spar segment cap and web ends are derived by interpolation between adjacent control stations. A constant rate of taper of cap and web dimensions is assumed between segment endpoints. Web stiffener dimensions are assumed constant along the length of the segment, and equal to those dimensions arrived at by interpolation at the inboard end of the segment.

Optimum weights for the caps, webs, and web stiffeners are computed utilizing interpolated structural synthesis dimensions. The general form of equation is the same as that used for the cover panels. The program next adjusts these dimensions to account for actual manufacturing considerations. In particular, flange sizes are checked to

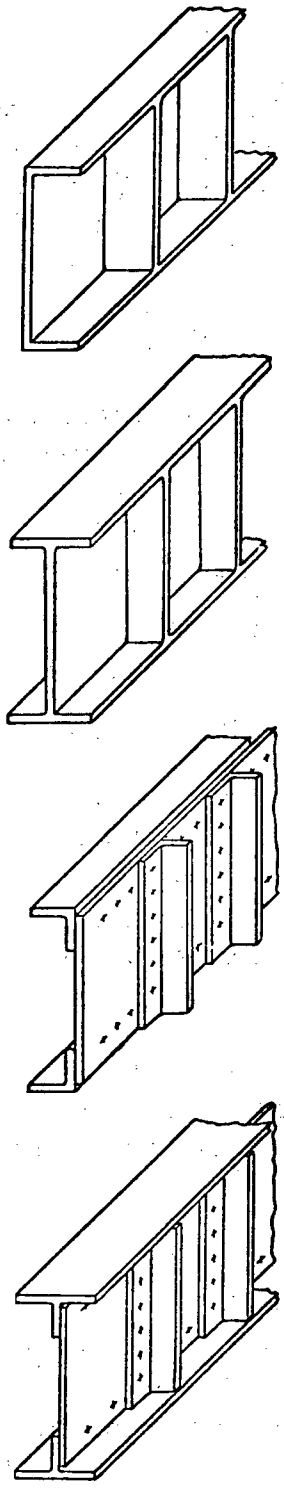

Integral Angle/Integral Blade

Integral Tee/Integral Blade

Joined Angle/Joined Angle

Joined Tee/Joined Angle

Figure 3-6. Summary of the Spar Configurations Currently Available in the Parts Definition Routines

see that they are large enough to allow for proper clearances, edge distances, fastener spacing, etc. The thicknesses of components fabricated from sheet stock are readjusted to the next higher standard material gage, joint overlaps are checked, etc. Actual weights are then computed using the revised dimensions.

Material weight for the integrally machined spar segment are computed by assuming a solid bar of material with dimensions slightly greater than the maximum spar external dimensions to account for cutoff and machining of the segment. The builtup spar is assumed to be comprised of extruded caps, sheet webs, and bentup sheet web stiffeners. Material weights for each of these elements are computed using the actual weight computation dimensions plus allowances for machining, cutoff, etc.

One spar web splice plate is assumed for each spar segment except the last one. Splice plates are sized to fit on the spar web inside the spar cap flanges. The width is derived by assuming a total of four fastener rows across the splice with appropriate clearances, spacing, and edge distances. Thickness is set equal to the spar web thickness. The optimum weight is set equal to the actual weight in this case since the plate is sized initially by functional logic and not the structural synthesis. Material weight is computed by assuming fabrication from flat sheet stock with a thickness equal to the next higher standard sheet gage. Extra length and width of 5.08 cm are added to the actual dimensions to account for initial cutting size.

Rib stiffeners are specified along the spar web at each rib attachment point if the local web stiffener spacing is greater than 30.48 cm. These stiffeners serve as attachment clips for the rib webs and are not utilized if truss type ribs are present. One set of rib stiffeners are specified for external spars, and two sets (one on each side of the spar web) for interior spars.

Rib stiffeners are assumed to be bentup angles with a thickness and riser height equal to those of the web stiffeners. They are sized for an attachment flange width carrying a single row of fasteners. Length is set equal to the web height. Optimum weight is again set equal to the actual weight. Material weight is computed by assuming fabrication from the next higher standard sheet gage. The length and width are increased by 5.08 cm and 2.54 cm respectively, for the material weight computation.

Fittings are specified on the exterior spars for attachment of the leading and trailing edge elements. These fittings attach to spar web stiffeners directly and to the adjacent skin panels through a clip and doubler arrangement. Each machined fitting has associated with it two clips and two doublers.

Fittings are sized on the basis of the local spar height. A generalized fitting design is assumed and the actual weight is computed by deriving dimensions in proportion to the spar height. Appropriate dimensions and attachment flanges are checked for fastener allowances and readjusted if necessary. Optimum weight is again set equal

to the actual weight. Material weight is computed by assuming the fitting to be machined from a block of thick plate. The dimensions of the block are assumed to be those of the maximum fitting dimensions in each direction with an additional (5.08 cm on the length, 2.54 cm on the width, and a 1.27 cm on the thickness.

The two doublers associated with each fitting are assumed to be cut from .160 cm sheet. The length and width are computed as a function of the fitting size with minimum values set for four rows of four fasteners each. Optimum weight is set equal to actual weight. Material weight is computed with an additional 5.08 cm added to the length and width dimensions.

The two clips associated with each fitting are assumed to be short pieces cut from a tee shaped extrusion. The length and riser height are computed as a function of fitting size. The base flange is sized to carry a single row of fasteners along each side of the riser. The thickness of both the base flange and the riser is assumed to be .127 cm. Optimum weight is set equal to actual weight. Material weight is computed by assuming 5.08 cm of additional length plus an allowance for the material removed from the riser.

The total number of assembly fasteners required is computed by summing the number of fasteners necessary to assemble each detail part as it is looked at individually. The following assembly operations are accounted for: attachment of the segment spar caps to the web, splicing the webs to attain a full length spar, attachment of the web and rib stiffeners to the web, attachment of the doublers and clips to the skin panels, and attachment of the fittings. The appropriate assembly operations are bypassed for the case of an integrally machined spar.

No changes were made to the manufacturi ng process listings or to the manufacturing cost analysis portion of the program during this effort. Spar detail parts are assumed to use those process listings previously specified for similar parts. It is recommended that future refinements include the addition of new structural configuration alternatives, but also an updated and expanded process listing for the concepts currently available.

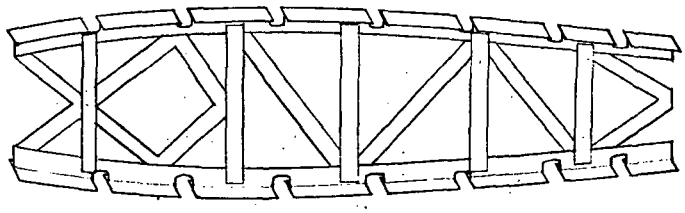

Figure 3-7. Assumed Arrangement of a Builtup Truss Type of Rib

3.3. RIB PART DEFINITION

The existing parts definition routine for ribs was converted from the BOXSIZ synthesis driver to APAS directly without any additions or modifications to the mathematical model. A single rib configuration, a builtup truss, is available in the parts definition. All other rib types available in the structural synthesis revert to a builtup truss rib when the program reaches the parts definition process.

The assumed arrangement of the rib is illustrated in Figure 3-7. Detail parts include *the upper and lower (or left and right) caps, 45 degree angle braces, right angle braces,* skin panel attachment clips, and assembly fasteners. The rib cap is assumed to be comprised of an extruded modified jay section with cutouts to allow for passage of the skin panel spanwise stiffeners. The rib caps are attached directly to the skin panels along the length of the caps except where spanwise skin panel splices occur. Here, clips are specified for attachment of the rib cap to the skin panel. The clips are assumed to be short pieces of extruded angle, and the number of clips associated with each rib is set equal to the number of spanwise panel splices.

The number of angle braces is computed by assuming a brace angle of 45 degrees with a single right angle brace between adjacent 45 degree angle braces. The braces are assumed to be extrusions with a cruciform section. Fasteners are required for attachment of the braces and clips to the rib cap, and attachment of the rib cap to the skin panels and spars. Aluminum, steel, or titanium fasteners are available in the program.

Input to the rib parts definition routine includes variables from both the lifting surface geometry and structural synthesis routines. The required geometry data includes the number and location of the control stations, the number of control station nodes, the number of ribs (up to a maximum of 100 are allowed per semi-span), rib spacing, and surface span. The structural synthesis provides at each control station the rib cap area and length, brace area and weight, and the structural box average height. Panel cross section dimensions (and panel type) are also required at each control station to determine the rib cap cutout size for clearance of panel stiffeners.

Ribs are sized by the structural synthesis routine at each control station. The rib parts definition routine derives an actual spanwise rib location based on the specified rib spacing. The dimensions of the actual ribs are obtained by interpolating dimensions between the control stations. Each actual rib is then analyzed individually. No changes were made to the manufacturing process listing or to the basic rib design during this study.

SECTION 4

CONCLUSIONS

As a result of the work performed under this study the following conclusions are drawn:

1. The overall objective of this program was to provide a user oriented computer program capable of assessing the impact of fatigue and fracture criteria on weight and cost of transport aircraft. VDEP-II meets this objective.

2. The direct approaches adopted in the fatigue, flaw growth, and residual strengths analysis routines, although not specified in the work statement, were necessary to meet the overall objective. Allowable stress nomograph approaches were initially considered but they required extensive analyses external to the program for each selected criteria (i.e., crack size, inspection interval, load spectrum). Such a program would not be user oriented and would not provide the required accuracy, versatility and future growth capability.

3. The APAS structural synthesis module developed under this study is a powerful tool for evaluating all types of design criteria. It enables the user to rapidly perform preliminary design trade studies involving static strength factors as well as fatigue and fracture criteria.

4. The sparsity of S-N data for structural components is a severe restriction on conventional fatigue analysis performed during preliminary design. Considering the wide range of parameters that effect fatigue life, it is unlikely that an adequate data bank for component construction types will ever be available. Unnotched coupon data covering the required range of cycles and stress ratios is available for most aerospace structural materials. Therefore, analysis methods which rely more heavily on this type of data should be developed.

5. The applicability of linear elastic fracture mechanics to composite materials is not clearly established. Crack growth has seldom been observed. No data on growth rates or predictive methods was available for this program. Damage tolerance has been investigated for various types of construction. From the data reviewed it appears reasonable to treat unstiffened laminates of graphite/epoxy by conventional fracture mechanics methods. This can be done with the present program by inputting the proper K_c for each particular lay-up.

SECTION 5

RECOMMENDATIONS

During the course of the study a number of problems surfaced. These involve program capability, analysis methods, and data input and storage requirements. The following recommendations are offered to correct or alleviate these problems.

1. The method of Appendix B, used to plot S-N Curves, should be built into the fatigue analysis subprogram, PRODAM. This would reduce fatigue data input and storage requirements, and speed up computer run time.

2. PRODAM should be upgraded to handle biaxial stresses. At present, biaxial stresses generated at each section cut are converted to principal stresses before they are sent to PRODAM where they are treated as collinear uniaxial stresses. A more rational approach using octahedral stresses has been developed (Ref. 12) and can be incorporated directly in PRODAM.

3. An input loads subprogram should be added. The present requirement to externally generate shears, moments, and torques for six fatigue conditions plus static strength conditions for each structural component is very time consuming and is regarded as the major hurdle for potential users of VDEP-II to overcome. Input for this subprogram would consist of airplane geometry, weight distributions, and aerodynamic parameters. Most of this data is available in other parts of the program.

4. The data storage approach used in PROGRO and RESIDS should be modified to reduce core size requirements. At present the entire data bank of stress intensity factor coefficients for riveted, stiffened panels is held in core at once. This requirement sets the core size for the entire program, and it can be reduced by improved data handling techniques.

5. The flight profile required to develop the load spectra used in fatigue and flaw growth analysis should be input as a user option. At present a flight profile representative of medium range operation of large commercial transports is installed in the program. A subprogram should be developed to generate load spectra from user inputs consisting of weight, range, speed, altitude, and aerodynamic parameters.

6. The program should be exercised to fully validate its accuracy and demonstrate its usefulness. VEDP-II as delivered has much greater analysis capability than originally planned and a more comprehensive checkout is required. The limited test cases which have been run as part of the program development are not sufficient to establish the needed user confidence and operating strategy.

7. The program should be modified to include additional types of flaws commonly found in aircraft structure. As a minimum the following flaw types should be added:

a. Surface flaw
b. Corner crack emanating from a rivet or bolt hole
c. Single through crack emanating from a rivet or bolt hole
d. Double through crack emanating from a rivet or bolt hole

8. The program should be modified to automatically account for thickness effects on toughness. The program and data base should be modified so that as the thickness of structure is changed by the sizing routine, the proper toughness value is selected and used in the next iteration.

9. Flaw growth retardation due to overloads and spectrum effects should be accounted for. Several retardation models have been developed and one of these should be adopted for this program.

10. Environmental effects on flaw growth should be added. Data for aluminum and titanium alloys in various environments (i.e., R.T. air, JP fuel, LH_2) should be collected and stored in the program. The input routine should allow the user to specify different environments for different segments of the flight.

11. A direct method for calculating critical stress intensity factors, K_c, in composite laminates should be added. Residual strength of flawed composite laminates can be considered in the present version of the program only to the extent that the user may input K_c for a specific laminate. A test program is needed to define K_c as a function of ply orientation for several composite materials. These functions should then be incorporated in the program so that residual strength of arbitrary angle-plied laminates can be calculated directly.

12. Capability for analyzing multi-material construction types is needed. Mixing materials within a component has generally been avoided in past transport aircraft designs; however, this technique is known to be effective in dealing with crack growth and residual strength requirements. A procedure to optimize multi-material panels (e.g., aluminum skin with titanium stiffeners) for static strength and then augment the section to meet fatigue and fracture criteria would be a unique and valuable capability to add to VDEP-II.

SECTION 6

REFERENCES

1. "Fracture Toughness Testing and its Applications," American Society for Testing and Materials Special Technical Publication (ASTM STP-381), 1964.

2. "Damage Tolerant Design Handbook," Metals and Ceramics Information Center, Columbus, Ohio, December 1972.

3. Irwin, G. R., "Analytical Aspects of Crack Stress Field Problems," University of Illinois, TNAM Report 212, March 1962.

4. Kuhn, P., "Residual Strength in the Presence of Fatigue Cracks," NASA/Langley Research Center, April 1967.

5. Tada, H., Paris, P. C., and Irwin, G. R., "The Stress Analysis of Cracks Handbook", Del Research Corporation, Hellertown, Pa. 1973.

6. Poe, C. C., Jr., "Stress-Intensity Factor for a Cracked Sheet with Riveted and Uniformly Spaced Stringers," NASA TR R-358, Washington, D. C., May 1971.

7. "Computer Program to Perform Cost and Weight Analysis of Transport Aircraft," NASA CR 13262, Nov. 1973.

8. Trelease, R. H., et al, "Estimation of Airframe Manufacturing Costs," Convair Aerospace Report GDCA-BJF71-918, July 1972.

9. Levenson, G. S., Barro, J. M., "Cost Estimating Relationships for Aircraft Airframes," Rand Report RM-4845-PR (Abridged), May 1966.

10. Kenyon, R. E., "Techniques for Estimating Weapon System Structural Costs," Air Force Report AFFDL-TR-71-74, April 1972.

11. Kruse, G. S., and Peterson, L. M., "Automated Structural Sizing Techniques for Aircraft and Aerospace Vehicle Structures", General Dynamics/Convair Report GDCA-ERR-1748, Dec. 1972.

12. Tanner, C. J., "Fatigue Memo No. 2 - Combined Stresses," General Dynamics/Convair, Memo No. ASA-72-002.

REFERENCES (Continued)

13. Bruhn, E. F., "Analysis and Design of Flight Vehicle Structures," Tri-State Offset Co., Cincinnati, Ohio, 1965.

14. Fletcher, R., and Powell, M. J. D., "A Rapidly Convergent Descent Method for Minimization", The Computer Journal, Vol. 6, April, 1963 - January 1964.

15. Kruse, G. S., Tanner, C. J., and Wilson, P. J., "Fatigue and Fracture Mechanics Technology - Analysis", General Dynamics/Convair Report CASD-ERR-74-052, Dec. 1974.

16. Miner, M. A., "Cumulative Damage in Fatigue", Journal of Applied Mechanics, Vol. 12, No. 3, Sept., 1945.

17. MIL-HDBK-5B, "Metallic Materials and Elements for Aerospace Vehicle Structures", U. S. Government Printing Office, Washington, D. C., 31 Aug. 1973.

18. Shanley, F. R., "Weight-Strength Analysis of Aircraft Structures", Dover Publications, Inc., New York, N. Y., March 1960.

19. Peery, D. J., "Aircraft Structures," McGraw-Hill Book Company, New York N.Y., 1950.

20. "Astronautics Structures Manual," NASA Marshall Space Flight Center.

21. "Advanced Composites Design Guide," Third Edition, Vol. I, AFML, Wright-Patterson AFB, Ohio, 1973.

APPENDIX A

S-N CURVES

All of the fatigue data stored in the structural synthesis routine, APAS, is shown as S-N curves in this Appendix. These curves were plotted with the Hewlett-Packard 9100B computer program shown in Appendix B. The program requires input in the form of fatigue equation coefficients for each material and fatigue notch factors for each construction type. These are developed below.

FATIGUE EQUATION COEFFICIENTS

Unnotched coupon data is required to determine the coefficients, C, M, and n for Equation (B-1). All of the data needed for Aluminum and Titanium is given in Reference 17 and is shown in Tables A-1 and A-2. Values of C, m, and n shown in the tables were calculated by a second H-P 9100B computer program which is also shown in Appendix B.

Table A-1. Fatigue Equation Coefficients for Unnotched 2024-T3

F_{tu} = 503 MN/m^2 (73 ksi)

	NORMALIZED MAX. STRESS, S_{max}/F_{tu} *							
R	10^0	10^4	10^5	10^6	10^7	C	m	n
+1.0								
.8	1.000	.999	.993	.985	.980	17220	.6674	-103.7
.6		.997	.945	.897	.856	2611	.1205	-27.85
.4		.993	.856	.733	.688	13960	.3137	-5.103
.2		.984	.753	.589	.551	21140	.3904	-1.763
0		.956	.670	.493	.453	22370	.4964	-1.299
-.2		.908	.603	.432	.401	36060	.8378	-.3845
-.5		.822	.534	.370	.342	73220	1.551	.2462
-1.0	1.000	.692	.462	.308	.281	410200	3.632	1.206
-2.0								
$-\infty$								

* Ref. 17, page 3-77

Table A-2. Fatigue Equation Coefficients for Unnotched Ti-6AL-4V

F_{tu} = 1186 MN/m^2 (172 ksi)

R	NORMALIZED MAX STRESS, S_{max}/F_{tu} *					C	m	n
	10^0	10^4	10^5	10^6	10^7			
+1.0								
0.8	1	0.988	0.913	0.837	0.802	17070	0.5628	-9.408
0.6		0.974	0.837	0.721	0.680	18940	0.5427	-4.479
0.4		0.953	0.767	0.628	0.593	32510	0.7472	-1.747
0.2		0.924	0.716	0.564	0.535	87370	1.202	0.1836
0		0.890	0.657	0.506	0.483	152800	1.582	1.142
-0.2		0.843	0.599	0.459	0.436	107200	1.709	0.6288
-0.5		0.773	0.529	0.407	0.384	40380	1.634	-0.3238
-1.0	1	0.650	0.420	0.335	0.310	8280	1.501	-1.593

* Ref. 17, page 5-95

Data for Graphite/Epoxy 0/±45/90 is given in Reference 21 for R = +.1 only. The following method is used to expand this data proportional to the distribution of R values for unnotched Ti-6AL-4V.

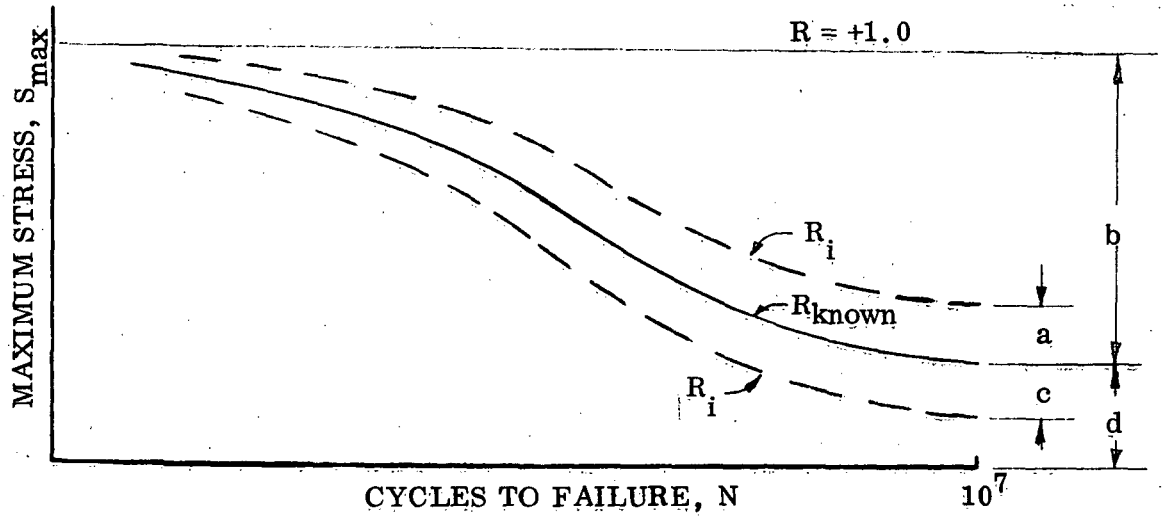

Figure A-1. Method for Distributing Stress Ratio Curves

For $R > R_{known}$:

$$S_{max} = S_{known} + \left(\frac{a}{b}\right)_{Titanium} \cdot \left(b\right)_{composite}$$

For $R < R_{known}$:

$$S_{max} = S_{known} - \left(\frac{c}{d}\right)_{Titanium} \cdot \left(d\right)_{composite}$$

Tables A-3 and A-4 show the results of this data expansion and the calculated values of C, m, and n for the composite materials over the range of R = +1.0 to R = -1.0.

Table A-3. Fatigue Equation Coefficients for Unnotched Graphite/Epoxy $0/\pm45/90$

F_{tu} = 379 MN/m^2 (55 KSI)

R	Normalized Max. Stress S_{max}/F_{tu}				C	m	n
	10^3	10^5	10^6	10^7			
+1.0	1.0	1.0	1.0	1.0			
.8	.989	.900	.860	.824	709.29	.4000	-31.252
.6	.977	.830	.771	.716	373.61	.2212	-20.448
.4	.935	.757	.690	.640	422.13	.4851	-14.398
.2	.864	.703	.640	.590	490.82	1.2632	-13.252
0	.800	.644	.585	.535	82.614	1.2067	-13.927
-.2	.762	.590	.525	.485	3506.06	3.1790	-7.4508
-.5	.720	.530	.460	.425	21782.9	4.4478	-4.1401
-1.0	.635	.440	.375	.345	6488.49	4.8300	-3.8756

Table A-4. Fatigue Equation Coefficients for Unnotched Boron/Epoxy $0/\pm45/90$

F_{tu} = 448 MN/m^2 (65 KSI)

R	Normalized Max. Stress S_{max}/F_{tu}				C	m	n
	10^3	10^5	10^6	10^7			
+1.0	1.0	1.0		1.0			
.8	.980	.860	.804	.752	1751.5	.6256	-20.216
.6	.959	.740	.655	.600	1655.0	.6070	-9.8069
.4	.870	.630	.547	.495	682.45	.8609	-8.3125
.2	.757	.547	.470	.420	1686.6	2.4226	-6.5261
0	.665	.475	.410	.368	234.93	2.5095	-7.3017
-.2	.620	.432	.370	.330	85.762	2.3291	-7.2630
-.5	.585	.385	.322	.292	1406.2	4.3362	-4.1876
-1.0	.530	.322	.260	.236	6533.8	6.0582	-2.3200

Regarding the data for the composite materials (Boron/Epoxy and Graphite/Epoxy), it must be realized that an infinite variety of laminates is possible. Each layup will have different fatigue characteristics. A pseudo isotropic layup, $0/\pm 45/90$, was selected for this program because it is a common layup and some fatigue data was available.

Figures A-2 thru A-5 show S-N curves for unnotched materials (2024-T3, Ti-6AL-4V, Graphite/Epoxy, and Boron/Epoxy) plotted from the data in Tables A-1 thru A-4. These curves are normalized to the material tensile ultimate strength, F_{tu}.

Figure A-2. S-N Curves for Unnotched 2024-T3

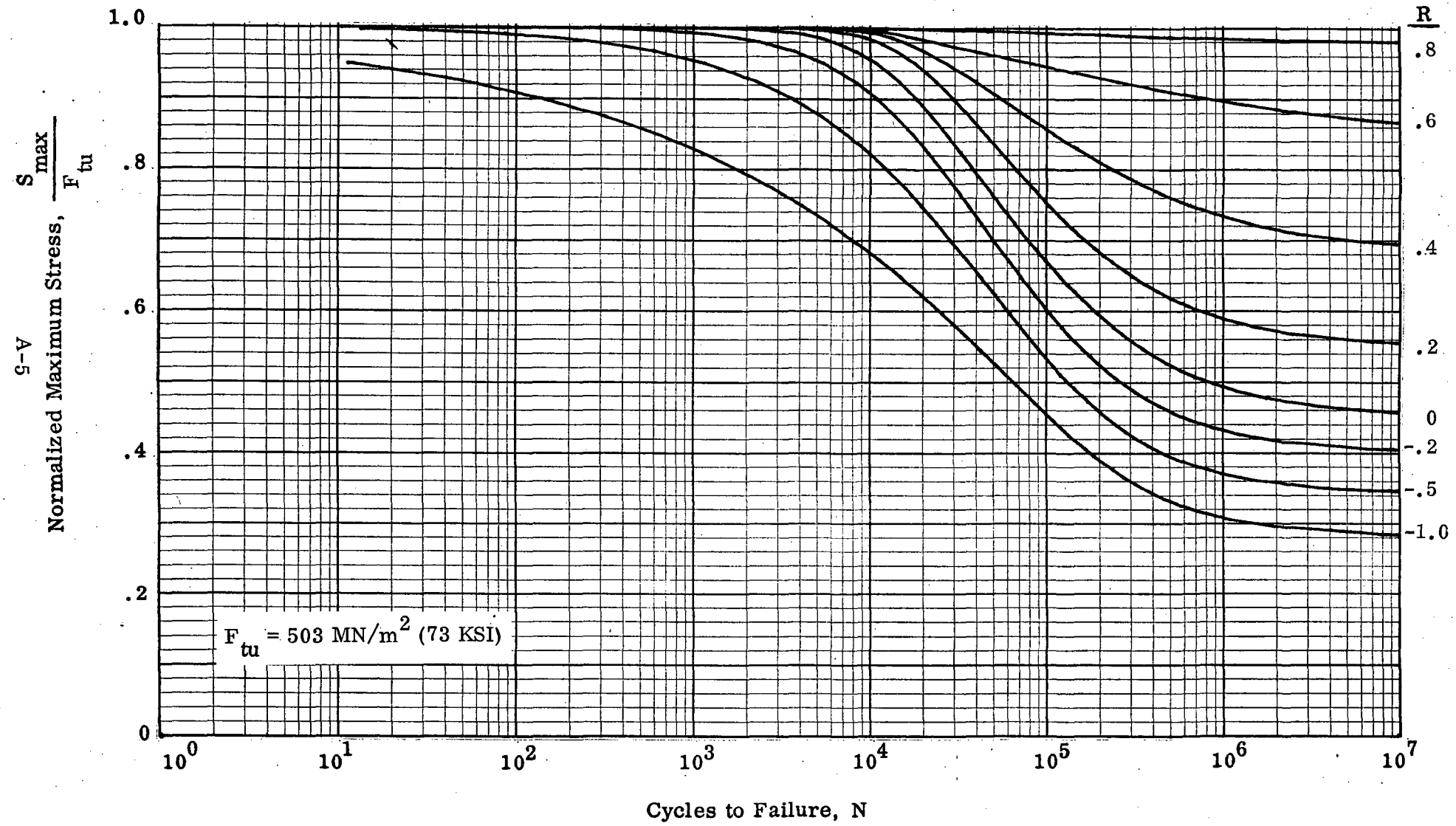

Figure A-3. S-N Curves for Unnotched Ti-6Al-4V

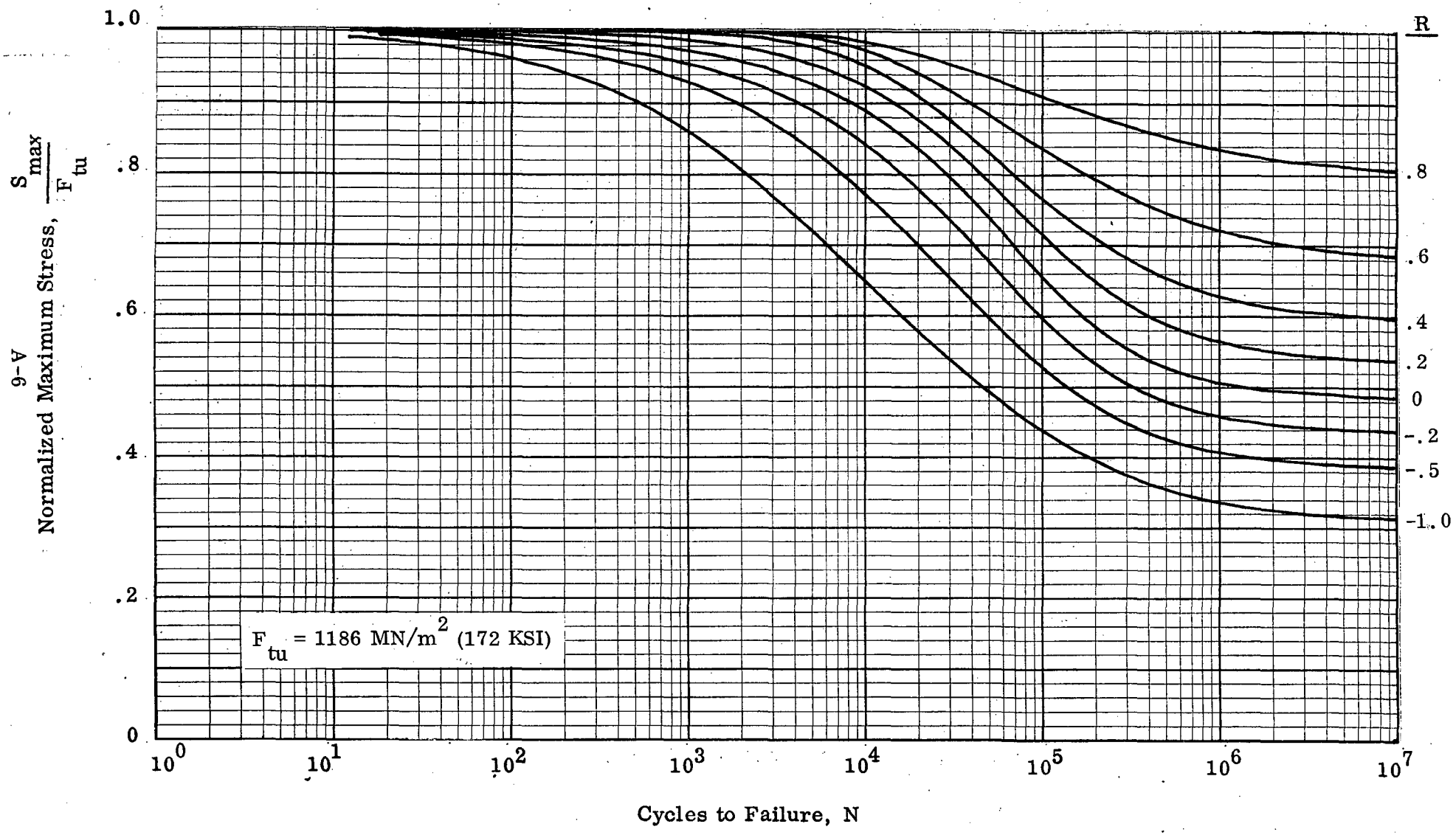

Figure A-4. S-N Curves for Unnotched Graphite/Epoxy 0/±45/90

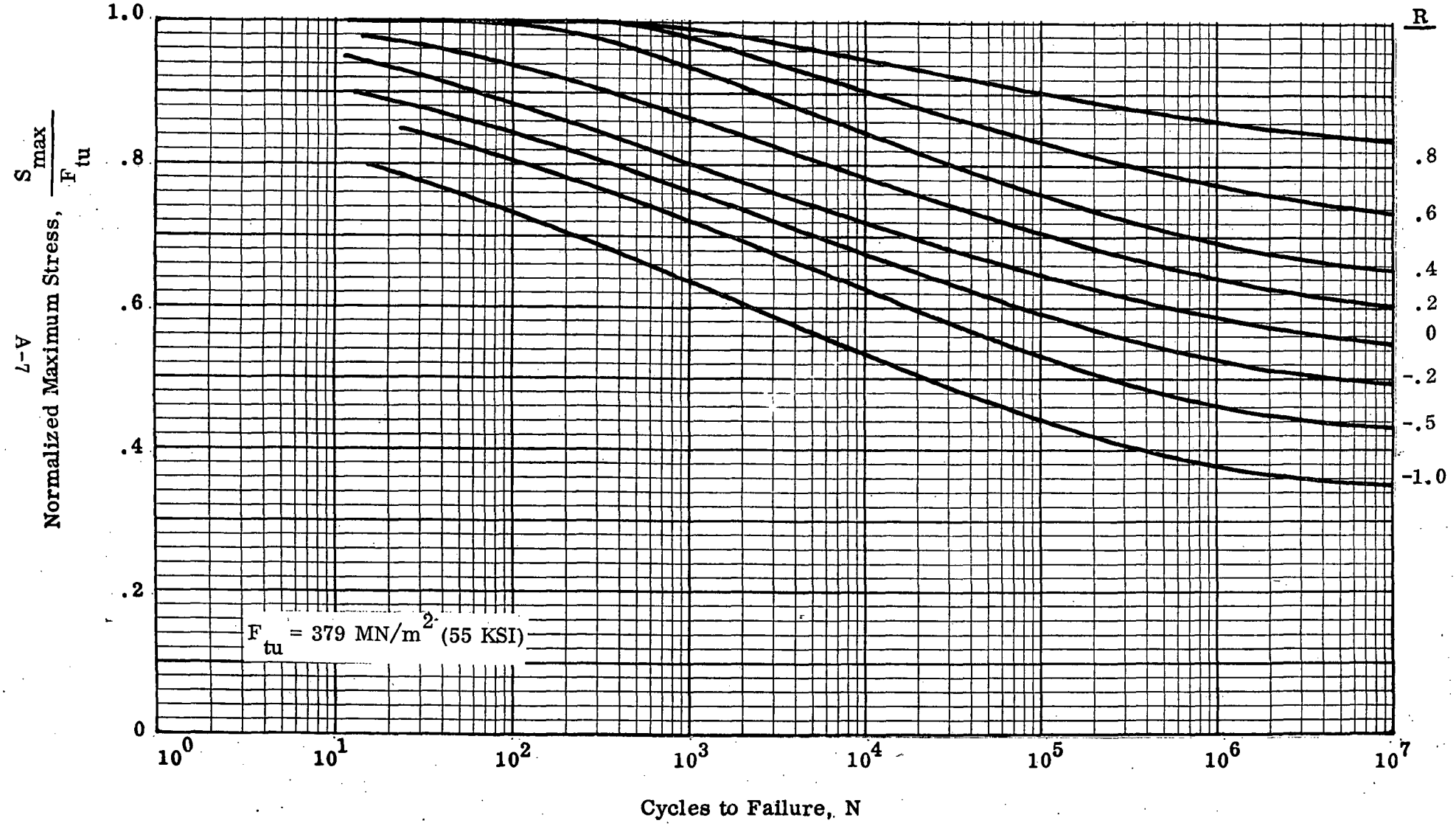

Figure A-5. S-N Curves for Unnotched Boron/Epoxy 0/±45/90

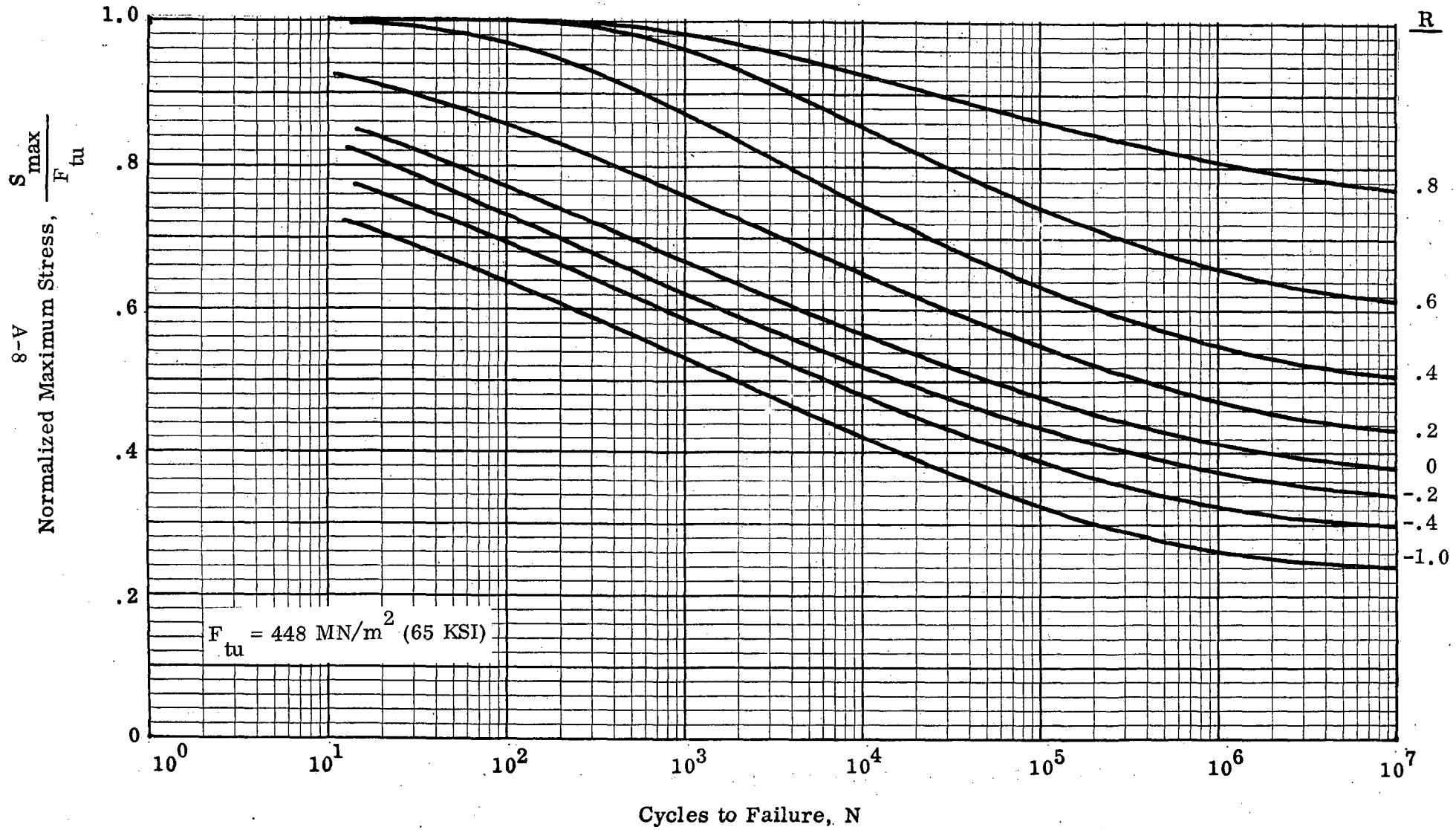

FATIGUE NOTCH FACTORS

Fatigue behavior of structural components can be approximated by factoring unnotched fatigue data. The ratio of unnotched fatigue strength to notched fatigue strength at any number of cycles, N, is defined as the fatigue notch factor, K_f. The variation of K_f with cycles is given by Equation (B-5). The notch factors at the endurance limit, K_{fe}, and at one cycle, K_{fs}, are required input for the S-N plotter program. Figure B-2 is an estimate of the variation of K_{fe} with stress ratio, R, for several types of construction. Table A-5 summarizes all of the fatigue notch factors needed to generate S-N curves for the construction types required in this program.

COMPONENT S-N CURVES

The component S-N curves shown in Figures A-8 thru A-19 were generated with the Appendix B procedure utilizing the fatigue equation coefficients (C, m, n) in Tables A-1 thru A-4 and the fatigue notch factors (K_{fs}, K_{fe}) in Table A-5. All curves are normalized to the net section static strength, S_s. These curves provide fatigue data for all of the component construction types currently allowed in the structural synthesis module, APAS. Values of constant life cuts thru these curves are stored in the FATTAB subroutine of APAS. New data may easily be installed by the user. The format is described on comment cards in FATTAB.

Table A-5. Summary of Fatigue Notch Factors, K_{fe}

Material		2024 -T3					Ti-6Al-4V					Graphite Epoxy 0/±45/90				Boron/Epoxy 0/±45/90			
Constr. Type		Un-notched	Riveted	Integral	Welded	Bonded	Un-notched	Riveted	Integral	Welded	Bonded	Un-notched	Riveted	Integral	Bonded	Un-notched	Riveted	Integral	Bonded
F_{tu} MN/m^2 (ksi)		503 (73)	455 (66)	441 (64)	455 (66)	455 (66)	1185 (172)	958 (139)	896 (130)	958 (139)	958 (139)	379 (55)	379 (55)	379 (55)	379 (55)	448 (65)	448 (65)	448 (65)	448 (65)
SF		1.0	.75	.95	.95	.95	1.0	.75	.95	.95	.95	1.0	.75	.95	.95	1.0	.75	.95	.95
K_{fs}		1.0	1.48	1.20	1.16	1.16	1.0	1.65	1.39	1.30	1.30	1.0	1.333	1.053	1.053	1.0	1.333	1.053	1.053
R	1.0	1.0	1.48	1.20	1.16	1.16	1.0	1.65	1.39	1.30	1.30	1.0	1.333	1.053	1.053	1.0	1.333	1.053	1.053
	.8	1.0	2.17	1.74	2.65	1.72	1.0	2.22	1.80	2.70	1.77	1.0	1.917	1.527	1.527	1.0	1.917	1.527	1.527
	.6	1.0	2.50	2.00	3.59	2.00	1.0	2.50	2.00	3.39	2.00	1.0	2.50	2.00	2.00	1.0	2.50	2.00	2.00
	.4	1.0	2.50	2.00	3.39	2.00	1.0	2.50	2.00	3.39	2.00	1.0	2.50	2.00	2.00	1.0	2.50	2.00	2.00
	.2	1.0	2.50	2.00	3.39	2.00	1.0	2.50	2.00	3.39	2.00	1.0	2.50	2.00	2.00	1.0	2.50	2.00	2.00
	0	1.0	2.50	2.00	3.39	2.00	1.0	2.50	2.00	3.39	2.00	1.0	2.50	2.00	2.00	1.0	2.50	2.00	2.00
	-.2	1.0	2.66	2.13	3.61	2.13	1.0	2.66	2.13	3.61	2.13	1.0	2.66	2.13	2.13	1.0	2.66	2.13	2.13
	-.5	1.0	2.90	2.32	3.93	2.32	1.0	2.90	2.32	3.93	2.32	1.0	2.90	2.32	2.32	1.0	2.90	2.32	2.32
	-1.0	1.0	3.30	2.64	4.47	2.64	1.0	3.30	2.64	4.47	2.64	1.0	3.30	2.64	2.64	1.0	3.30	2.64	2.64
	-2.0																		
	-∞																		

Figure A-6. S-N Curves for Riveted Aluminum Components

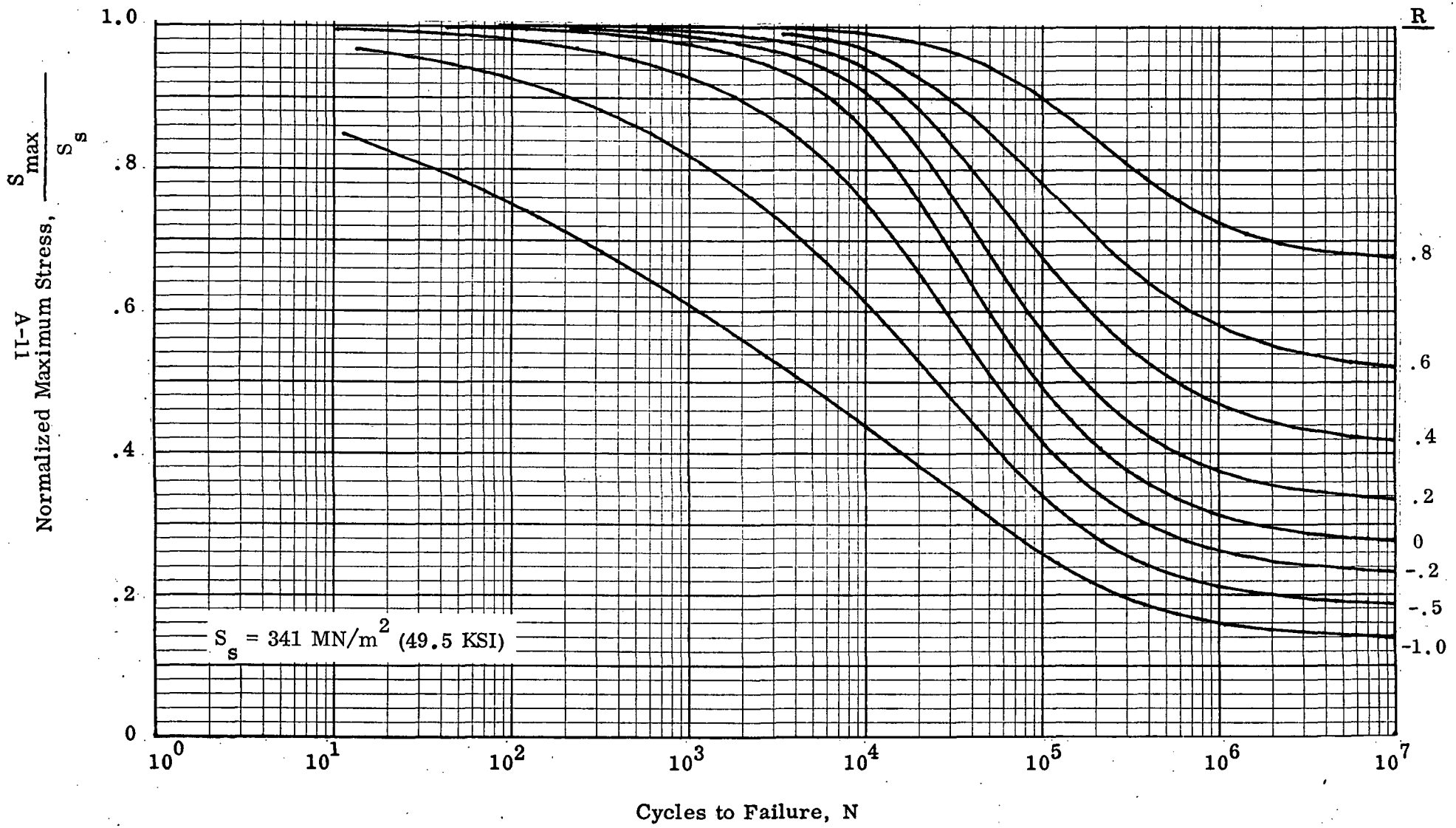

Figure A-7. S-N Curves for Integral Aluminum Components

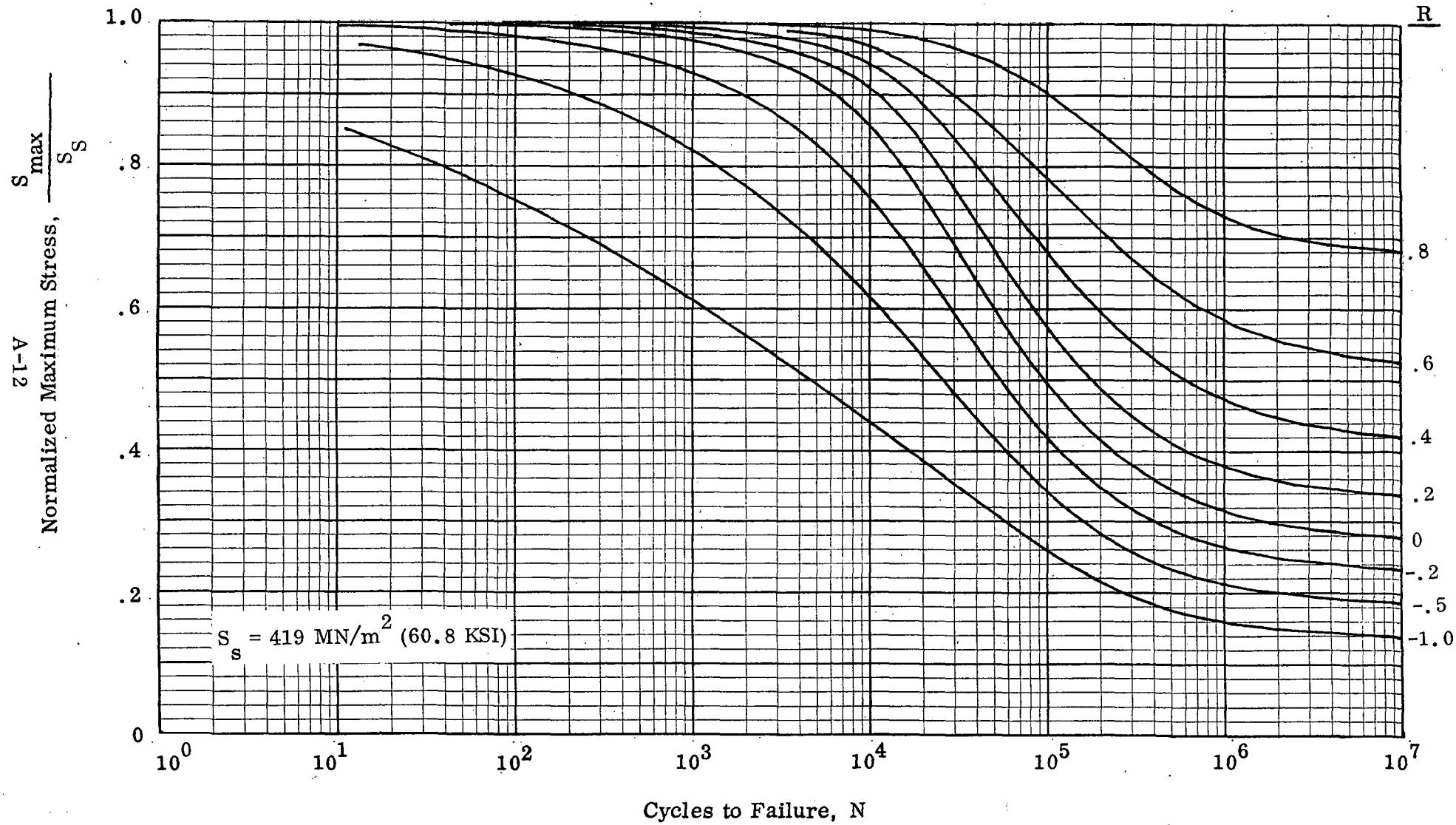

Figure A-8. S-N Curves for Spot Welded Aluminum Components

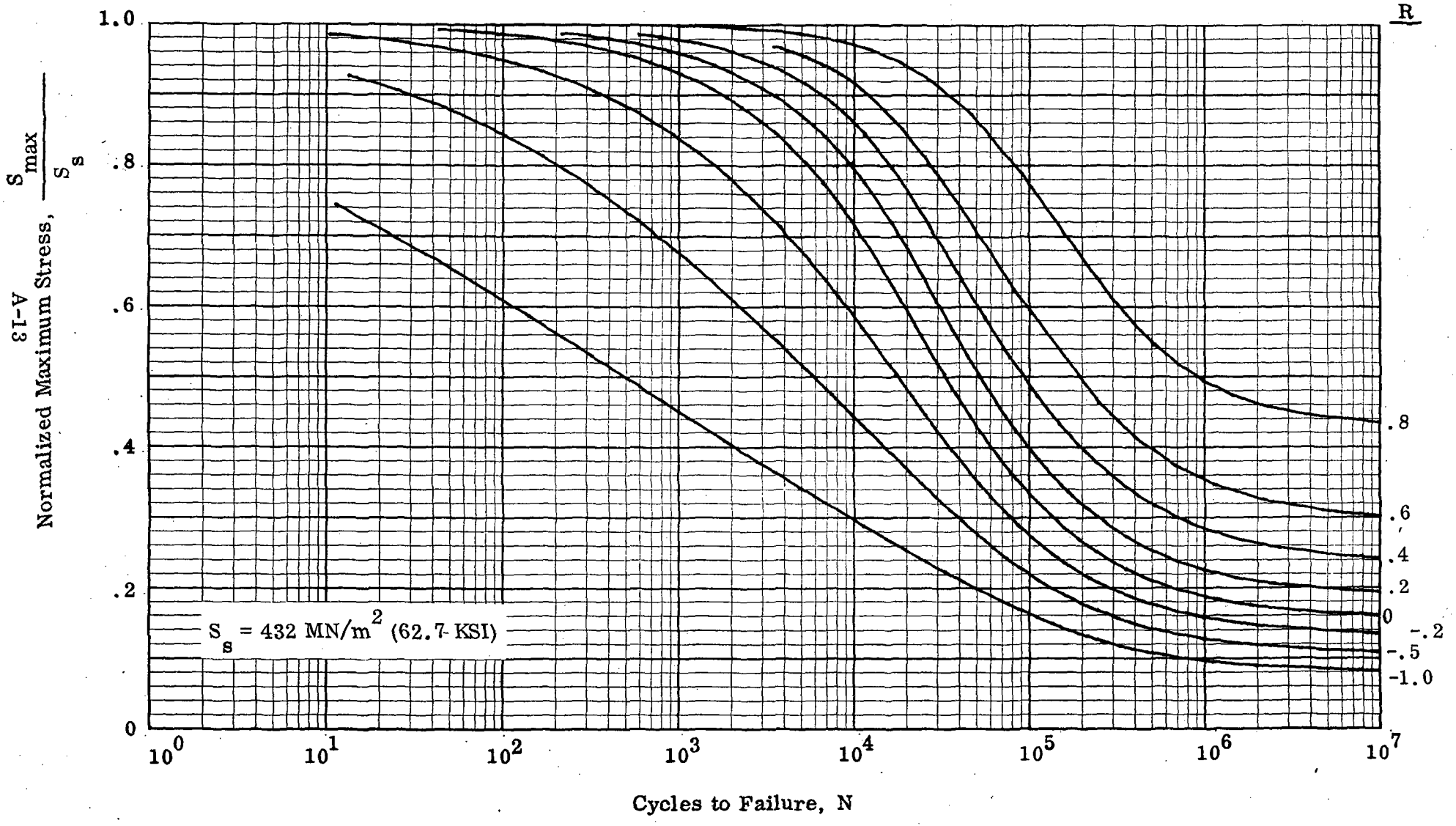

Figure A-9. S-N Curves for Bonded Aluminum Components

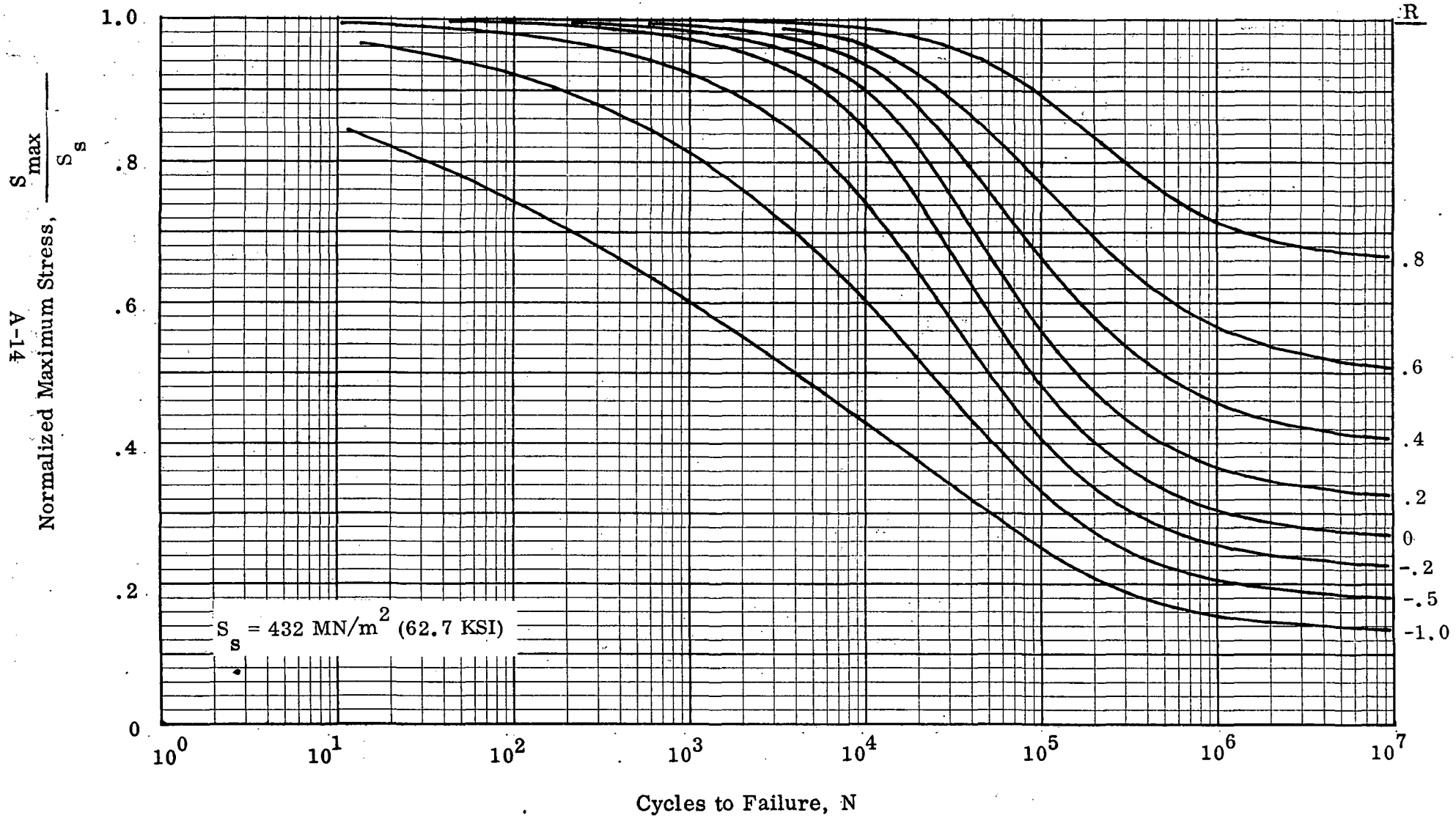

Figure A-10. S-N Curves for Riveted Titanium Components

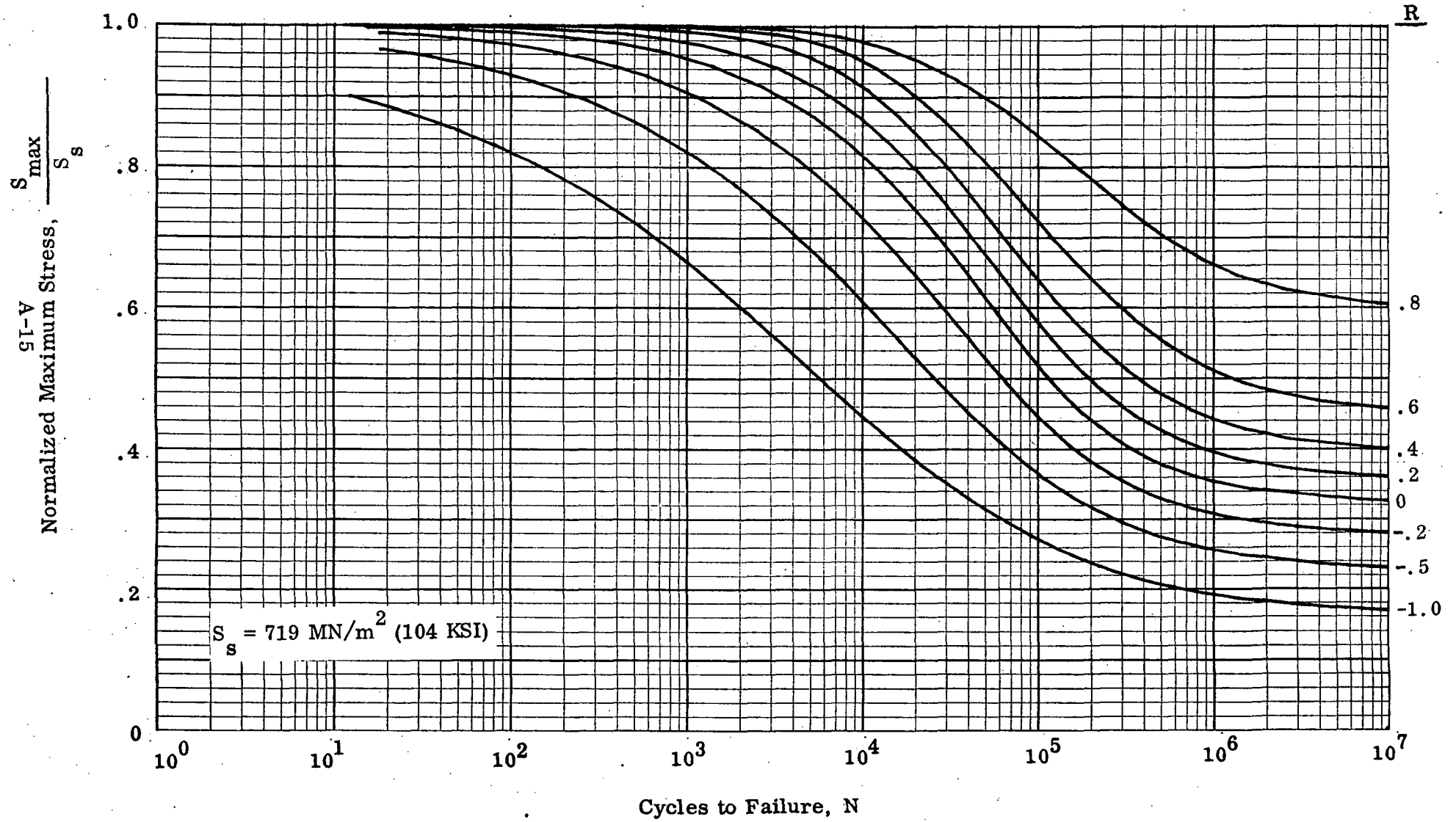

Figure A-11. S-N Curves for Integral Titanium Components

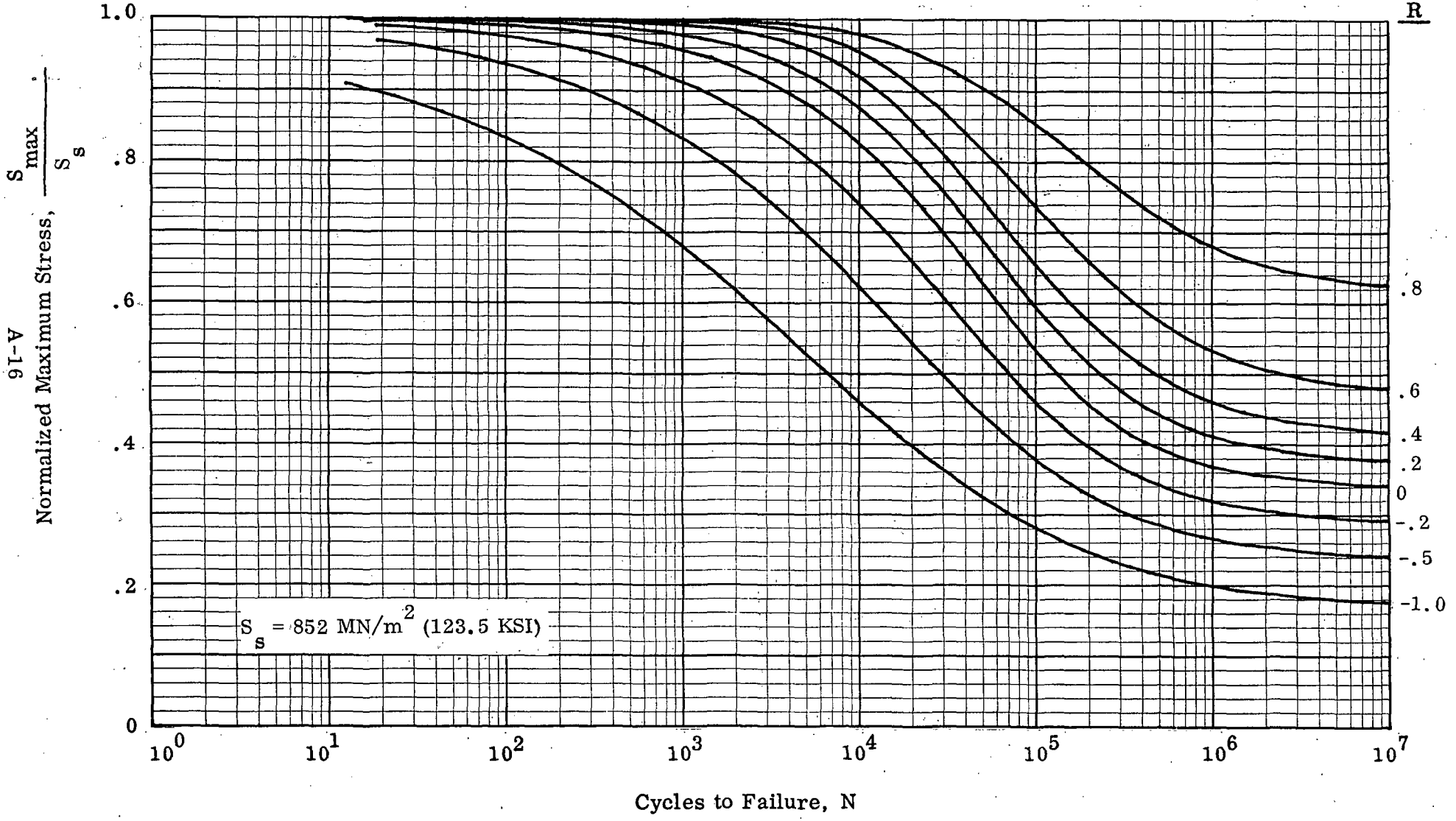

Figure A-12. S-N Curves for Spot Welded Titanium Components

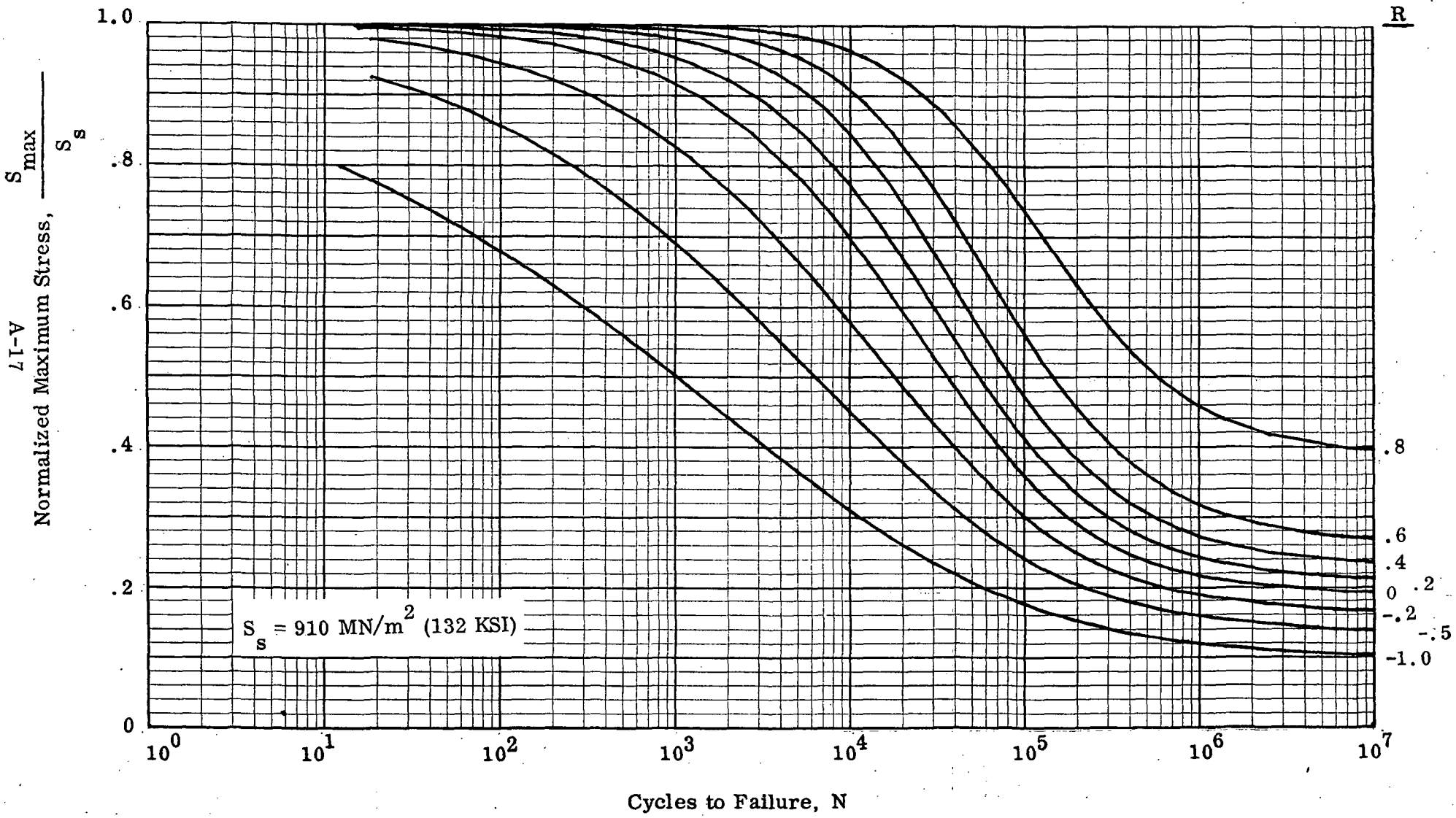

Figure A-13. S-N Curves for Bonded Titanium Components

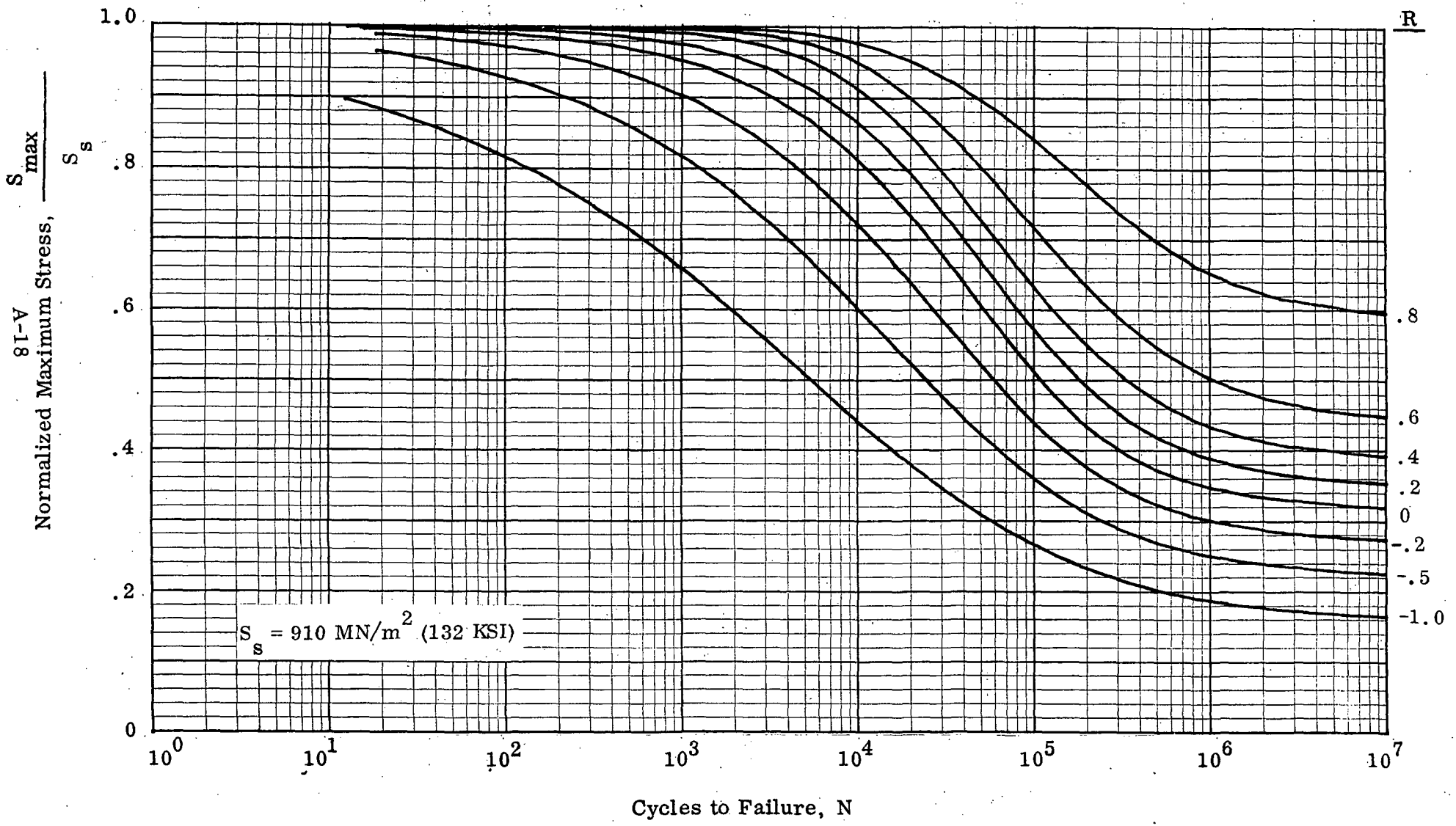

Figure A-14. S-N Curves for Riveted Graphite/Epoxy, 0/±45/90, Components

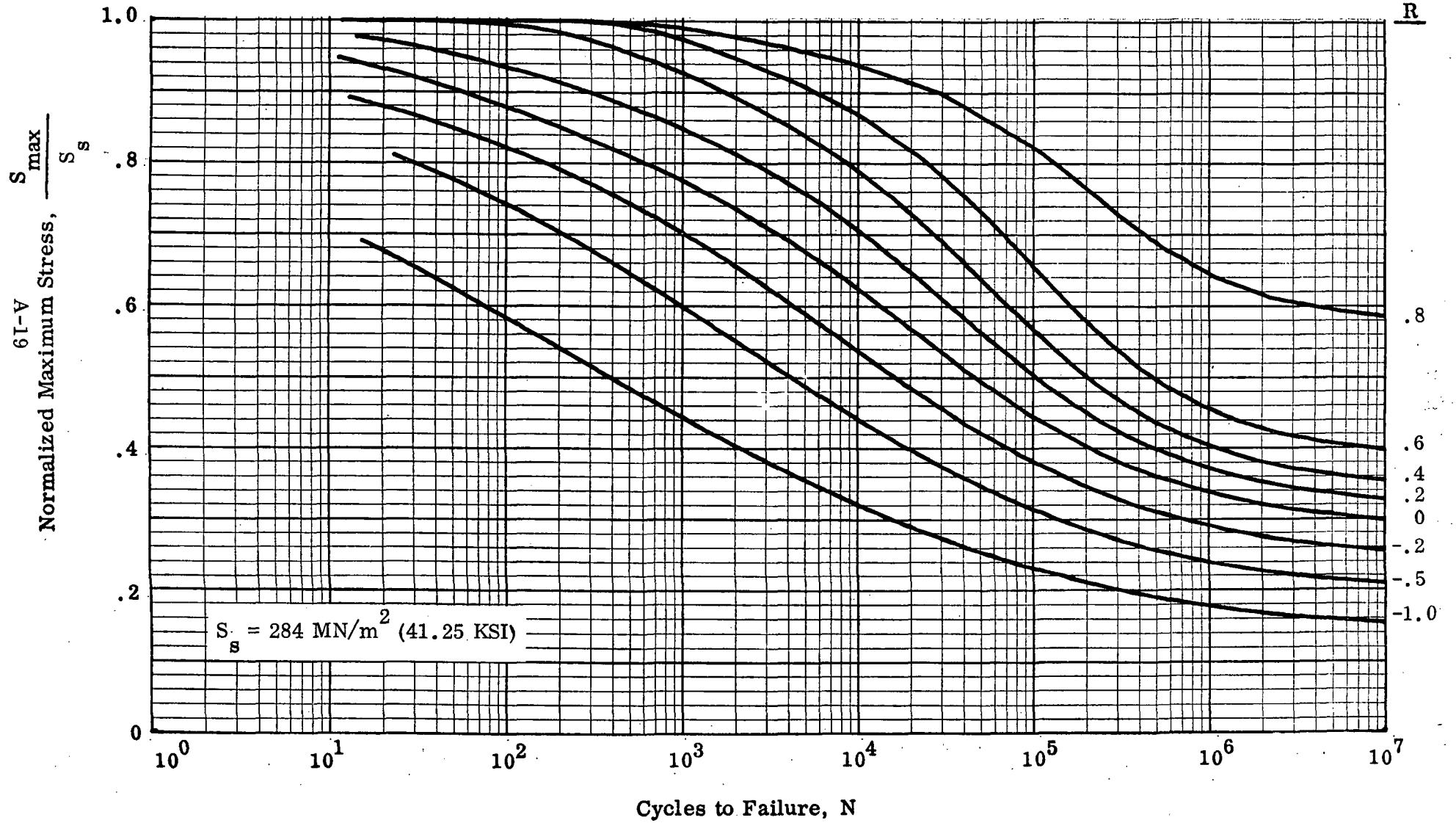

Figure A-15. S-N Curves for Integral or Bonded Graphite/Epoxy, $0/\pm 45/90$, Components

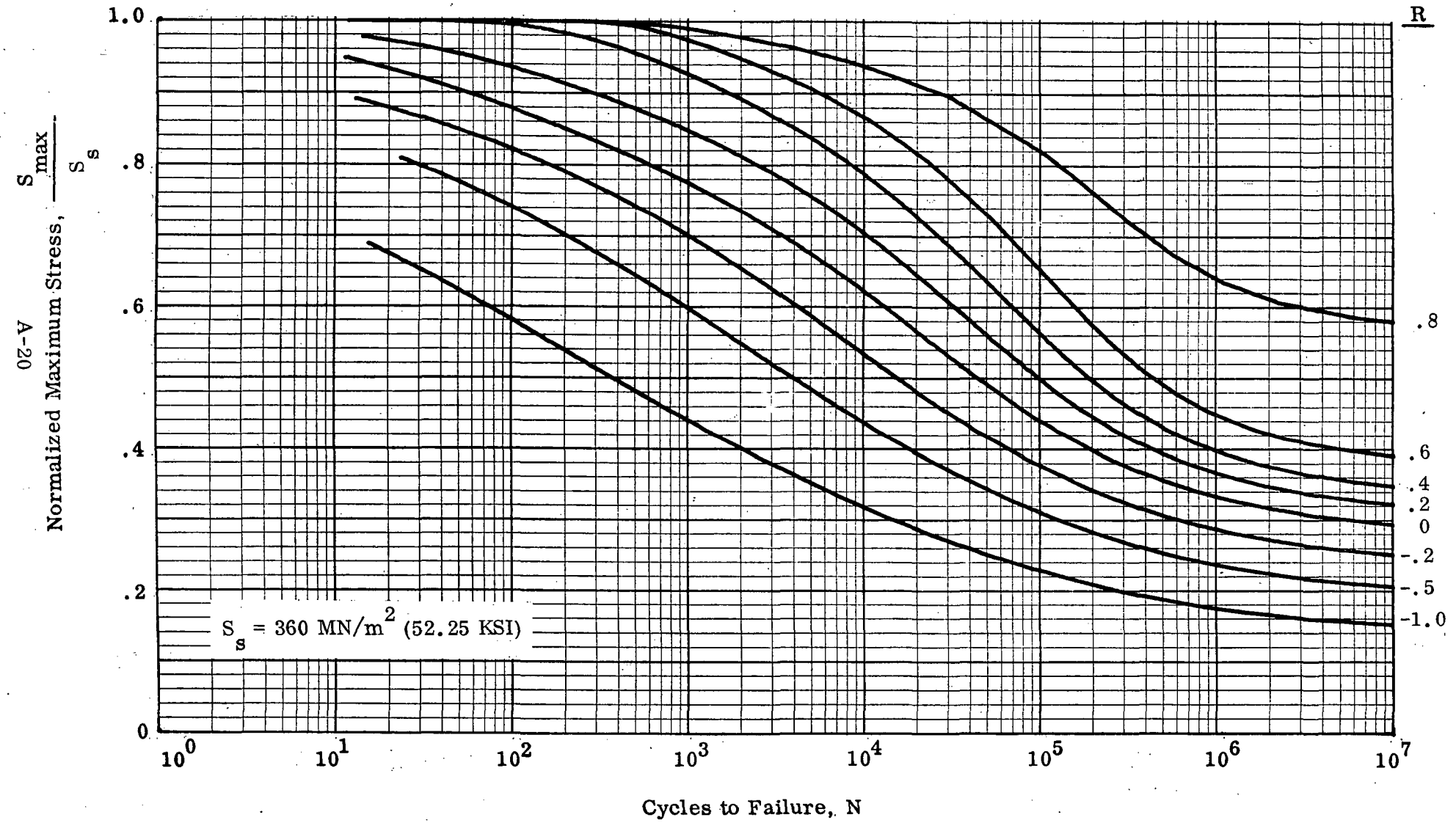

Figure A-16. S-N Curves for Riveted Boron/Epoxy, $0/\pm 45/90$, Components

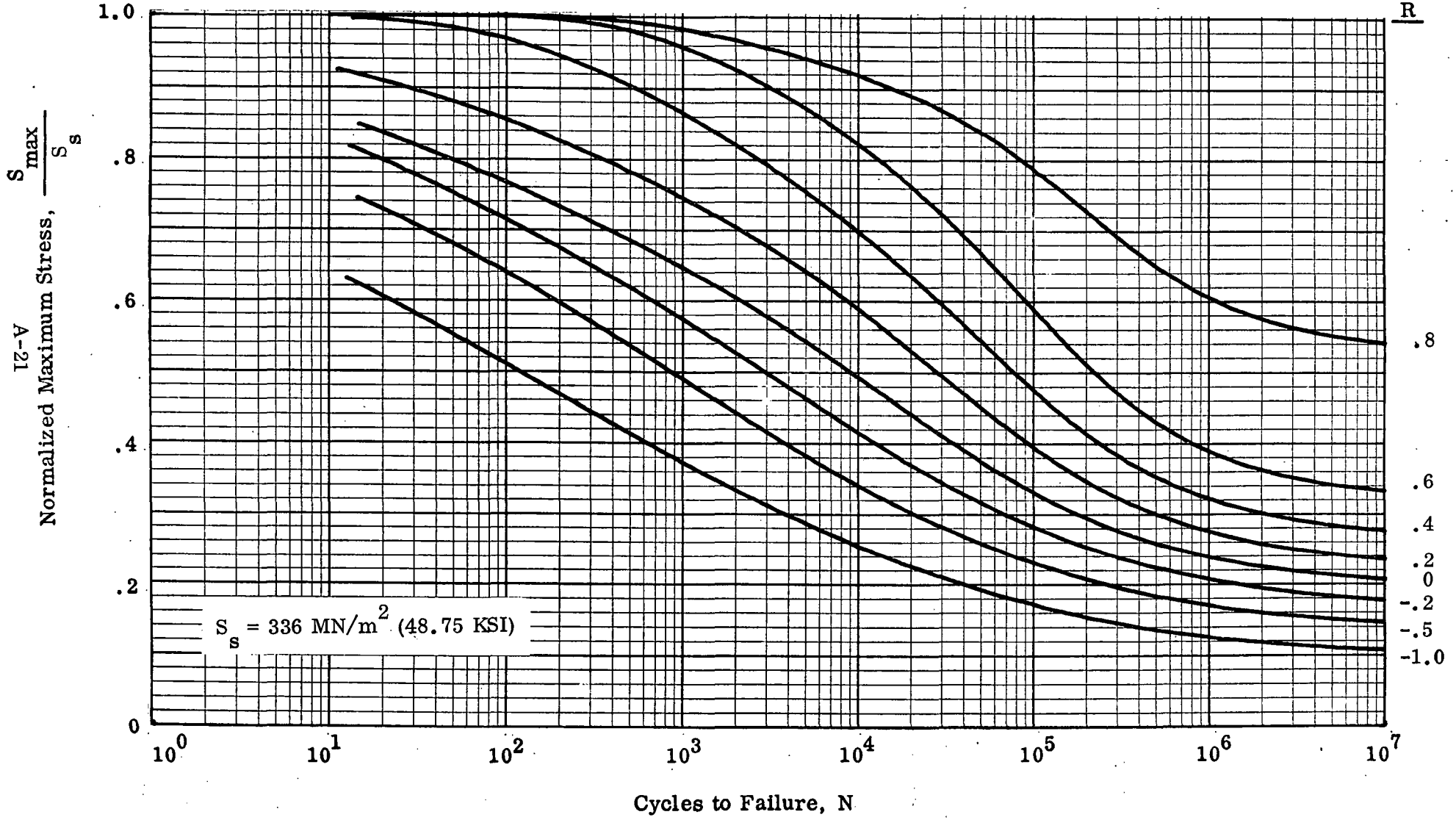

Figure A-17. S-N Curves for Integral or Bonded Boron/Epoxy, 0/±45/90, Components

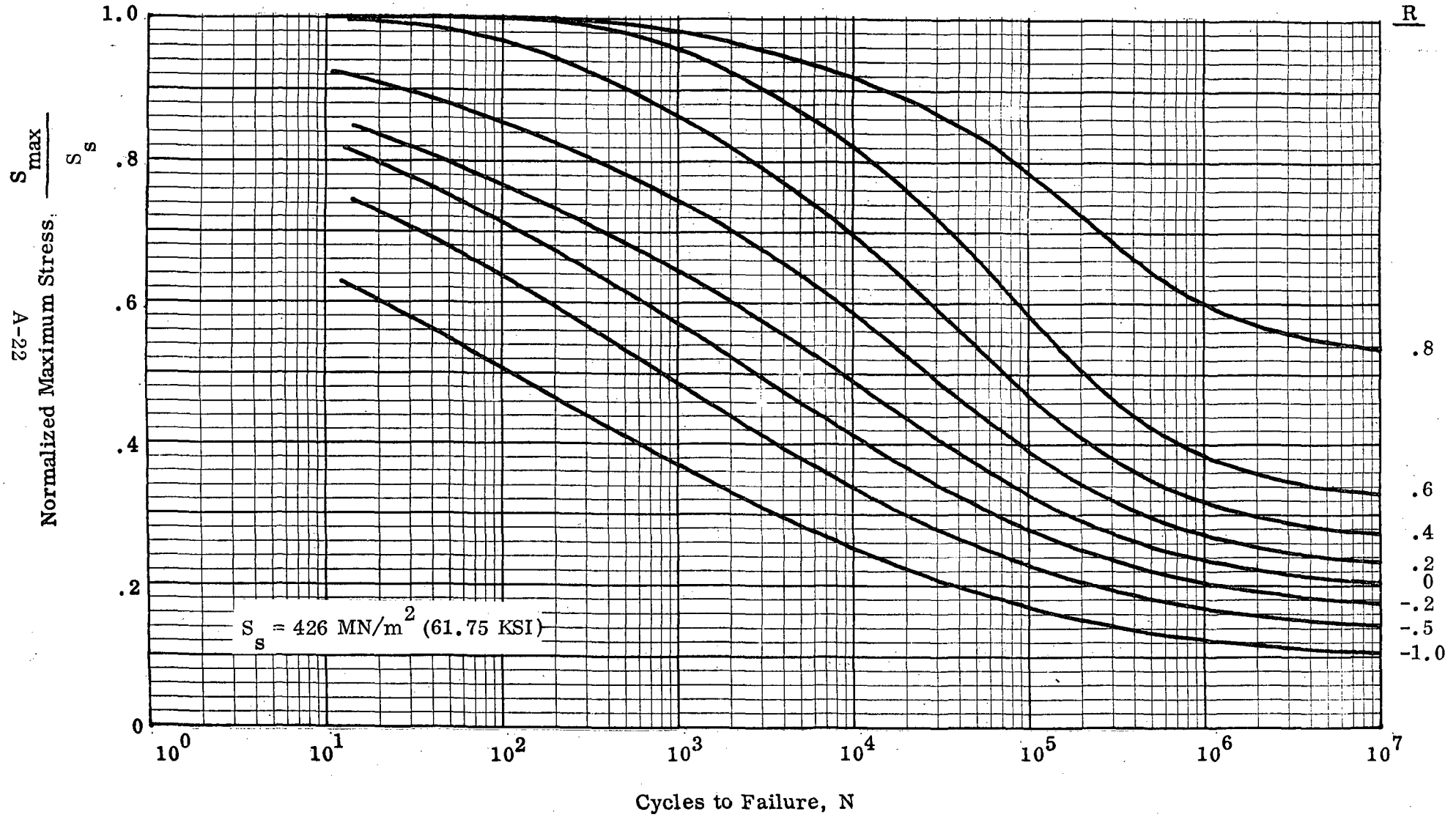

APPENDIX B
AUTOMATED PLOTTING OF S-N DATA FOR STRUCTURAL COMPONENTS

INTRODUCTION

Fatigue analysis is frequently needed but seldom accomplished early in the design phase of aerospace structures. A major obstacle to such timely analysis is the sparsity of component S-N data. There is no source of fatigue design data comparable to the static strength design data available in MIL-HDBK-5B. Fatigue life is affected by a wide range of parameters that include cyclic stress, mean stress, product form and orientation, temperature, environment, structural geometry, notch effects, metallurgical effects, and surface finish. An almost infinite variety of materials and fabrication methods would have to be tested to build an adequate S-N data bank. Since this is out of the question, the fatigue life of most aerospace vehicles is verified by tests and analysis performed late in the development of the structure. This after-the-fact analysis cannot produce optimum structures. Tradeoff studies performed in the preliminary design phase may be compromized by lack of rational fatigue considerations.

As a result of the circumstance outlined above the fatigue analyst must improvise with limited fatigue data in the early design phases. The usual approach is to select and plot the most appropriate data available from the literature and previous in-house programs. S-N curves are cross-plotted into constant life diagrams to facilitate interpolation for additional stress ratio values and extrapolation to extend the cycle range. With some intuition and judgement S-N curves are then drawn and faired-in to form preliminary design criteria for a particular component.

A procedure for rapidly plotting S-N curves from limited data has been developed under a Convair IRAD study (Ref. 15). This method was used to generate the S-N curves for structural components shown in Appendix A. The procedure, employing two Hewlett-Packard 9100B Computer Programs, is presented here for convenience. The first H-P program is used to calculate curve-fit coefficients for unnotched coupon data. The second program is used to factor and plot the data as derived S-N curves for structural components.

S-N EQUATION

The characteristic sigmoidal shape of typical S-N data can be described with the following equation.

$$N = C \frac{\left(1 - \frac{S_{max}}{S_s}\right)^m \left(\frac{S_{max}}{S_s}\right)^n}{\left(\frac{S_{max}}{S_s} - \frac{S_e}{S_s}\right)} \qquad \text{(B-1)}$$

where:

S_{max} is the maximum cyclic stress

S_s is the net section static strength, $F_{tu} \times SF$

S_e is the maximum cyclic stress at the endurance limit

C, m, n, are data fit coefficients

Solving for C, m, and n gives:

$$C = \frac{y_1 (x_1 - x_e)}{(1-x)^m (x_1)^n} \tag{B-2}$$

$$n = \frac{\ln\left[\frac{y_1(x_1 - x_e)}{y_2(x_2 - x_e)}\right] - m \cdot \ln\left(\frac{1 - x_1}{1 - x_2}\right)}{\ln\left(\frac{x_1}{x_2}\right)} \tag{B-3}$$

$$m = \frac{\ln\left[\frac{y_1(x_1 - x_e)}{y_3(x_3 - x_e)}\right] - \frac{\ln\left(\frac{x_1}{x_3}\right)}{\ln\left(\frac{x_1}{x_2}\right)} \ln\left[\frac{y_1(x_1 - x_e)}{y_2(x_2 - x_e)}\right]}{\ln\left(\frac{1 - x_1}{1 - x_3}\right) - \frac{\ln\left(\frac{x_1}{x_3}\right)}{\ln\left(\frac{x_1}{x_2}\right)} \ln\left(\frac{1 - x_1}{1 - x_2}\right)} \tag{B-4}$$

Where:

$y = N$

$x = \frac{S_{max}}{S_s}$

$x_e = \frac{S_e}{S_s}$

Provided the static ultimate stress, S_s, and the endurance limit stress, S_e, are known, the coefficients C, m, and n can be found by substituting N and S values for three data points into Equations B-2, B-3, B-4. Equation 1 then describes a smooth sigmoidal curve which fits five data points : S_s, S_e and 3 intermediate points. Thus Equation B-1 can be fitted to any known fatigue data such as the constant life diagrams presented in MIL-HDBK-5B.

The following Hewlett-Packard 9100B program incorporates the above equations to solve for the coefficients C, m, and n.

S-N DATA FIT PROGRAM OPERATING INSTRUCTIONS

To execute the program to calculate C, m, and n perform the following steps in order.

1. PRESS "CLEAR"
2. PRESS "END"
3. ENTER PROGRAM - SIDES A AND B OF MAGNETIC CARD
4. TURN ON PRINT X
5. PRESS "END"
6. PRESS "CONT"
7. ENTER STRESS RATIO R, "CONT"
8. ENTER STATIC ULTIMATE STRESS S_s, "CONT"
9. ENTER ENDURANCE LIMIT STRESS S_e, "CONT"
10. ENTER ANY THREE INTERMEDIATE DATA POINTS AS FOLLOWS:
    a. ENTER CYCLES N_1, "CONT" AND STRESS S_1, "CONT"
    b. ENTER CYCLES N_2, "CONT" AND STRESS S_2, "CONT"
    c. ENTER CYCLES N_3, "CONT" AND STRESS S_3, "CONT"
11. THE PROGRAM WILL PRINT C, m, and n.
12. THE PROGRAM RETURNS TO STEP 7.

The programming code is listed on pages B-14, 15, and 16.

NOTCH FACTOR EQUATION

The ratio of unnotched fatigue strength to notched fatigue strength at any number of cycles, N, is defined as the fatigue notch factor, K_f. Examination of notched and unnotched data indicates the variation of K_f with N can be represented by the following inverse hyperbolic tangent equation. See Figure B-1.

$$\text{LnN} = \text{Ln}C_1 + C_2 \, \text{Tanh}^{-1} \frac{2K_f - K_{fs} - K_{fe}}{K_{fe} - K_{fs}} \qquad \text{(B-5)}$$

Where:

K_f is the ratio of unnotched fatigue strength to notched fatigue strength.

K_{fs} equals K_f at one cycle (static).

K_{fe} equals K_f at endurance limit (assumed to be $N = 10^7$).

C_1 and C_2 define the inflection point and slope respectively.

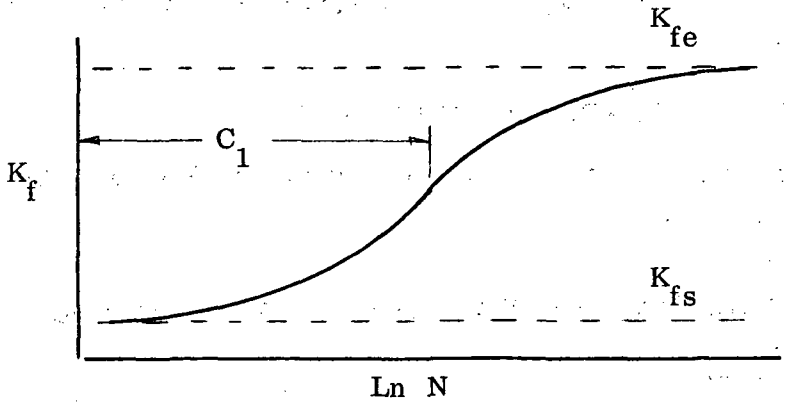

Figure B-1. Inverse Hyperbolic Tangent Function

Equation B-5 is solved for K_f as follows:

Expressing the inverse hyperbolic function in logarithmic form gives

$$\text{Tanh}^{-1} x = 1/2 \ln\left(\frac{1+x}{1-x}\right)$$

Substituting into Equation B-5 gives

$$\text{LnN} = \text{LnC}_1 + C_2 \left(1/2 \text{ Ln } \frac{1 + \dfrac{2K_f - K_{fe} - K_{fs}}{K_{fe} - K_{fs}}}{1 - \dfrac{2K_f - K_{fe} - K_{fs}}{K_{fe} - K_{fs}}} \right)$$

Let $a = \dfrac{C_2}{2}$ and simplify

$$\text{LnN} = \text{Ln } C_1 + a \cdot \ln \left(\frac{K_{fs} - K_f}{K_f - K_{fe}} \right) \qquad \text{(B-6)}$$

And solving for K_f yields

$$K_f = \frac{K_{fs} + K_{fe}\left(\frac{N}{C_1}\right)^{1/a}}{1 + \left(\frac{N}{C_1}\right)^{1/a}} \qquad \text{(B-7)}$$

The component static strength factor, K_{fs}, is equal to the unnotched material ultimate strength divided by the component net section ultimate strength

$$K_{fs} = \frac{(F_{tu})_{\text{unnotched}}}{(F_{tu} \cdot SF)_{\text{component}}} = \frac{(F_{tu})_{\text{unnotched}}}{(S_s)_{\text{component}}} \qquad \text{(B-8)}$$

where:

F_{tu} is the material ult. strength.

SF is the net sect. factor, (i.e., rivet factor).

S_s is the net sect. static strength

The endurance limit factor, K_{fe}, must either be determined from test data or estimated when data is not available. A review of available data shows K_{fe} (at $N = 10^7$ cycles) to vary with the stress ratio, R, as shown in Figure B-2. At R equal plus one K_{fe} must equal K_{fs}. These trends may not hold for all materials, construction types, and load spectra therefore data from components tested to realistic load spectra is preferred.

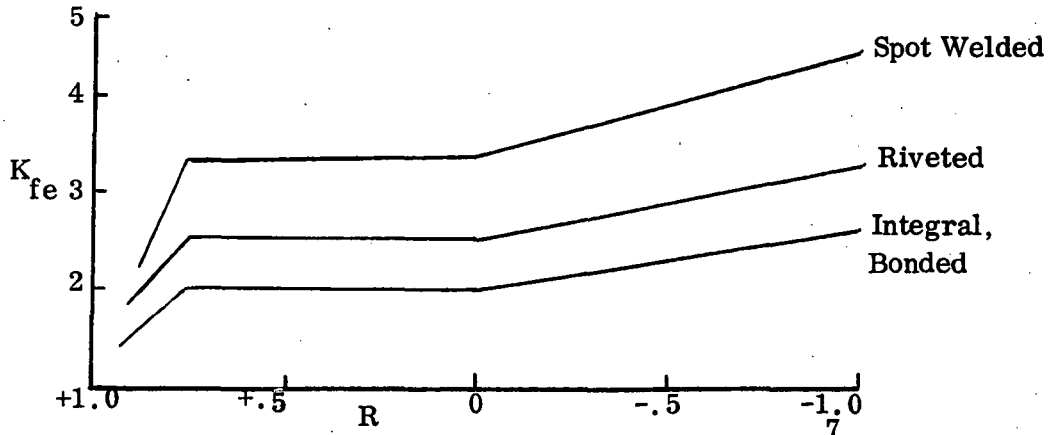

Figure B-2. Variation of Fatigue Notch Factor at 10^7 Cycles with Stress Ratio

It also appears that C_1 and a can be defined as functions of R . The following equations are proposed.

$$C_1 = e^{\left(\frac{R+7.07}{1.43}\right)\ln \cdot 10} \qquad \text{(B-9)}$$

$$a = -.6R - 1.4 \qquad \text{For } R > 0 \qquad \text{(B-10a)}$$

$$a = -1.9R + 1.4 \qquad \text{For } R \leq 0 \qquad \text{(B-10b)}$$

The development of Equations B-5 thru B-10b was facilitated by a Hewlett-Packard 9100B Plotting Routine. Figure B-3 was obtained with this H-P program and is a plot of Equations B-6, B-9, B-10a, and B-10b.

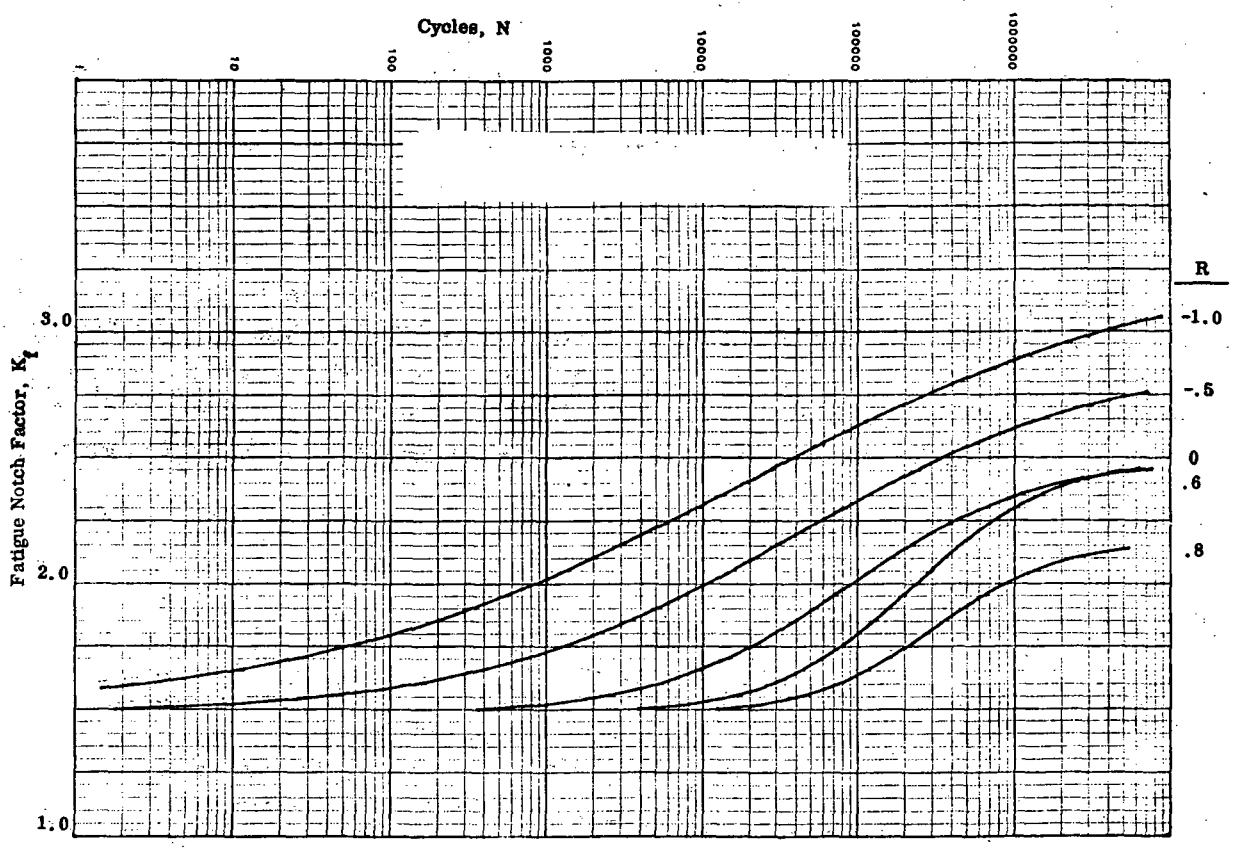

Figure B-3. Fatigue Notch Factors for Riveted Aluminum Components

S-N PLOTTER OPERATING INSTRUCTIONS

A plotting routine incorporating Equations B-1, B-7, B-9, B-10a, and B-10b has been programmed for the Hewlett-Packard 9100B. To operate the program execute the following steps:

1. PRESS "CLEAR"
2. PRESS "END"
3. ENTER PROGRAM - SIDES A AND B OF MAGNETIC CARD
4. TURN ON PRINT X
5. TURN ON PLOTTER
6. INSERT AND ADJUST PLOT PAPER (See Note 3).
7. PRESS "END"
8. PRESS "CONT"
9. ENTER STRESS RATIO, R, "CONT"
10. ENTER STATIC STRESS FACTOR, K_{fs}, "CONT"
11. ENTER ENDURANCE STRESS FACTOR, K_{fe}, "CONT"
12. ENTER ENDURANCE STRESS, S_e, "CONT" (See Note 2)
13. ENTER COEFFICIENT, C, "CONT" (See Note 3)
14. ENTER COEFFICIENT, m, "CONT"
15. ENTER COEFFICIENT, n, "CONT"
16. THE PROGRAM WILL PLOT AN S-N CURVE NORMALIZED TO NET SECTION STATIC STRENGTH, S_s.
17. THE PROGRAM WILL RETURN TO STEP 9.

Notes:

1. The program will plot both notched and unnotched S-N curves. For unnotched curves set K_{fs} and K_{fe} equal to one in Steps 10 and 11.
2. The value of S_e entered in Step 12 must be normalized by dividing by S_s for the material from which C, m and n were calculated.
3. The coefficients C, m, and n may be easily calculated with the H-P program presented previously.
4. The program is set for semi-log paper with 7 cycles × 60 divisions. (K&E No. 466463). If different plot paper is used it will be necessary to change the scale factors. Referring to the program listing, the x and y scale factors are located at Steps 62 and 57 respectively.
5. To correct anomalies in plotted curves, it may be necessary to recalculate C, m, and n using more judicious input stresses. Equation B-1 is very sensitive to C, m, and n.

The programming code is listed on Pages B-17, B-18 and B-19.

EXAMPLE PROBLEMS -- DATA FIT PROGRAM

Tables B-1 and B-2 show the required input data and the calculated values of C, m and n for unnotched 2024-T3, and for typical riveted aluminum components. Also shown is a partial listing of the H-P printout.

Table B-1. Fatigue Equation Coefficients for Unnotched 2024-T3

F_{tu} = 503 MN/m^2 (73 ksi)

R	NORMALIZED MAX. STRESS, S_{max}/F_{tu} *					C	m	n
	10^0	10^4	10^5	10^6	10^7			
+1.0								
.8	1.000	.999	.993	.985	.980	17220	.6674	-103.7
.6	↓	.997	.945	.897	.856	2611	.1205	-27.85
.4		.993	.856	.733	.688	13960	.3137	-5.103
.2		.984	.753	.589	.551	21140	.3904	-1.763
0		.956	.670	.493	.453	22370	.4964	-1.299
-.2		.908	.603	.432	.401	36060	.8378	-.3845
-.5	↑	.822	.534	.370	.342	73220	1.551	.2462
-1.0	1.000	.692	.462	.308	.281	410200	3.632	1.206
-2.0								
- ∞								

* Ref. 17, page 3-77

Sample H-P Printout:

```
 .4 ———— R

 1. ———— Ss
 .688 ——— Se

 10000. ———— N1
 .993 ——— S1
 100000. ———— N2
 .856 ——— S2
 1. 06 ——— N3
 .733 ——— S3

 13956.3474 —— C
 .3137 —— m
 -5.1029 —— n
```

Table B-2. Fatigue Equation Coefficients for Typical Riveted Aluminum Component

$S_s = 345\ MN/m^2$ (50 ksi)

R	NORMALIZED MAX. STRESS*, S_{max}/S_s					C	m	n
	10^0	10^4	10^5	10^6	10^7			
+1.0	1.0							
.8		.970	.850	.704	.684	501000	1.437	4.193
.6		.950	.724	.530	.498	108600	1.050	.6764
.4		.924	.638	.442	.404	52170	.9027	-.2568
.2		.882	.552	.350	.318	69100	1.157	.2584
0		.818	.482	.296	.266	64050	1.413	.2156
-.2		.720	.420	.250	.224	119860	2.343	.6162
-.5		.592	.344	.200	.174	130450	3.539	.5115
-1.0		.434	.256	.148	.126	219170	6.532	.6556
-2.0	1.0							

* Ref. Design criteria for a transport aircraft fuselage.

Sample H-P Printout:

```
-.2 ——— R

1. ——— Ss
.224 ——— Se

10000. ——— N1
.720 ——— S1
100000. ——— N2
.420 ——— S2
1. 06 ——— N3
.250 ——— S3

119868.3605 ——— C
2.3430 ——— m
.6162 ——— n
```

EXAMPLE PROBLEMS — S-N PLOTTER PROGRAM

The S-N curves for unnotched 2024-T3 shown in Figure B-4 were plotted from the data shown in Table B-1. These curves are not factored, i.e., K_{fs} and K_{fe} were set equal to one.

Figure B-5 shows S-N curves for typical riveted aluminum components plotted from the data in Table B-2. Again K_{fs} and K_{fe} were set equal to one.

Figure B-6 is an example of component S-N curves derived by factoring unnotched data. The unnotched data for 2024-T3 in Table B-1 is used. The static strength factor, K_{fs} is found by Equation B-8. A rivet factor of 0.75 is assumed.

$$K_{fs} = \frac{73}{66 \times 0.75} = 1.48$$

The fatigue notch factors, K_{fe}, are from Figure B-2. The derived S-N curves of Figure B-6 agree within six percent with the data based S-N curves of Figure B-5.

Figure B-4. S-N Curves for Unnotched 2024-T3

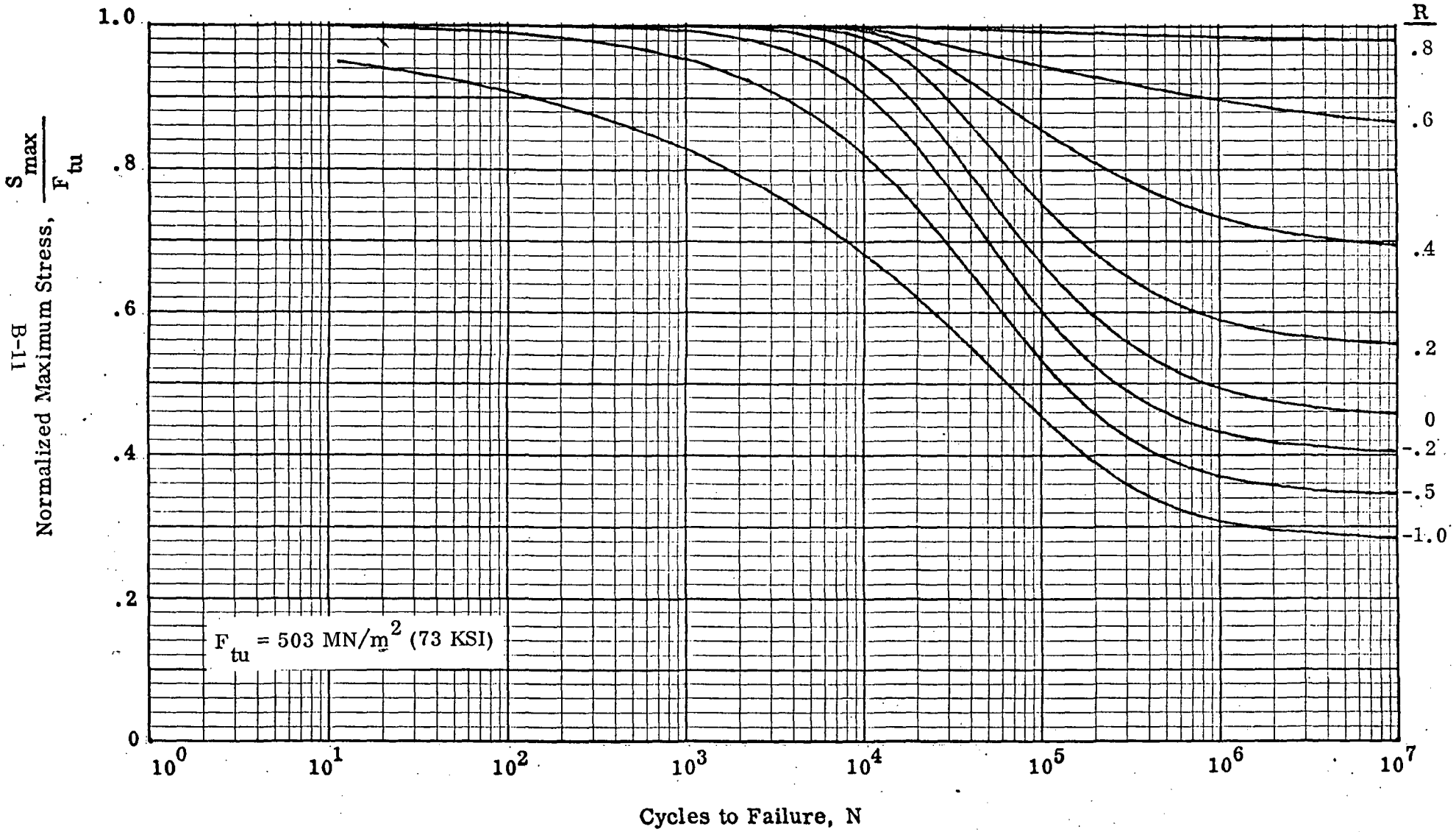

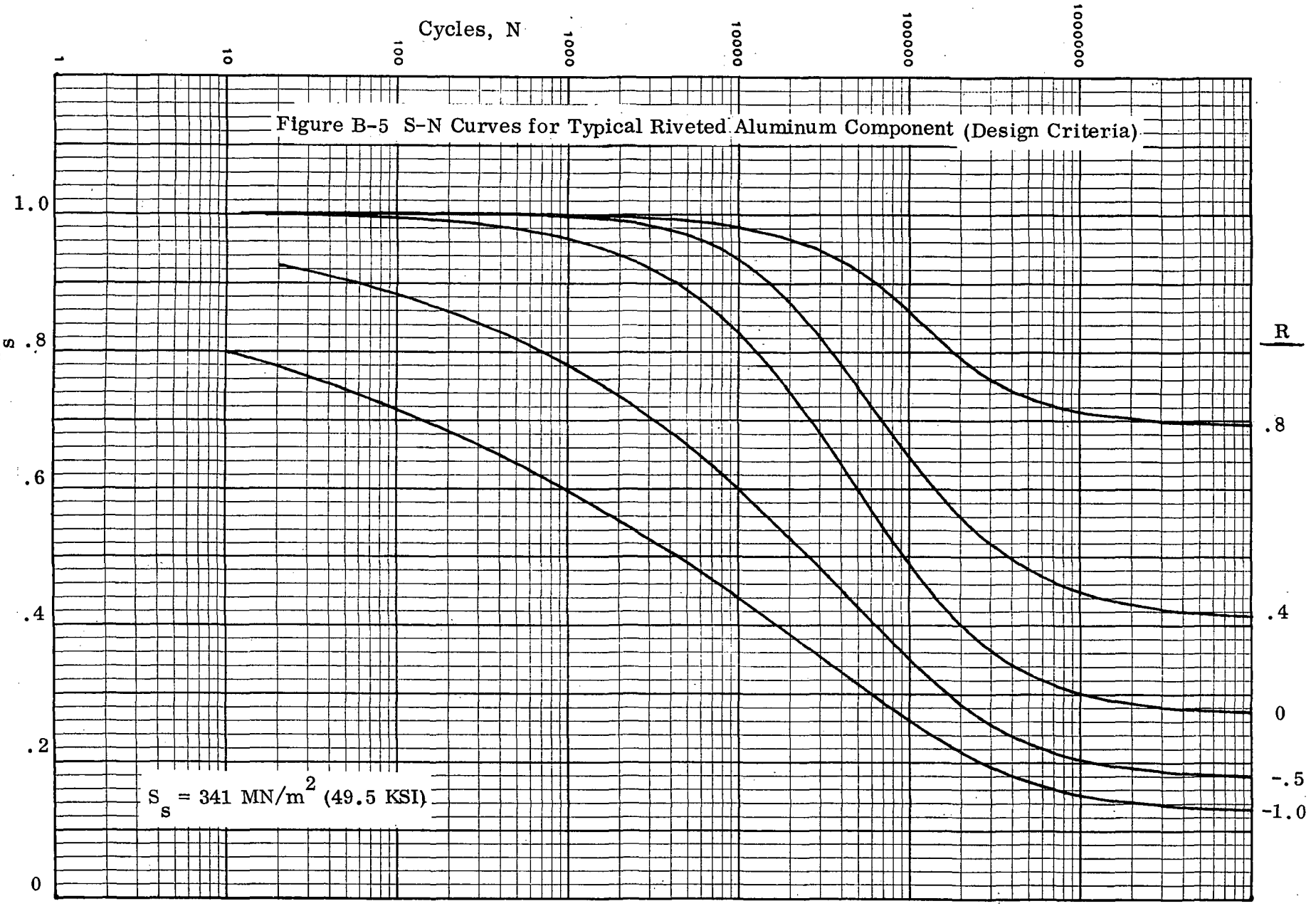

Figure B-5 S-N Curves for Typical Riveted Aluminum Component (Design Criteria)

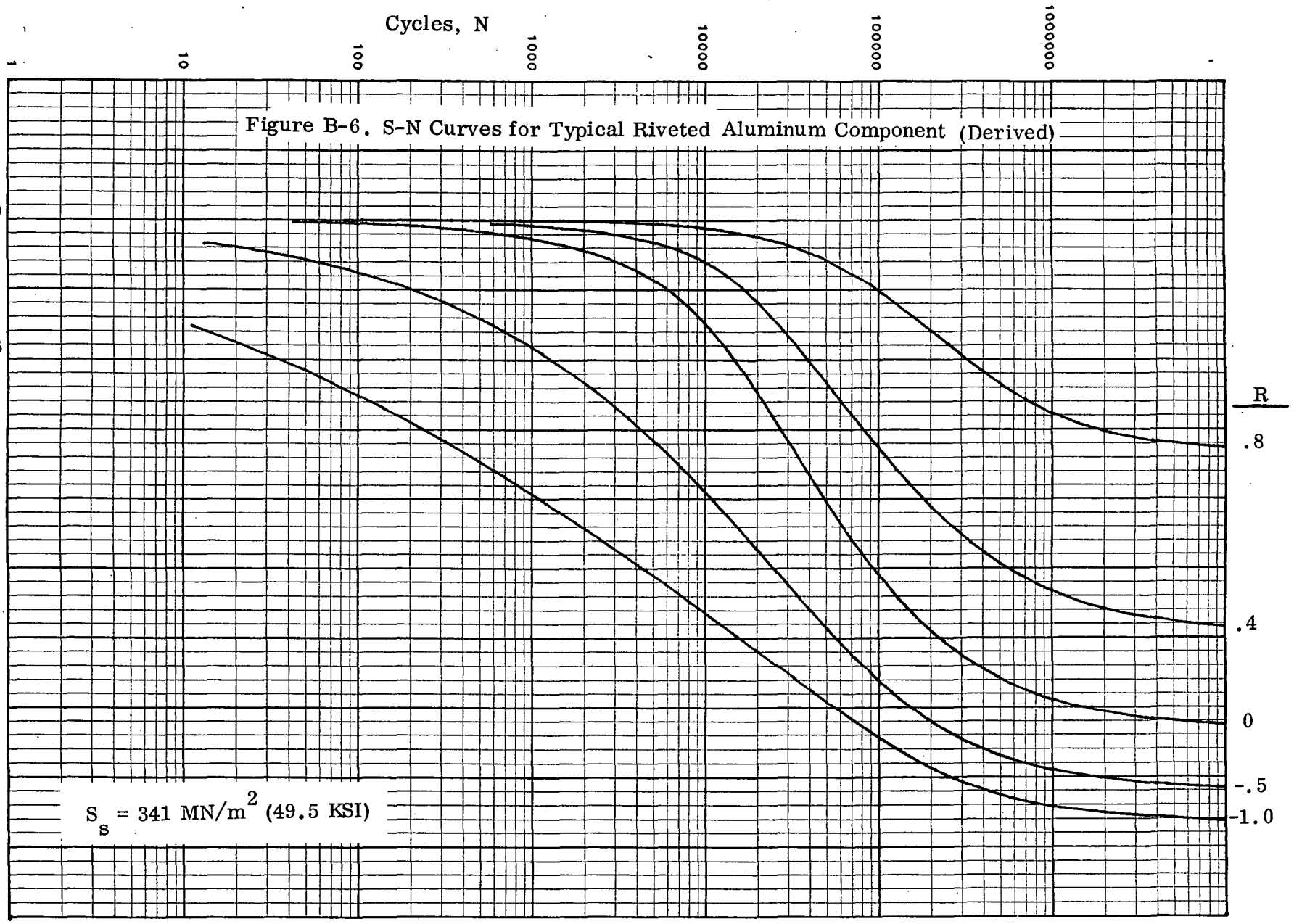

Figure B-6. S-N Curves for Typical Riveted Aluminum Component (Derived)

S-N DATA FIT COEFFICIENTS - - C, m, n
(Hewlett-Packard Programming Code)

S-N Data Fit - - C, m, n

Title _____

HEWLETT-PACKARD

Step	Key	Code	Display x	Display y	Display z
0 0	CL				
1	S		R		
2	PR				
3	SP				
4	S		S_S		
5	x→				
6	f				
7	PR				
8	S		S_e		
9	PR				
a	SP				
b	↑				
c	f				
d	÷			X_1	
1 0	y→				
1	e				
2	S		N_1		
3	x→				
4	d				
5	PR				
6	S		S_1		
7	PR				
8	↑				
9	f				
a	÷			X_1	
b	y→				
c	c				
d	S		N_2		
2 0	x→				
1	b				
2	PR				
3	S		S_2		
4	PR				
5	↑				
6	f				
7	÷			X_2	
8	y→				
9	a				
a	S		N_3		
b	x→				
c	9				
d	PR				

HEWLETT-PACKARD

Step	Key	Code	Display x	Display y	Display z
3 0	S		S_2		
1	PR				
2	SP				
3	↑				
4	f				
5	÷			X_3	
6	y→				
7	g				
8	GO TO				
9	SUB				
a	−				
b	0				
c	0				
d	↓		C		
4 0	PR				
1	f		m		
2	PR				
3	b		n		
4	PR				
5	SP				
6	SP				
7	GO TO				
8	0				
9	0				
a	S				
b	S				
c	S				
d	S				
0					
1					
2					
3					
4					
5					
6					
7					
8					
9					
a					
b					
c					
d					

HEWLETT-PACKARD

Step	Key	Code	Display x	Display y	Display z
0					
1					
2					
3					
4					
5					
6					
7					
8					
9					
a					
b					
c					
d					

Storage

F	S_S	m
E	X_1	
D	$N_1 = Y_1$	
C	X_1	
B	$N_2 = Y_2$	n
A	X_2	C
9	$N_3 = Y_3$	
8	X_3	
7		
6		
5		
4		
3		
2		
1		
0		

S-N Data Fit -- C, m, n

Title _____

HEWLETT-PACKARD

Step	Key	Code	Display x	Display y	Display z
0 0	C		X_1		
1	↑				
2	e		X_7		
3	−				
4	a		X_2		
5	↑				
6	e		X_7		
7	−				
8	↓				
9	÷				
a	d		Y_1		
b	X				
c	b		Y_2		
d	÷				
1 0	↓				
1	Ln X				
2	↓				
3	C		X_1		
4	↑				
5	X←				
6	8		X_3		
7	÷				
8	↓				
9	Ln X				
a	X				
b	C		X_1		
c	↑				
d	a		X_2		
2 0	÷				
1	↓				
2	Ln X				
3	÷				
4	Y→				
5	−				
6	f				
7	C		X_1		
8	↑				
9	e		X_7		
a	−				
b	X←				
c	8		X_3		
d	f				

Step	Key	Code	Display x	Display y	Display z
3 0	e		X_7		
1	−				
2	↓				
3	÷				
4	d		Y_1		
5	X				
6	X←				
7	9		Y_3		
8	÷				
9	↓				
a	Ln X				
b	↑				
c	X←				
d	−				
4 0	f		A		
1	−			NUM	
2	Y→				
3	−				
4	f				
5	1		1		
6	↑				
7	C		X_1		
8	−				
9	1				
a	↑				
b	CONT				
c	a		X_2		
d	−				
5 0	↓				
1	÷				
2	↓				
3	Ln X				
4	↑				
5	C		X_1		
6	↑				
7	X←				
8	8		X_3		
9	÷				
a	↓				
b	Ln X				
c	X				
d	C		X_1		

Step	Key	Code	Display x	Display y	Display z
6 0	↑				
1	a		X_2		
2	÷				
3	↓				
4	Ln X				
5	÷			③	
6	Y→				
7	−				
8	e				
9	1		1		
a	↑				
b	C		X_1		
c	−				
d	1		1		
7 0	↑				
1	X←				
2	8		X_3		
3	−				
4	↓				
5	÷				
6	↓				
7	Ln X				
8	↑				
9	X←				
a	−				
b	e		B		
c	−			DEM	
d	X←				

Storage

f	①	NUM ②
e	③	
d		
c		
b		
a		
9		
8		
7		
6		
5		
4		
3		
2		
1		
0		

S-N Data Fit -- C, m, n

Title _____

HEWLETT-PACKARD

Step	Key	Code	Display x	Display y	Display z
8 0	—				
1	f		Num		
2	X⇄Y				
3	÷			m	
4	Y→				
5	f				
6	1		1		
7	↑				
8	C		X_1		
9	—				
a	1		1		
b	↑				
c	a		X_2		
d	—				

HEWLETT-PACKARD

Step	Key	Code	Display x	Display y	Display z
9 0	↓				
1	÷				
2	↓				
3	Ln X				
4	↓				
5	f		m		
6	X			C	
7	Y→				
8	—				
9	f				
a	C		X_1		
b	↑				
c	e		X_7		
d	—				

HEWLETT-PACKARD

Step	Key	Code	Display x	Display y	Display z
a 0	a		X_2		
1	↑				
2	e		X_7		
3	—				
4	↓				
5	÷				
6	d		Y_1		
7	X				
8	b		Y_2		
9	÷				
a	↓				
b	Ln X		C_1		
c	↑				
d	X←				

Step	Key	Code	Display x	Display y	Display z
b 0	—			C_1	
1	f				
2	—			Num	
3	C		X_1		
4	↑				
5	a		X_2		
6	÷				
7	↓				
8	Ln X		Z_1		
9	÷			n	
a	Y→				
b	b				
c	C		X_1		
d	↑				

Step	Key	Code	Display x	Display y	Display z
c 0	e		X_7		
1	—				
2	d		Y_1		
3	X			Num	
4	C		X_1		
5	Ln X				
6	↓				
7	b		n		
8	X				
9	↓				
a	e^x				
b	÷				
c	1		1		
d	↑				

Step	Key	Code	Display x	Display y	Display z
d 0	C		X_1		
1	—				
2	↓				
3	Ln X				
4	↑				
5	f		m		
6	X				
7	↓				
8	e^x				
9	÷			C	
a	Y→				
b	a				
c	RET				
d	S				

Step	Key	Code	Display x	Display y	Display z
0					
1					
2					
3					
4					
5					
6					
7					
8					
9					
a					
b					
c					
d					

Storage

f	
e	
d	
c	
b	
a	
9	
8	
7	
6	
5	
4	
3	
2	
1	
0	

S-N PLOTTER FOR STRUCTURAL COMPONENTS
(Hewlett-Packard Programming Code)

S-N Plotter

Title

H-P #9100B PROGRAMMING SHEET

5333 (7-70)

Step	Key	Code	Display x	Display y	Display z
00	CL				
01	S		R		
02	X→				
03	e				
04	PR				
05	S		Kfs		→
06	X→				
07	−				
08	c				
09	PR				
0a	S		Kfe		→
0b	X→				
0c	−				
0d	a				
10	PR				
11	S		Se		
12	X→				
13	d				
14	PR				
15	S		c		
16	X→				
17	−				
18	f				
19	PR				
1a	S		m		
1b	X→				
1c	−				
1d	e				
20	PR				→
21	S		n		
22	X→				
23	−				
24	d				
25	PR				
26	SP				
27	1		1		
28	EN EX				
29	CH SI				
2a	6		Δ S		
2b	X→				
2c	f				
2d	↑				

Step	Key	Code	Display x	Display y	Display z
30	1		1		
31	X⇄Y		Δ S	1	
32	−				
33	Y→				
34	C				
35	GO TO				
36	SUE				
37	−				
38	0				
39	0				
3a	1		1	Log N	→
3b	IF X>Y				
3c	6				
3d	a				
40	7		7		
41	IF X<Y				
42	9				
43	C				
44	X←				
45	−				
46	a		Kfe		
47	↑				
48	1		1		
49	IF X<Y		1	Kfe	
4a	SUB				
4b	−				
4c	A				
4d	0				
50	C		S		
51	X⇄Y				
52	÷				
53	X←				
54	−				
55	C		Kfs		
56	X				
57	2				
58	5				
59	0				
5a	0				
5b	X			SF·Y	
5c	X←				
5d	−				

Step	Key	Code	Display x	Display y	Display z
60	b		Log N		
61	↑			X	
62	6				
63	2				
64	5				
65	•				
66	X			SF·X	
67	↓				
68	FMT		SF·X	SF·Y	
69	↓				
6a	X←				
6b	−				
6c	b		Log N		
6d	↑				
70	5				
71	IF X<Y		5	Log N	
72	8				
73	7				
74	f		Δ S		
75	↑				
76	•				
77	0				
78	2				
79	IF X<Y		.02	Δ S	
7a	8				
7b	d				
7c	1				
7d	•				

Storage

f	Δ S	−f	c
e	R	−e	m
d	Se	−d	n
c	S	−c	Kfs
b		−b	Log N
a		−a	Kfe
9			
8			
7			
6			
5			
4			
3			
2			
1			
0			

S-N Plotter

Title _____

H-P #9100B PROGRAMMING SHEET

Step	Key	Code	Display x	Display y	Display z
80	5				
81	X				
82	Y→				
83	f				
84	GO TO				
85	8				
86	d				−
87	.				
88	0				
89	1				
8a	0				
8b	X →				
8c	f				
8d	C		S		
90	↑				−
91	f		ΔS		
92	−				
93	Y→				
94	C				
95	d		Se	S	
96	IF X>Y				
97	9				
98	C				
99	GO TO				
9a	3				
9b	5				
9c	C		S		
9d	↑			S	
20	f		ΔS		−
21	+				
22	Y→				
23	C				
24	↑			ΔS	
25	.				
26	1		.1		
27	X				
28	Y→				
29	f				
2a	1		1		
2b	EN EX				
2c	CH SI				
2d	4				
b0	IF X>Y		10⁻⁴	ΔS	−
b1	b				
b2	6				
b3	GO TO				
b4	8				
b5	d				
b6	FIX				
b7	↑				
b8	GO TO				
b9	0				
ba	0				
bb	S				
bc	S				
bd	S				
c0	1		1		−
c1	↑				
c2	C		S		
c3	−				
c4	↓				
c5	Ln X				
c6	↑				
c7	X←				
c8	−				
c9	e		m		
ca	X				
cb	↓				
cc	e^x				
cd	↑				
f0	C		S		
f1	CONT				
f2	Ln X				
f3	↑				
f4	X←				
f5	−				
f6	d		n		
f7	X				
f8	↓				
f9	e^x				
fa	X				
fb	X←				
fc	−				
fd	f		C		
30	−				
31	b				
32	↑				
33	RET			LogN	
34	S				
35	S				
36	S				
37					
38					
39					
3a					
3b					
3c					
3d					
20	X				
21	C		S		
22	↓				
23	d		Se		
24	÷				
25	↓				
26	÷				
27	1		1	N	
28	IF X>Y				
29	CONT				
2a	X←Y				
2b	↓				
2c	Log X		LogN		
2d	X→				

Storage	
f	
e	
d	
c	
b	
a	
9	
8	
7	
6	
5	
4	
3	
2	
1	
0	

5333 (7-70)

Title S-N Plotter

H-P #9100B PROGRAMMING SHEET

Step	Key	Code	Display x	Display y	Display z
40	x⇐				
41	−				
42	b		LogN		
43	↑				
44	1				
45	0		10		
46	Ln X				
47	X				
48	↓				
49	e^x				
4a	↑			N	
4b	e		R		
4c	↑				
4d	7				
50	.				
51	0				
52	7				
53	+				
54	1				
55	.				
56	4				
57	3				
58	÷				
59	1				
5a	0				
5b	Ln X				
5c	X				
5d	↓				
60	e^x		C_1		
61	÷			$\frac{N}{C_1}$	
62	e		R		
63	↑				
64	0		0	R	
65	IFX>Y				
66	7				
67	6				
68	.				
69	6				
6a	0				
6b	CH SI				
6c	X				
6d	1				
70	.				
71	4				
72	+			n	
73	GO TO				
74	8				
75	1				
76	1			R	
77	.				
78	9				
79	CH SI				
7a	X				
7b	1				
7c	.				
7d	4				
80	+		.	n	
81	1				
82	X⇐Y				
83	÷				
84	↓				
85	X⇐Y				
86	Ln X				
87	X				
88	↓				
89	e^x				
8a	↑				
8b	↑				
8c	X⇐				
8d	−				
90	a		Kfe		
91	X				
92	X⇐				
93	−				
94	C		Kfs		
95	+			NUM	
96	1				
97	ROLL ↑		( )	1	NUM
98	+			DEN	
99	↓				
9a	÷			Kf	
9b	RET			Kf	
9c	S				
9d	S				
0					
1					
2					
3					
4					
5					
6					
7					
8					
9					
a					
b					
c					
d					

Storage

f	
e	
d	
c	
b	
a	
9	
8	
7	
6	
5	
4	
3	
2	
1	
0	

5333 (7-70)

DISTRIBUTION LIST
NAS1-12506

	No. Copies
NASA Langley Research Center Hampton, VA 23665	
Attn: Report & Manuscript Control Office, Mail Stop 180A	1
Clarence C. Poe, Jr., Mail Stop 188E	57
NASA Ames Research Center Moffett Field, CA 94035	
Attn: Library, Mail Stop 202-3	1
NASA Flight Research Center Edwards, CA 93523	
Attn: Library	1
NASA Goddard Space Flight Center Greenbelt, MD 20771	
Attn: Library	1
Jet Propulsion Laboratory 4800 Oak Grove Drive Pasadena, CA 91103	
Attn: Library, Mail 111-113	1
NASA Lyndon B. Johnson Space Center Houston, TX 77058	
Attn: JM6/Library	1
NASA John F. Kennedy Space Center Kennedy Space Center, FL 32899	
Attn: Library, IS-DOC-1L	1
NASA Lewis Research Center 21000 Brookpark Road Cleveland, OH 44135	
Attn: Library, Mail Stop 60-3	1
NASA Marshall Space Flight Center Marshall Space Flight Center, AL 35812	
Attn: Library, AS61L	1
National Aeronautics & Space Administration Washington, DC 20546	
Attn: KSS-10/Library	1
RW/NASA Headquarters	1
Materials Sciences Corporation Blue Bell Office Campus 1777 Walton Road Blue Bell, PA 19422	
Attn: Nancy Sabia	1

NASA CR-132648

DISTRIBUTION LIST
NAS1-12506

	No. Copies
E. I. Du Pont De Nemours & Company, Inc. Wilmington, DE 19898 Attn: Carl Zweben, Bldg. 262/Room 316, Experimental Station	1
NASA Scientific & Technical Information Facility 6571 Elkridge Landing Road Linthicum Heights, MD 21090	30 plus reproducible